

Technical University of Crete
Department of Electrical & Computer Engineering



**QUANTUM RANDOM WALKS:
QUANTUM TO CLASSICAL PHASE TRANSITIONS**

A Thesis

In partial fulfillment of the requirements for the degree of
Integrated Master of Science in Electrical & Computer Engineering

Thesis Chair:
Demosthenes Ellinas, Ph.D.

Committee Members:
Dimitris G. Angelakis, Ph.D.
Ioannis Tsohantjis, Ph.D.

by
Aristotelis Symeonakis

Chania, May 2022

Dedications

To future scientists.

Acknowledgements

Firstly, I would like to thank my thesis advisor, professor Demosthenes Ellinas who upped my thinking patterns for mathematical and practical solutions and was always there for me. I also thank the committee members Dimitrios Angelakis and Ioannis Smyrnakis for valuable feedback and patience during the presentation. I'm grateful to prof. A. Bracken for making available his program code on which part of the numerical work of the thesis was based. I'm really appreciative for the love and support received from my friends during this stage of my life, and not only. Most of all I owe to my family who believed in me, stood by my side and sculpted me to what I am today.

Thank you.

Abstract

Quantum walks (QW) are systems consisting of parts identified as the quantum coin, the quantum walker and procedures simulating coin tossing and spreading along a space. They constitute quantum versions of the proverbial classical random walk (CRW) which now is reformulated to admit its quantization to a QW. Quantization rules for the CRW to QW passage, the novel effects of enhanced mobility of a QW, its demonstrated computational universality, as well as a wealth of scientific-technological applications and physical implementation scenarios constitute a vibrant subfield of quantum information science and technology. This work deals with an additional problem: the controlled and designed quantum-to-classical (Q – C) transition in random walks. Utilizing recent progress in that problem, employs classical randomness imposed on the quantum coin subsystem of a QW and studies the induced onset of Q – C transition. Guided by a crossover condition, (involving the number of evolution steps-time and the strength of imposed randomness), governing the existence of Q – C transition two QW models are studied. These are models of QWs on the lattices of integer and natural numbers. Distributions of lattice cite occupation probabilities as well as standard deviation parameter vs. number of steps and/or strength of the imposed randomness are systematically investigated as quantitative measures of the Q – C transition. The transition is manifested as a passage from the quadratically enhanced diffusion rate (ballistic regime) to a decelerated diffusion rate (classical regime). Next a switch like designed Q – C transition is introduced: in terms of a layered QW diffusion model, the operational and applied character of that switch is manifested. A novel figure of merit for the performance of the switch is finally introduced: the Inverse Participation Ratio (IPR) of the distribution of occupation probabilities. The IPR demonstrates that the Q – C transition is a phenomenon similar to Anderson localization that entails a randomness induced suppression of QW hyper-diffusion.

Περίληψη

Οι κβαντικοί περίπατοι (ΚβΠ) είναι συστήματα αποτελούμενα από μέρη που αναγνωρίζονται ως το κβαντικό νόμισμα, ο κβαντικός περιπατητής και διαδικασίες που προσομοιώνουν τη ρίψη νομισμάτων και την εξάπλωση κατά μήκος ενός χώρου. Αυτά αποτελούν τις κβαντικές εκδοχές των παρόμοιων κλασικών τυχαίων περιπάτων (ΚΤΠ) οι οποίοι αναδιατυπώνονται έτσι ώστε να κβαντοποιηθούν σε ΚβΠ. Κανόνες κβαντοποίησης για το πέρασμα από ΚΤΠ σε ΚβΠ, οι καινούργιες ιδιότητες ενισχυμένης κινητικότητας ενός ΚβΠ, η αποδεδειγμένη υπολογιστική καθολικότητα, καθώς και ένας πλούτος από σενάρια επιστημονικών τεχνολογικών εφαρμογών και υλοποιήσεις, αποτελούν ζωντανά υποπεδία της επιστήμης-τεχνολογίας της κβαντικής πληροφορίας. Αυτή η εργασία ασχολείται με ένα επιπλέον πρόβλημα: Την ελεγχόμενη και σχεδιασμένη κβαντική-σε-κλασική (Κβ – Κλ) μετάβαση σε τυχαίους περιπάτους. Αξιοποιώντας την πρόσφατη πρόοδο για το θέμα αυτό, χρησιμοποιείται κλασική τυχαιότητα που επιβάλλεται στο υποσύστημα κβαντικών νομισμάτων και μελετά την επαγομένη έναρξη της Κβ – Κλ μετάβασης. Καθοδηγημένο από μια συνθήκη διασταύρωσης (που περιλαμβάνει το πλήθος των βημάτων-χρόνου εξέλιξης και την ισχύ της επιβλημένης τυχειότητας), που διέπει την ύπαρξη της Κβ – Κλ μετάβασης, μελετώνται δύο μοντέλα ΚβΠ. Τα μοντέλα αυτά είναι ΚβΠ στα πλέγματα των ακεραίων και των φυσικών αριθμών. Κατανομές πιθανοτήτων κατάληψης των σημείων του πλέγματος καθώς και η παράμετρος της τυπικής απόκλισης έναντι του πλήθους βημάτων και/ή την ισχύς της επιβληθείσας τυχειότητας διερευνώνται συστηματικά ως ποσοτικά μέτρα της Κβ – Κλ μετάβασης. Η μετάβαση εκδηλώνεται ως ένα πέρασμα από τον τετραδικά ενισχυμένο ρυθμό διάχυσης (βαλλιστικό καθεστώς) σε έναν επιβραδυμένο ρυθμό διάχυσης (κλασικό καθεστώς). Στη συνέχεια, εισάγεται μια Κβ – Κλ μετάβαση στη μορφή διακόπτη: Όσον αφορά ένα πολυεπίπεδο μοντέλο διάχυσης ΚβΠ, εκδηλώνεται ο λειτουργικός και εφαρμοσμένος χαρακτήρας αυτού του διακόπτη. Τελικά, εισάγεται ένα καινοτόμο μέτρο ποιότητας για την απόδοση του διακόπτη: ο Αντίστροφος Λόγος Συμμετοχής (ΑΛΚ) της κατανομής πιθανοτήτων κατάληψης. Ο ΑΛΚ καταδεικνύει ότι η Κβ – Κλ μετάβαση είναι ένα φαινόμενο παρόμοιο με τον εντοπισμό του Άντερσον που συνεπάγεται μια επαγομένη λόγω τυχειότητας καταστολή υπερ-διάχυσης ΚβΠ.

Table of Contents

Abstract	iv
Introduction	1
1 Mathematical Preliminaries	3
1.1 Definitions	3
1.1.1 Quantum bit	3
1.1.2 Tensor Product	4
1.1.3 Qudit	5
1.1.4 Superposition	6
1.1.5 ‘Double-Wedge’ Notation	7
1.1.6 Unitary – Hermitian – Normal	7
1.1.7 Vector Inner Product and Normalization	7
1.2 Tools	9
1.2.1 Gates – Operators – Pauli Matrices	9
1.2.2 Single Qubit Gates	10
1.2.3 Entanglement	15
1.2.4 Trace – Partial Trace	15
1.2.5 Density Matrix – Operator	17
1.2.6 Reduced Density Matrix	17
1.2.7 Super-operator – CPTP Maps	19
1.2.8 Quantum Measurement	20
1.3 General Statistics	22
1.3.1 Random Variables	22
1.3.2 Probability Density Function	22
1.3.3 Mean, Mode, Median	22
1.3.4 Variance	23
1.3.5 Standard Deviation	23
1.3.6 Inverse Participation Ratio	24
2 Classical Random Walk and Quantum Walk Theory	25
2.1 Classical Random Walk	25
2.1.1 On Integers	25
2.1.2 Quantization	27
2.2 Quantum Walk	31
2.2.1 Introduction	31

2.2.2	Density Matrix	32
2.2.3	Asymptotics and the Double Horn Distribution	34
3	Quantum – Classical Transitions	39
3.1	The ε -Model	41
3.2	Detection of a Hidden Random Layer via Q – C Transition	62
3.3	The χ -Model	75
	Conclusion	85
A	Appendix	87
A.1	The Adjoint Action	87
A.2	Euclidean Group $E(2)$	88
A.3	Discrete Time Fourier Transform	89
A.4	Qiskit QW Circuit Implementation	90
	References	92

Introduction

The quantum walk [1], [2] has been related with other objects of quantum computing, like quantum search algorithms in general [3] or even more specific ones, like searching in graphs [4]. If a graph is used to model the locality of a database, then the QW can provide a natural framework for the spatial search problem [5]. QWs have been involved in research for different types of processes like decision processes in trees, which utilize some quantum advantages [6] with the most known quality being the exponential algorithmic speed-up in various applications [7]. Exact solutions for exact one-dimensional problems are already given [8], [9], [10], and random walks on boundless systems have been solved analytically [11]. The problem of quantization has implicated researchers, to some extent, to more systematically find ways on how to quantize the walk [12], [13]. One of the more theoretical aspects of the QW theories have to do with what is the exact kind of relation between the classical and quantum and the passing from one to the other [14]. The asymptotic behaviour can tell us lots of useful details about the QW. Also, phenomena correlated to memory effects have been studied [15].

In this thesis we aim to expose some interesting points of the random walks, as much as classical as quantum modes, as we talk about their combination and transferral from one to the other and back, in one experiment. Such behaviour is found in nature, say, in the atmosphere of neutron stars where there are layers of different gasses, as well as in liquid thermometer gadgets. But what is it to us? Through the study of such kind of transition in a controlled environment, we can look into classical noise, affecting a given quantum system, in a way that we can take advantage of [9], [11]. Future heuristic algorithms and simulation applications could be assisted by these transitions.

The key that makes it all happen is a noise strength parameter introduced in the reshuffling matrix which is then infused in the random walk's coin operator which distorts

it's diagonality and, thus, the behaviour of the walk's deviation. We will study this classical noise infusion and behaviour in two unique mathematical models.

Thesis outline

chapter 1. Mathematical Preliminaries.

We describe the basic tools of quantum information and statistical theory, without which we cannot continue. In case you are acquainted with these terms and concepts, feel free to skip this chapter.

chapter 2. Classical Random Walk and Quantum Walk Theory.

A crash course on random walk theory from the basics of the CRW, to quantization rules and asymptotic behaviour of the QW is necessary and available here.

chapter 3. Quantum – Classical Transitions.

Development and proving of the theory of the present topic of interest on two different models and a small practical experiment using one of the models.

Chapter 1

Mathematical Preliminaries

1.1 Definitions

1.1.1 Quantum bit

Since we focus on the informational domain, we define a unit that carries our bits of information, namely, the quantum bit or simply, the qubit. In physical implementation, it can be a cold ion or a photon or something of the kind [16], but we won't deal with that here. One qubit can have values of 0 or 1 or anything in between. Keep in mind that a qubit represents one bit of classical information only when stored or measured! Upon processing, a qubit can behave as an infinite number of classical bits because of its property to obtain any value from the space continuum $[0, 1]$. We will describe the qubit states using Dirac's formalization, as shown below.

We consider a Hilbert space $H = \mathbb{C}^{n \times 1}$ which contains vectors, polynomials, and matrices. Each column vector is noted as $|a\rangle \in H$, and it is called *ket*. Its dual space is $H^* = \mathbb{C}^{1 \times n}$ and each row vector is noted as $\langle a| \in H^*$, which is called *bra* [17], [18].

Ket, qubit representation for the '0, 1' basis, also known as computational basis:

$$|0\rangle = \begin{pmatrix} 1 \\ 0 \end{pmatrix}, \quad |1\rangle = \begin{pmatrix} 0 \\ 1 \end{pmatrix} \quad (1)$$

Bra, qubit representation for the computational basis:

$$\langle 0| = \begin{pmatrix} 1 & 0 \end{pmatrix}, \quad \langle 1| = \begin{pmatrix} 0 & 1 \end{pmatrix} \quad (2)$$

1.1.2 Tensor Product

To combine Hilbert spaces say in the case of multiparticle systems, we note as tensor product (\otimes) the mathematical tool for convolutional multiplication of space terms.

Suppose

$$A = \begin{pmatrix} \alpha_{11} & \cdot & \cdot & \cdot & \alpha_{1n} \\ \cdot & \cdot & & & \cdot \\ \cdot & & \cdot & & \cdot \\ \cdot & & & \cdot & \cdot \\ \alpha_{m1} & \cdot & \cdot & \cdot & \alpha_{mn} \end{pmatrix}, \quad (3)$$

and

$$B = \begin{pmatrix} \beta_{11} & \cdot & \cdot & \cdot & \beta_{1q} \\ \cdot & \cdot & & & \cdot \\ \cdot & & \cdot & & \cdot \\ \cdot & & & \cdot & \cdot \\ \beta_{p1} & \cdot & \cdot & \cdot & \beta_{pq} \end{pmatrix}, \quad (4)$$

two matrices having dimensions $m \times n$ and $p \times q$, respectively. The tensor product of A and B is given by

$$A \otimes B = \begin{pmatrix} \alpha_{11} & \cdot & \cdot & \cdot & \alpha_{1n} \\ \cdot & \cdot & & & \cdot \\ \cdot & & \cdot & & \cdot \\ \cdot & & & \cdot & \cdot \\ \alpha_{m1} & \cdot & \cdot & \cdot & \alpha_{mn} \end{pmatrix} \otimes \begin{pmatrix} \beta_{11} & \cdot & \cdot & \cdot & \beta_{1q} \\ \cdot & \cdot & & & \cdot \\ \cdot & & \cdot & & \cdot \\ \cdot & & & \cdot & \cdot \\ \beta_{p1} & \cdot & \cdot & \cdot & \beta_{pq} \end{pmatrix}$$

$$A \otimes B = \begin{pmatrix} \alpha_{11}B & \cdot & \cdot & \cdot & \alpha_{1n}B \\ \cdot & \cdot & \cdot & \cdot & \cdot \\ \cdot & \cdot & \cdot & \cdot & \cdot \\ \cdot & \cdot & \cdot & \cdot & \cdot \\ \alpha_{m1}B & \cdot & \cdot & \cdot & \alpha_{mn}B \end{pmatrix}, \quad (5)$$

with $A \otimes B$ having dimensions $mp \times nq$.

We can simplify the tensor product notation of $|\alpha \otimes \beta\rangle$ as $|\alpha, \beta\rangle$ or just $|\alpha\beta\rangle$. In case we have a tensor product of $|\alpha\rangle$ with itself n times giving $\underbrace{|\alpha\rangle \otimes |\alpha\rangle \otimes \dots \otimes |\alpha\rangle}_n$, we can use the notation $|\alpha\rangle^{\otimes n}$.

Four key properties of the tensor product are

- $z(|\alpha\rangle \otimes |\beta\rangle) = (z|\alpha\rangle) \otimes |\beta\rangle = |\alpha\rangle \otimes (z|\beta\rangle)$
- $(|\alpha_1\rangle + |\alpha_2\rangle) \otimes |\beta\rangle = |\alpha_1\rangle \otimes |\beta\rangle + |\alpha_2\rangle \otimes |\beta\rangle$
- $|\alpha\rangle \otimes (|\beta_1\rangle + |\beta_2\rangle) = |\alpha\rangle \otimes |\beta_1\rangle + |\alpha\rangle \otimes |\beta_2\rangle$
- $A \otimes B(|\alpha\rangle \otimes |\beta\rangle) = A|\alpha\rangle \otimes B|\beta\rangle$

where $|\alpha\rangle$ and $|\beta\rangle$ are arbitrary basis vectors, A and B are arbitrary linear operators, and z is an arbitrary scalar [18].

1.1.3 Qudit

We define, as qudit a multiple qubit register [18].

For example, a 2-qubit register:

$$|u_0\rangle = |00\rangle = |0\rangle|0\rangle = |0\rangle \otimes |0\rangle = \begin{pmatrix} 1 \\ 0 \end{pmatrix} \otimes \begin{pmatrix} 1 \\ 0 \end{pmatrix} = \begin{pmatrix} 1 \\ 0 \\ 0 \\ 0 \end{pmatrix}$$

The above is one of the four computational basis states for 2-qubits. The remaining three are

$$\begin{aligned}
 |u_1\rangle &= |01\rangle = |0\rangle|1\rangle = |0\rangle \otimes |1\rangle = \begin{pmatrix} 1 \\ 0 \end{pmatrix} \otimes \begin{pmatrix} 0 \\ 1 \end{pmatrix} = \begin{pmatrix} 0 \\ 1 \\ 0 \\ 0 \end{pmatrix}, \\
 |u_2\rangle &= |10\rangle = |1\rangle|0\rangle = |1\rangle \otimes |0\rangle = \begin{pmatrix} 0 \\ 1 \end{pmatrix} \otimes \begin{pmatrix} 1 \\ 0 \end{pmatrix} = \begin{pmatrix} 0 \\ 0 \\ 1 \\ 0 \end{pmatrix}, \\
 |u_3\rangle &= |11\rangle = |1\rangle|1\rangle = |1\rangle \otimes |1\rangle = \begin{pmatrix} 0 \\ 1 \end{pmatrix} \otimes \begin{pmatrix} 0 \\ 1 \end{pmatrix} = \begin{pmatrix} 0 \\ 0 \\ 0 \\ 1 \end{pmatrix}. \tag{6}
 \end{aligned}$$

As it seems, only one '1' exists in every vector corresponding to each position.

1.1.4 Superposition

Quantum property of occupying multiple states at once, until collapse by, say, measurement.

So upon measurement, there is some probability $|\alpha|^2$ of getting an outcome of $|0\rangle$ and a probability of $|\beta|^2$ getting $|1\rangle$.

Thus,

$$|\psi\rangle = \alpha|0\rangle + \beta|1\rangle. \tag{7}$$

If the state is normalized, we get that $|\alpha|^2 + |\beta|^2 = 1$.

1.1.5 ‘Double-Wedge’ Notation

The vectorization of any arbitrary matrix \mathbf{A} may be represented by the double-wedge notation $|A\rangle\rangle$ [18] as

$$|A\rangle\rangle = \left| \begin{pmatrix} a_{00} & a_{01} \\ a_{10} & a_{11} \end{pmatrix} \right\rangle\rangle = \begin{pmatrix} a_{00} \\ a_{01} \\ a_{10} \\ a_{11} \end{pmatrix}. \quad (8)$$

1.1.6 Unitary – Hermitian – Normal

A complex square matrix U is *unitary* if its conjugate transpose U^* is also its inverse, that is, if

$$UU^* = U^*U = \mathbf{1}, \quad \mathbf{1} = \begin{pmatrix} 1 & 0 \\ 0 & 1 \end{pmatrix}, \quad (9)$$

where $\mathbf{1}$ is the so-called identity matrix.

The hermitian adjoint of a matrix is denoted with a dagger (\dagger). If the matrix is hermitian, then

$$UU^\dagger = U^\dagger U = \mathbf{1}. \quad (10)$$

We call an operator *normal* when

$$AA^\dagger = A^\dagger A. \quad (11)$$

1.1.7 Vector Inner Product and Normalization

To compute the length of a vector, even if it’s a length in an abstract sense, we need a way to find the *inner product*. This is a generalization of the dot product used with ordinary vectors in Euclidean space. While the dot product takes two vectors and maps

them into a real number, in our case the inner product will take two vectors from \mathbb{C}^2 and map them to a *complex* number. We write the inner product between two vectors $|u\rangle, |v\rangle$ with the notation $\langle u|v\rangle$. If the inner product between two vectors is zero,

$$\langle u|v\rangle = 0, \tag{12}$$

we say that $|u\rangle, |v\rangle$ are *orthonormal* to one another. The inner product is a complex number. The conjugate of this complex number satisfies

$$\langle u|v\rangle^* = \langle v|u\rangle. \tag{13}$$

We can use the inner product to define a norm (or length) – by computing the inner product of a vector with itself

$$\|u\| = \sqrt{\langle u|u\rangle}. \tag{14}$$

Notice that the norm is a real number, and hence can define a length. For any vector $|u\rangle$ we have

$$\langle u|u\rangle \geq 0, \tag{15}$$

with equality, if and only if $|u\rangle = 0$.

When the norm of a vector u is $\|u\| = 1$, we say that vector u is *normalized*. We can generate a normalized vector by computing the norm, which is just a number, and dividing the vector by it. If each element of a set of vectors is normalized and the elements are orthogonal with respect to each other, we say the set is *orthonormal*. For example, consider the set $|0\rangle, |1\rangle$. By inner product definition, we have

$$\langle 0|0\rangle = \begin{pmatrix} 1 & 0 \end{pmatrix} \begin{pmatrix} 1 \\ 0 \end{pmatrix} = 1,$$

$$\begin{aligned}
\langle 0|1\rangle &= \begin{pmatrix} 1 & 0 \end{pmatrix} \begin{pmatrix} 0 \\ 1 \end{pmatrix} = 0, \\
\langle 1|0\rangle &= \begin{pmatrix} 0 & 1 \end{pmatrix} \begin{pmatrix} 1 \\ 0 \end{pmatrix} = 0, \\
\langle 1|1\rangle &= \begin{pmatrix} 0 & 1 \end{pmatrix} \begin{pmatrix} 0 \\ 1 \end{pmatrix} = 1.
\end{aligned} \tag{16}$$

By showing that $\langle 0|0\rangle = \langle 1|1\rangle = 1$, we showed the vectors are normalized, while showing that $\langle 0|1\rangle = \langle 1|0\rangle = 0$, we showed they were orthogonal. Hence, the set is orthonormal [18].

Another orthonormal basis set for \mathbb{C}^2 is

$$|+\rangle = \frac{1}{\sqrt{2}} \begin{pmatrix} 1 \\ 1 \end{pmatrix}, \quad |-\rangle = \frac{1}{\sqrt{2}} \begin{pmatrix} 1 \\ -1 \end{pmatrix}. \tag{17}$$

1.2 Tools

1.2.1 Gates – Operators – Pauli Matrices

As in classical computation, we are in the need of tools capable of physically implementing our mathematical calculations. In place of the classical gates, we now have quantum gates or, otherwise, quantum operators. They are usually represented in the form of a squared matrix with dimensions corresponding to the number of qubits they will act on.

1.2.2 Single Qubit Gates

Some basic operators are the Pauli sigma or rotations

$$\begin{aligned}\sigma_0 = \sigma_I = \mathbf{1} &= \begin{pmatrix} 1 & 0 \\ 0 & 1 \end{pmatrix}, \quad (\text{Identity gate}) \\ \sigma_1 = \sigma_X = X &= \begin{pmatrix} 0 & 1 \\ 1 & 0 \end{pmatrix}, \quad (\text{Not gate}) \\ \sigma_2 = \sigma_Y = Y &= \begin{pmatrix} 0 & -i \\ i & 0 \end{pmatrix}, \\ \sigma_3 = \sigma_Z = Z &= \begin{pmatrix} 1 & 0 \\ 0 & -1 \end{pmatrix}, \quad (\text{Phase gate})\end{aligned}\tag{18}$$

and it's easy to prove that they are unitary and hermitian, thus,

$$\mathbf{1}^2 = X^2 = Y^2 = Z^2 = \mathbf{1}.\tag{19}$$

Pauli sigma gates actions

- $\mathbf{1}|0\rangle = |0\rangle, \quad \mathbf{1}|1\rangle = |1\rangle$
- $X|0\rangle = |1\rangle, \quad X|1\rangle = |0\rangle$
- $Y|0\rangle = i|1\rangle, \quad Y|1\rangle = -i|0\rangle$
- $Z|0\rangle = |0\rangle, \quad Z|1\rangle = |-1\rangle$

Another notable gate is the Hadamard gate

$$H = \frac{1}{\sqrt{2}} \begin{pmatrix} 1 & 1 \\ 1 & -1 \end{pmatrix},\tag{20}$$

a single-qubit operation that maps the basis states as

- $H|0\rangle = \frac{|0\rangle+|1\rangle}{\sqrt{2}}$
- $H|1\rangle = \frac{|0\rangle-|1\rangle}{\sqrt{2}}$

thus, creating an equal superposition of the two basis states.

An interesting gate transformation is that of the square root of the not gate (\sqrt{X}). We find this gate matrix by exploiting its eigenvalues $\in \{\pm 1\}$ and its eigenvectors $|0'\rangle = \frac{1}{\sqrt{2}}(|0\rangle + |1\rangle)$ and $|1'\rangle = \frac{1}{\sqrt{2}}(|0\rangle - |1\rangle)$ [18].

We have

$$|0'\rangle\langle 0'| = \begin{pmatrix} \frac{1}{2} & \frac{1}{2} \\ \frac{1}{2} & \frac{1}{2} \end{pmatrix}, \quad (21)$$

and

$$|1'\rangle\langle 1'| = \begin{pmatrix} \frac{1}{2} & -\frac{1}{2} \\ -\frac{1}{2} & \frac{1}{2} \end{pmatrix}. \quad (22)$$

From eq. (21) and eq. (22) the not matrix is written as

$$X = 1 \begin{pmatrix} \frac{1}{2} & \frac{1}{2} \\ \frac{1}{2} & \frac{1}{2} \end{pmatrix} - 1 \begin{pmatrix} \frac{1}{2} & -\frac{1}{2} \\ -\frac{1}{2} & \frac{1}{2} \end{pmatrix}. \quad (23)$$

From eigenvalues properties we have

$$\begin{aligned} \sqrt{X} &= \sqrt{1} \begin{pmatrix} \frac{1}{2} & \frac{1}{2} \\ \frac{1}{2} & \frac{1}{2} \end{pmatrix} + \sqrt{-1} \begin{pmatrix} \frac{1}{2} & -\frac{1}{2} \\ -\frac{1}{2} & \frac{1}{2} \end{pmatrix} \\ &= \begin{pmatrix} \frac{1}{2} & \frac{1}{2} \\ \frac{1}{2} & \frac{1}{2} \end{pmatrix} + i \begin{pmatrix} \frac{1}{2} & -\frac{1}{2} \\ -\frac{1}{2} & \frac{1}{2} \end{pmatrix} \\ &= \begin{pmatrix} \frac{1+i}{2} & \frac{1-i}{2} \\ \frac{1-i}{2} & \frac{1+i}{2} \end{pmatrix}. \end{aligned} \quad (24)$$

1.2.2.1 Multi Qubit Gates With quantum interference and entanglement (section 1.2.3), we are capable of making use of a number of qubits simultaneously. That's where the multiple qubit gates come in handy, and especially a category of those that allow us to control qubits by exploiting other qubits, called the control gates. Generally, a control gate is of the form

$$CU = P_0 \otimes \mathbf{1} + P_1 \otimes U = \begin{pmatrix} \mathbf{1} & \mathbf{0} \\ \mathbf{0} & U \end{pmatrix} = \begin{pmatrix} 1 & 0 & 0 & 0 \\ 0 & 1 & 0 & 0 \\ 0 & 0 & u_{11} & u_{12} \\ 0 & 0 & u_{21} & u_{22} \end{pmatrix}, \quad (25)$$

with CU acting on a two qubit system as

- $CU |00\rangle = (\mathbf{1} \otimes \mathbf{1})(|0\rangle \otimes |0\rangle) = \mathbf{1}|0\rangle \otimes \mathbf{1}|0\rangle = |0\rangle \otimes |0\rangle = |00\rangle$
- $CU |01\rangle = (\mathbf{1} \otimes \mathbf{1})(|0\rangle \otimes |1\rangle) = \mathbf{1}|0\rangle \otimes \mathbf{1}|1\rangle = |0\rangle \otimes |1\rangle = |01\rangle$
- $CU |10\rangle = (\mathbf{1} \otimes \mathbf{U})(|1\rangle \otimes |0\rangle) = \mathbf{1}|1\rangle \otimes U|0\rangle = |1\rangle \otimes U|0\rangle$
- $CU |11\rangle = (\mathbf{1} \otimes \mathbf{U})(|1\rangle \otimes |1\rangle) = \mathbf{1}|1\rangle \otimes U|1\rangle = |1\rangle \otimes U|1\rangle$

representing an if-else statement, operating on the target qubits by checking the control qubits.

The most notable control gate is the Controlled-Not

$$CNOT = CN = CX = P_0 \otimes \mathbf{1} + P_1 \otimes X = \begin{pmatrix} 1 & 0 & 0 & 0 \\ 0 & 1 & 0 & 0 \\ 0 & 0 & 0 & 1 \\ 0 & 0 & 1 & 0 \end{pmatrix}, \quad (26)$$

with CX acting on a two qubit system as

- $CX |00\rangle = \mathbf{1} \otimes \mathbf{1} |00\rangle = |00\rangle$

- $CX |01\rangle = \mathbf{1} \otimes \mathbf{1} |01\rangle = |01\rangle$
- $CX |10\rangle = \mathbf{1} \otimes X |10\rangle = |11\rangle$
- $CX |11\rangle = \mathbf{1} \otimes X |11\rangle = |10\rangle$

Another interesting multi qubit gate that does not belong to the control gates is the swap gate which, as the name suggests, it swaps the terms it acts on. It's defined as

$$SWAP = S = \begin{pmatrix} 1 & 0 & 0 & 0 \\ 0 & 0 & 1 & 0 \\ 0 & 1 & 0 & 0 \\ 0 & 0 & 0 & 1 \end{pmatrix}, \quad (27)$$

with S acting on a two qubit system as

- $S|00\rangle = |00\rangle$
- $S|01\rangle = |10\rangle$
- $S|10\rangle = |01\rangle$
- $S|11\rangle = |11\rangle$

Suppose we need to find the matrix of some arbitrary operator U with the following actions

- $|u_{00}\rangle = U |00\rangle$
- $|u_{01}\rangle = U |01\rangle$
- $|u_{10}\rangle = U |10\rangle$
- $|u_{11}\rangle = U |11\rangle$

The matrix elements of an arbitrary operator U , acting on some given basis, are extracted by the inner product of the different basis states combinations, with the operating element

acting in between. To distinguish the abstract operator U from its matrix representation, we should name the matrix representation as something different e.g., P_U , but for simplicity we're going to use the same symbol for both, so

$$U = \begin{pmatrix} \langle 00|U|00\rangle & \langle 00|U|01\rangle & \langle 00|U|10\rangle & \langle 00|U|11\rangle \\ \langle 01|U|00\rangle & \langle 01|U|01\rangle & \langle 01|U|10\rangle & \langle 01|U|11\rangle \\ \langle 10|U|00\rangle & \langle 10|U|01\rangle & \langle 10|U|10\rangle & \langle 10|U|11\rangle \\ \langle 11|U|00\rangle & \langle 11|U|01\rangle & \langle 11|U|10\rangle & \langle 11|U|11\rangle \end{pmatrix} = \begin{pmatrix} \langle 00|u_{00}\rangle & \langle 00|u_{01}\rangle & \langle 00|u_{10}\rangle & \langle 00|u_{11}\rangle \\ \langle 01|u_{00}\rangle & \langle 01|u_{01}\rangle & \langle 01|u_{10}\rangle & \langle 01|u_{11}\rangle \\ \langle 10|u_{00}\rangle & \langle 10|u_{01}\rangle & \langle 10|u_{10}\rangle & \langle 10|u_{11}\rangle \\ \langle 11|u_{00}\rangle & \langle 11|u_{01}\rangle & \langle 11|u_{10}\rangle & \langle 11|u_{11}\rangle \end{pmatrix}. \quad (28)$$

E.g., suppose $U = CX$ so

- $|u_{00}\rangle = U|00\rangle = |00\rangle$
- $|u_{01}\rangle = U|01\rangle = |01\rangle$
- $|u_{10}\rangle = U|10\rangle = |11\rangle$
- $|u_{11}\rangle = U|11\rangle = |10\rangle$

Then eq. (28) becomes

$$\begin{pmatrix} \langle 00|00\rangle & \langle 00|01\rangle & \langle 00|11\rangle & \langle 00|10\rangle \\ \langle 01|00\rangle & \langle 01|01\rangle & \langle 01|11\rangle & \langle 01|10\rangle \\ \langle 10|00\rangle & \langle 10|01\rangle & \langle 10|11\rangle & \langle 10|10\rangle \\ \langle 11|00\rangle & \langle 11|01\rangle & \langle 11|11\rangle & \langle 11|10\rangle \end{pmatrix} = \begin{pmatrix} 1 & 0 & 0 & 0 \\ 0 & 1 & 0 & 0 \\ 0 & 0 & 0 & 1 \\ 0 & 0 & 1 & 0 \end{pmatrix} = CX. \quad (29)$$

The same applies for any other linear operator [18].

1.2.3 Entanglement

Quantum entanglement is a physical resource, like energy, associated with the peculiar non-classical correlations that are possible between separated quantum systems. Entanglement can be measured, transformed, and purified. A pair of quantum systems in an entangled state can be used as a quantum information channel to perform computational and cryptographic tasks that are impossible for classical systems. The general study of the information-processing capabilities of quantum systems is the subject of quantum information theory.

The most known entangled states are the bell states. The general bell equation is

$$|\beta_{xy}\rangle = \frac{|0,y\rangle + (-1)^x |1,\bar{y}\rangle}{\sqrt{2}}, \quad (30)$$

where $x, y \in \{0, 1\}$ and \bar{y} is the negation of y [17].

eq. (30) gives the four bell states

$$\begin{aligned} |\beta_{00}\rangle &= \frac{|00\rangle + |11\rangle}{\sqrt{2}} = |\Phi_+\rangle, \\ |\beta_{01}\rangle &= \frac{|01\rangle + |10\rangle}{\sqrt{2}} = |\Psi_+\rangle, \\ |\beta_{10}\rangle &= \frac{|00\rangle - |11\rangle}{\sqrt{2}} = |\Phi_-\rangle, \\ |\beta_{11}\rangle &= \frac{|01\rangle - |10\rangle}{\sqrt{2}} = |\Psi_-\rangle. \end{aligned} \quad (31)$$

1.2.4 Trace – Partial Trace

Suppose a matrix

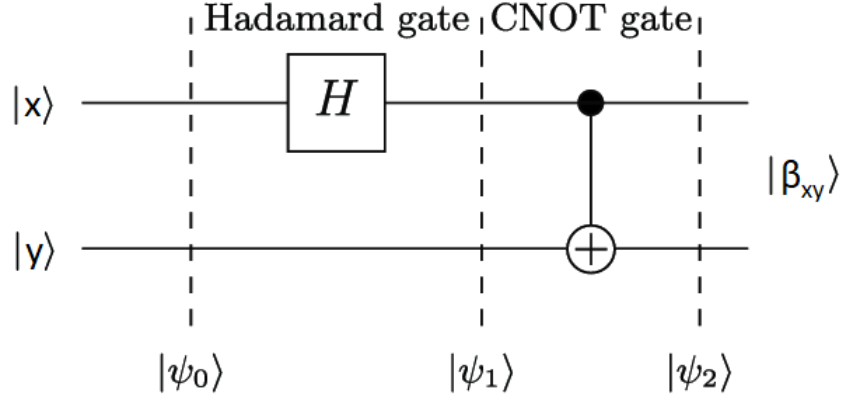


Figure 1: The circuit that achieves the bell states is composed of a Hadamard and a CX gate. With an initial state $|\psi_0\rangle = |x\rangle + |y\rangle$, where $|x\rangle = x_1|0\rangle + x_2|1\rangle$ and $|y\rangle = y_0|0\rangle + y_1|1\rangle$, the Hadamard gate sets the first input qubit in a superposition giving $|\psi_1\rangle = H|x\rangle + |y\rangle = (\frac{x_0}{\sqrt{2}}|0\rangle + \frac{x_1}{\sqrt{2}}|1\rangle) + |y\rangle$, and then the CX gate disperses that superposition on the rest of the circuit giving eq. (30).

$$A = \begin{pmatrix} a & b \\ c & d \end{pmatrix}, \quad (32)$$

the trace of this operator is the sum of its diagonal elements

$$Tr(A) = a + d. \quad (33)$$

This stands for any array of dimensions $n \times n$.

Now, consider two square matrices X, Y with H_X and H_Y , respectively. The partial trace on the space H_X is defined as

$$Tr_X(X \otimes Y) = Tr(X)Y, \quad (34)$$

and the partial trace on the space H_Y is defined as

$$Tr_Y(X \otimes Y) = Tr(Y)X. \quad (35)$$

In general,

$$\text{Tr}_k(X_1 \otimes X_2 \otimes \cdots \otimes X_n) = \text{Tr}(X_k)(X_1 \otimes \cdots \otimes X_{k-1} \otimes X_{k+1} \otimes \cdots \otimes X_n). \quad (36)$$

1.2.5 Density Matrix – Operator

When we are dealing with a multiple number of qubits, called an ensemble, we have to be able to split our system, and we can do this with some kind of averaging operator. The Density operator does that work by holding all the probabilities of each qubit state to appear.

Three key properties that classify an arbitrary matrix ρ as a density matrix are

- $\rho\rho^\dagger = \rho^\dagger\rho = \mathbf{1}$
- $\langle\phi|\rho|\phi\rangle \geq 0$, ϕ some arbitrary matrix
- $\text{Tr}(\rho) = 1$

The density operator for a mixed state E_ϕ is represented as

$$\rho = \sum_{i=1} p_i |\phi_i\rangle \langle\phi_i|. \quad (37)$$

1.2.6 Reduced Density Matrix

We can remove components of a system by tracing upon specific elements. What we get is a *reduced density matrix*.

We will describe how we can calculate this very important function, which describes one of the two qubits, using the partial trace given the general density operator of a

bipartite system [18]. Suppose a bipartite density matrix

$$\rho_{AB} = \sum_{ijkl} \rho_{ijkl} |i\rangle \langle j| \otimes |k\rangle \langle l| = \begin{pmatrix} \rho_{0000} & \rho_{0001} & \rho_{0100} & \rho_{0101} \\ \rho_{0010} & \rho_{0011} & \rho_{0110} & \rho_{0111} \\ \rho_{1000} & \rho_{1001} & \rho_{1100} & \rho_{1101} \\ \rho_{1010} & \rho_{1011} & \rho_{1110} & \rho_{1111} \end{pmatrix}, \quad (38)$$

by grouping the above 4×4 matrix in four 2×2 matrices, we rewrite eq. (38) as

$$\rho_{AB} = \begin{pmatrix} \rho'_{00} & \rho'_{01} \\ \rho'_{10} & \rho'_{11} \end{pmatrix}, \quad \rho'_{kl} = \begin{pmatrix} \rho_{kl00} & \rho_{kl01} \\ \rho_{kl10} & \rho_{kl11} \end{pmatrix}. \quad (39)$$

We find that the reduced density operator ρ_A describes the first quantum system by tracing out the second density operator ρ_B as

$$\begin{aligned} \rho_A &= \sum_{ijkl} Tr_B(\rho_{ijkl} |i\rangle \langle j| \otimes |k\rangle \langle l|) \\ &= \sum_{ijkl} \rho_{ijkl} |i\rangle \langle j| \otimes Tr(|k\rangle \langle l|). \end{aligned} \quad (40)$$

From the identity

$$Tr(|k\rangle \langle l|) = \delta_{kl}, \quad (41)$$

eq. (40) becomes

$$\begin{aligned} \rho_A &= \sum_{ijk} \rho_{ijkk} |i\rangle \langle j| \\ &= \begin{pmatrix} \rho_{0000} + \rho_{0011} & \rho_{0100} + \rho_{0111} \\ \rho_{1000} + \rho_{1011} & \rho_{1100} + \rho_{1111} \end{pmatrix} \\ &= \begin{pmatrix} Tr(\rho'_{00}) & Tr(\rho'_{01}) \\ Tr(\rho'_{10}) & Tr(\rho'_{11}) \end{pmatrix}. \end{aligned} \quad (42)$$

Similarly

$$\begin{aligned}
\rho_B &= \sum_{ijkl} Tr_A(\rho_{ijkl} |i\rangle \langle j| \otimes |k\rangle \langle l|) \\
&= \rho_{ijkl} Tr(|i\rangle \langle j|) \otimes |k\rangle \langle l| \\
&= \sum_P ijk \rho_{iikl} |k\rangle \langle l| \\
&= \begin{pmatrix} \rho_{0000} + \rho_{1100} & \rho_{0001} + \rho_{1101} \\ \rho_{0010} + \rho_{1110} & \rho_{0011} + \rho_{1111} \end{pmatrix} \\
&= \rho'_{00} + \rho'_{11}. \tag{43}
\end{aligned}$$

1.2.7 Super-operator – CPTP Maps

As super-operator (\mathcal{E}) we name an operator which acts on a system's density matrix ρ with the action noted as

$$\rho \xrightarrow{\mathcal{E}} \mathcal{E}(\rho). \tag{44}$$

A super-operator must satisfy

$$\mathcal{E}\left(\sum_i \alpha_i \rho_i\right) = \sum_i \alpha_i \mathcal{E}(\rho_i), \tag{45}$$

and

$$0 \leq Tr(\mathcal{E}(\rho)) \leq 1. \tag{46}$$

We characterize a super-operator as completely positive trace preserving (CPTP) when

$$\forall \rho > 0 \implies \mathcal{E}(\rho) > 0, \tag{47}$$

and

$$Tr(\mathcal{E}(\rho)) = Tr(\rho). \tag{48}$$

If in addition to the properties

$$\text{Tr}(\mathcal{E}(\rho)) = \text{Tr}(\rho) = 1, \quad (49)$$

and

$$\mathcal{E}\left(\sum_i p_i \rho_i\right) = \sum_i p_i \mathcal{E}(\rho_i), \quad (50)$$

\mathcal{E} has also the property of complete positivity (CP), we can say that the super-operator can be represented in the form of

$$\mathcal{E}(\rho) = \sum_k A_k \rho A_k^\dagger, \quad (51)$$

with A_i and A_i^\dagger being a set of so-called Kraus generators which by themselves can represent the abstract map (\mathcal{E}) if at least

$$\sum_k A_k A_k^\dagger = \mathbf{1}, \quad (52)$$

or

$$\sum_k A_k^\dagger A_k = \mathbf{1}. \quad (53)$$

apply. A second way to represent the abstract map will be presented in eq. (72) [17], [18].

1.2.8 Quantum Measurement

Quantum measurements are described by a collection of *measurement operators*

$$P_m = |m\rangle \langle m|, \quad P_m = P_m^\dagger = P_m^2. \quad (54)$$

These are operators acting on the state space of the system being measured. If the state of the quantum system is $|\psi\rangle$, immediately before the measurement, then the

probability that the result m will occur is given by

$$p(m) = \langle \psi | P_m^\dagger P_m | \psi \rangle. \quad (55)$$

The measurement operators satisfy the *completeness equation*

$$\sum_m P_m = \sum_m P_m^\dagger P_m = \sum_m P_m^2 = 1. \quad (56)$$

From eq. (55) and eq. (56), we have the completeness equation expressing the fact that probabilities sum to one

$$\sum_m p(m) = \sum_m \langle \psi | P_m^\dagger P_m | \psi \rangle = 1. \quad (57)$$

A simple, but important example of a measurement is the *measurement of a qubit in the computational basis*. This is a measurement on a single qubit with two outcomes defined by two measurement operators. For the outcome $|0\rangle$, we have the operator

$$P_0 = |0\rangle \langle 0| = \begin{pmatrix} 1 \\ 0 \end{pmatrix} \begin{pmatrix} 1 & 0 \end{pmatrix} = \begin{pmatrix} 1 & 0 \\ 0 & 0 \end{pmatrix}, \quad (58)$$

and respectively for the outcome $|1\rangle$

$$P_1 = |1\rangle \langle 1| = \begin{pmatrix} 0 \\ 1 \end{pmatrix} \begin{pmatrix} 0 & 1 \end{pmatrix} = \begin{pmatrix} 0 & 0 \\ 0 & 1 \end{pmatrix}. \quad (59)$$

Suppose the state being measured is $|\psi\rangle = \alpha|0\rangle + \beta|1\rangle$. Then the probability of obtaining measurement outcome $|0\rangle$ is

$$p(0) = \langle \psi | P_0^\dagger P_0 | \psi \rangle = \langle P_0 | \psi \rangle = |\alpha|^2. \quad (60)$$

and respectively for $|1\rangle$

$$p(1) = \langle \psi | P_1^\dagger P_1 | \psi \rangle = \langle P_1 | \psi \rangle = |\beta|^2. \quad (61)$$

1.3 General Statistics

1.3.1 Random Variables

A random variable is a variable whose possible values are numerical outcomes of a random phenomenon. There are two types of random variables, discrete and continuous, but we will focus mostly on the discrete type.

A dichotomous random variable is a variable that has two outcome levels. A common example of a dichotomous variable is the tossing of a coin, which results in either of two possible outcomes, heads, or tails.

1.3.2 Probability Density Function

In probability theory, a probability density function (PDF), or density of a continuous random variable, is a function that describes the relative likelihood for this random variable to take on a given value and is defined by

$$P(\alpha \leq X \leq \beta) = \int_b^\alpha f(x) dx. \quad (62)$$

1.3.3 Mean, Mode, Median

Mean (μ), median, and mode are different measures of centre in a numerical data set. They each try to summarize a dataset with a single number to represent a typical data point from the dataset.

The mean is the average number, found by dividing the sum of numbers in a set by

the multitude of this set

$$\mu = \frac{1}{N} \sum_{i=1}^N x_i. \quad (63)$$

The median is the middle number, found by ordering all data points and picking out the one in the middle, if there are two middle numbers, taking the mean of those two numbers.

The mode is the most frequent number.

1.3.4 Variance

The variance (σ^2), is a measure of variability. It is calculated by

$$\sigma^2 = \frac{1}{N} \sum_{i=1}^N (x_i - \mu)^2. \quad (64)$$

Variance, tells us the degree of spread in a data set. The more spread the data is, the larger the variance is in relation to the mean. Parametric statistical tests are sensitive to variance. Comparing the variance of samples helps you assess group differences. Variance is important to consider before performing parametric tests. These tests require equal or similar variances when comparing different samples.

1.3.5 Standard Deviation

The standard deviation (σ) is the square root of variance and tells us, on average, how far each value lies from the mean.

The formula for the standard deviation is

$$\sigma = \sqrt{\frac{1}{N} \sum_{i=1}^N (x_i - \mu)^2}, \quad (65)$$

where N is the count of the values in the set, x_i is each of the values in the set, and μ is the mean value of the given set.

A data-driven quality control method is derived from σ is called the ‘Six Sigma’. The name comes from the area under the normal distribution curve, after moving six standard deviations away from the centre. The chance of hitting a point outside the 6σ distance is 3.4 per million.

1.3.6 Inverse Participation Ratio

The inverse participation ratio (IPR) is a simple way to quantify how many states a particle is distributed over when there is some intrinsic uncertainty about the particle’s whereabouts, and is expressed as

$$\text{IPR} = \frac{1}{\sum_i p_i^2}, \quad (66)$$

where p_i is the probability that the particle is in the state i .

This sort of intrinsic uncertainty arises in quantum mechanics, since a particle can exist in a quantum superposition of states over many locations. Big values of IPR suggest distribution localization, while small IPR values suggest distribution delocalization.

Chapter 2

Classical Random Walk and Quantum Walk Theory

A Random Walk is considered an algorithm in which a mobile unit called the *walker* has a degree of movement freedom determined by a stochastic random variable called the *coin*. This scheme can take place in the continuous or discrete time domain. In this work, the walker has a one-dimensional degree of freedom and the coin is a dichotomic random variable.

The drunkards walk.

Imagine a man returning home from the pub after some pints. Though he might take an accidental right step twice, maybe thrice, statistics tells us he will end up in a straight line from where he started. We will examine the variance of his position corresponding to the number of his steps.

2.1 Classical Random Walk

In classical computational systems, we call this algorithm a Classical Random Walk visualized as the moving of the walker to the left or the right depending on the random outcome of a coin toss. Below, we describe the mathematics of the CRW algorithm.

2.1.1 On Integers

The CRW consists of two interacting systems, the coin system, represented by the density matrix ρ_c which lives in the Hilbert space

$$H_c = \text{span}\{|0\rangle = \text{heads}, |1\rangle = \text{tails}\}, \quad (67)$$

and the walker system, represented by the density matrix ρ_w and lives in the Hilbert space

$$H_w = \text{span}\{|k\rangle\}_{k \in \mathbb{Z}}. \quad (68)$$

The total CRW space is $H_c \otimes H_w$ and is represented by the separable density matrix $\rho_c \otimes \rho_w$.

The relocation of the walker is decided by the toss of the coin. If the coin shows heads, the walker moves to the left, and in our case the negative side of the walker dimension. Respectively, if the coin shows tails, the walker moves to the right, and in our case the positive side of the walker dimension. This movement is made possible by the operators $\{P_+, P_-\} \in \text{End}(H_c)$ which act on the coin system to provide the coin measurement, and the operators E_\pm, L with $\{E_\pm, L\} \in \text{End}(H_w)$, which act on the walker system in order to move the walker and are combined to the unitary operator

$$V_{cl} = P_+ \otimes E_+ + P_- \otimes E_-, \quad (69)$$

which evolves the CRW by acting on the total system as

$$\rho_c \otimes \rho_w \xrightarrow{\text{Ad}(V_{cl})} V_{cl} V_{cl} (\rho_c \otimes \rho_w) V_{cl}^\dagger, \quad (70)$$

so we call eq. (69) the *step operator* or the *evolution operator*. Because we are mostly interested in the walker system and because the action of the step operator couples the two systems, we must decouple them using the partial trace upon the coin system. One step of the CRW algorithm looks like this

$$\rho_c \otimes \rho_w \xrightarrow{\text{step operation}} V_{cl} (\rho_c \otimes \rho_w) V_{cl}^\dagger \xrightarrow{\text{decoupling}} \text{Tr}_c \left\{ V_{cl} (\rho_c \otimes \rho_w) V_{cl}^\dagger \right\}, \quad (71)$$

and can also be expressed in the form of a CTPT map as

$$\mathcal{E}_{V_{cl}}(\rho_w) = Tr_c \left\{ V_{cl}(\rho_c \otimes \rho_w) V_{cl}^\dagger \right\}. \quad (72)$$

For further steps, we simply act $\mathcal{E}_{V_{cl}}(\rho_w)$ in a consecutive manner, giving

$$\mathcal{E}_{V_{cl}}^n(\rho_w) = \mathcal{E}_{V_{cl}}(\rho_w^{n-1}) = Tr_c \left\{ V_{cl}(\rho_w \otimes \rho_w^{n-1}) V_{cl}^\dagger \right\}, \quad (73)$$

with n being the number of steps.

The diagonal elements of $\mathcal{E}_{V_{cl}}(\rho_w)$ give the occupation probability distribution of the CRW as

$$p_k = \langle k | \mathcal{E}_{V_{cl}}(\rho_w) | k \rangle, \quad (74)$$

which can be generalized to

$$P_k^{(n)} = \langle k | \mathcal{E}_{V_{cl}}^n(\rho_w) | k \rangle, \quad k = 0, \pm 1, \pm 2, \dots \quad (75)$$

with n being the number of steps and $|k\rangle$ being the eigenbasis of the position operator L .

2.1.2 Quantization

We are capable of changing the nature of the CRW so that it adapts to quantum characteristics. Such a transformation is called quantization and leads to the quantum counterpart of the CRW. The key concept of quantization holds the unitary operator U , namely the *reshuffling matrix*, which is infused in the evolution operator V_{cl} giving the transformation

$$V_{cl} \rightarrow V_q = (V_{cl} U \otimes \mathbf{1}), \quad (76)$$

with V_q being the new evolution operator, promoting quantum characteristics to the

walk. Obviously, $U \neq \mathbf{1}$ or else $V_q = V_{cl}$. Some viable reshuffling matrix examples are

$$U = \frac{1}{\sqrt{2}} \begin{pmatrix} 1 & 1 \\ -1 & 1 \end{pmatrix}, U = \frac{1}{\sqrt{2}} \begin{pmatrix} 1 & 1 \\ 1 & -1 \end{pmatrix}, U = \frac{1}{\sqrt{2}} \begin{pmatrix} 1 & i \\ i & 1 \end{pmatrix}.$$

From eq. (71) and eq. (76) we see the QW evolution operator is now

$$\mathcal{E}_{V_q}(\rho_w) = Tr_c \left\{ V_q (\rho_c \otimes \rho_w) V_q^\dagger \right\}. \quad (77)$$

We can obtain eq. (77) with multiple ways, we call quantization rules. Quantization rules are formulas that consist of the evolution of the system and the tracing-out of the walker. We will examine two evolution rules, each having two tracing schemes, giving a total of four quantization rules [12], [13], [15]. Let's examine the quantization rules a bit more thoroughly.

U quantization rule with the Original Tracing Scheme

This rule implies that the number of steps n , come along as an exponent of the evolution matrix V_q and we then apply an original partial tracing procedure, giving the walker density matrix

$$\rho_w^{(n)} = \mathcal{E}_{V_q^n}(\rho_w) = Tr_c \left\{ (V_q^n) (\rho_c \otimes \rho_w) (V_q^n)^\dagger \right\}. \quad (78)$$

We can easily see that $V_q = V_{cl}U \otimes \mathbf{1}$ acts on the first term of $\rho_c \otimes \rho_w$ leaving ρ_w intact, so the walker density matrix is explicitly rewritten as

$$\begin{aligned} \rho_w^{(n)} &= \mathcal{E}_{V_q^n}(\rho_w) = Tr_c \left\{ (V_q^n) (\rho_c \otimes \rho_w) (V_q^n)^\dagger \right\} \\ &= Tr_c \left\{ (V_{cl}U \otimes \mathbf{1})^n (\rho_c \otimes \rho_w) ((V_{cl}U \otimes \mathbf{1})^n)^\dagger \right\} \\ &= Tr_c \left\{ (V_{cl}U)^n \rho_c ((V_{cl}U)^n)^\dagger \otimes \rho_w \right\} \\ &= \rho_w Tr \left\{ Ad^n (V_{cl}U) \rho_c \right\}. \end{aligned} \quad (79)$$

U quantization rule and V^k model

This rule implies that the number of steps n , remain as an exponent on the walker density matrix ρ_w and now k is the size of the step. Finally, we apply the partial tracing procedure, giving the walker density matrix

$$\rho_w^{(n)} = \mathcal{E}_{V_q^k}(\rho_w^{(n-1)}) = Tr_c\{(V_q^k)(\rho_c \otimes \rho_w^{(n-1)})(V_q^k)^\dagger\}. \quad (80)$$

Again, $V_q = V_{cl}U \otimes \mathbf{1}$ acts on the first term of $\rho_c \otimes \rho_w$ leaving ρ_w intact, so the walker density matrix is explicitly rewritten as

$$\begin{aligned} \rho_w^{(n)} &= \mathcal{E}_{V_q^k}(\rho_w^{(n-1)}) = Tr_c\{(V_q^k)(\rho_c \otimes \rho_w^{(n-1)})(V_q^k)^\dagger\} \\ &= Tr_c\{(V_{cl}U \otimes \mathbf{1})^k(\rho_c \otimes \rho_w^{(n-1)})[(V_{cl}U \otimes \mathbf{1})^k]^\dagger\} \\ &= Tr_c\{(V_{cl}U \otimes \mathbf{1})^k \rho_c [(V_{cl}U \otimes \mathbf{1})^k]^\dagger \rho_w^{(n-1)}\} \\ &= \rho_w^{(n-1)} Tr\{Ad^k(V_{cl}U)\rho_c\}. \end{aligned} \quad (81)$$

\mathcal{E} quantization rule and Original Tracing Scheme

A generalized version of the U quantization rule is the \mathcal{E} quantization rule. The \mathcal{E} quantization rule employs a CPTP map \mathcal{E} , which acts on the coin density matrix. The density matrix ρ_c for each step n is found as

$$\begin{aligned} \rho_c \xrightarrow{\mathcal{E}} \mathcal{E}(\rho_c) &= S_1 \rho_c S_1^\dagger + \dots + S_n \rho_c S_n^\dagger \\ &= Ad(S_1)\rho_c + \dots + Ad(S_n)\rho_c \\ &= \sum_i Ad(S_i)\rho_c, \end{aligned} \quad (82)$$

where (S_1, \dots, S_n) are Kraus generators. Then we apply $Ad(V_{cl})$ on $\rho_c \otimes \rho_w$ and obtain the action

$$Ad(V_{cl})(\mathcal{E} \otimes \mathbf{1}), \quad (83)$$

on the combined system, giving the walker density matrix

$$\begin{aligned}
\rho_w^{(n)} &= \mathcal{E}_{V_q^n}(\rho_w) = Tr_c\{[V_{cl}(\mathcal{E} \otimes \mathbf{1})]^n(\rho_c \otimes \rho_w)[V_{cl}^\dagger]^n\} \\
&= Tr_c\{[V_{cl}(\sum_i Ad(S_i) \otimes \mathbf{1})]^n(\rho_c \otimes \rho_w)[V_{cl}^\dagger]^n\} \\
&= \rho_w Tr\{(V_{cl} \sum_i Ad(S_i))^n \rho_c [V_{cl}^\dagger]^n\} \\
&= \rho_w Tr\{\sum_i Ad^n(V_{cl} S_i) \rho_c\}.
\end{aligned} \tag{84}$$

\mathcal{E} quantization rule and V^k model

The density matrix of the n step for the walker is defined as

$$\begin{aligned}
\rho_w^{(n)} &= \mathcal{E}_{V_q^k}(\rho_w^{(n-1)}) \\
&= Tr_c\{V_{cl}(\mathcal{E}_k \otimes \mathbf{1}) \dots V_{cl}((\mathcal{E}_1 \otimes \mathbf{1})(\rho_c \otimes \rho_w^{(n-1)})V_{cl}^\dagger \dots V_{cl}^\dagger)\} \\
&= \rho_w^{(n-1)} Tr\{Ad(V_{cl}^k)(\mathcal{E}_k \dots \mathcal{E}_1(\rho_c))\},
\end{aligned} \tag{85}$$

with $\mathcal{E}_1, \dots, \mathcal{E}_k$ being different CPTP maps.

Quantization Rules Summarized

	Original Scheme	V^k model
U -rule	$\rho_w^{(n)} = \rho_w Tr\{Ad^n(V_{cl}U)(\rho_c)\}$	$\rho_w^{(n)} = \rho_w^{(n-1)} Tr\{Ad^k(V_{cl}U)(\rho_c)\}$
ε -rule	$\rho_w^{(n)} = \rho_w Tr\left\{\sum_i Ad^n(V_{cl}S_i)(\rho_c)\right\}$	$\rho_w^{(n)} = \rho_w^{(n-1)} Tr\{Ad^k(V_{cl}^k)(\varepsilon_k \dots \varepsilon_1(\rho_c))\}$

Figure 2: *Quantization Rules*

2.2 Quantum Walk

2.2.1 Introduction

Imagine you toss a coin, and it spins airborne, then you spin another coin, and another, and another, and they all spin simultaneously and eventually, they fuse in one super coin which can move the walker as many steps as the number of coins thrown.

The QW is the quantum analogue of the CRW. The term *random* may be relinquished as the randomness in QW arises through quantum superposition of states, non-random, reversible unitary evolution operators and collapse of the wave function due to state measurements.

The coin and walker live in their respective Hilbert spaces H_c and, H_w , such that the total Hilbert space of the QW is $H = H_c \otimes H_w$.

A basic and important application of the QW is in the quantum algorithms, offering new methods for their designing. A famous category of algorithms affected by QW is the search algorithms. In 1996 Lov Grover was the inventor of a very important quantum search algorithm, which increased the speed of searching in very difficult search problems. Grover's algorithm solves any search problem with N possible solutions in time $O(\sqrt{N})$ [7], [8], [13], [1], [2].

Because quantum rules apply in the QW, we use quantum coins, which for simplicity we will refer to them just as coins, and they can evolve the QW in a balanced manner.

A frequently used balanced unitary coin is the Hadamard coin H

$$H = \frac{1}{\sqrt{2}} \begin{pmatrix} 1 & 1 \\ 1 & -1 \end{pmatrix}. \quad (86)$$

We can prove that the Hadamard coin is balanced

$$\begin{aligned}
|0\rangle \otimes |0\rangle &\xrightarrow{H} \frac{1}{\sqrt{2}}(|0\rangle + |1\rangle) \otimes |0\rangle \\
&\xrightarrow{E} \frac{1}{\sqrt{2}}(|0\rangle \otimes |1\rangle + |1\rangle \otimes |-1\rangle),
\end{aligned} \tag{87}$$

where E_{\pm} is the step operator mentioned earlier.

Upon measuring the system state in the computational basis, we obtain each of $\{|0\rangle \otimes |1\rangle, |1\rangle \otimes |-1\rangle\}$ with equal probability $p_{\pm 1} = \frac{1}{2}$, with the right kets $(|1\rangle, |-1\rangle)$ representing walker positions on the X -axis [1], [19].

2.2.2 Density Matrix

By density matrix definition, we easily get the discrete time density matrix of the walker in the discrete basis $|k\rangle$ as

$$\rho_w = \sum_{k, k' \in \mathbb{Z}} \rho_{kk'} |k\rangle \langle k'|. \tag{88}$$

Now, let's find the general matrix describing the QW in the continuous base $|\phi\rangle$ where $\phi \in [0, 2\pi)$ representing some arbitrary angle, for which the three density matrix qualities must apply (viz. section 1.2.5).

From our experience, the respective continuous version of eq. (88) in the said basis, will be of the normalized form

$$\rho_w = \int_0^{2\pi} \int_0^{2\pi} \rho(\phi, \phi') |\phi\rangle \langle \phi'| \frac{d\phi d\phi'}{(2\pi)^2}. \tag{89}$$

We can combine eq. (88) with eq. (89) with the help of Fourier discrete-continuous

inter-transformation (appendix A.3)

$$\begin{aligned}
\rho_w &= \sum_{m,m' \in \mathbb{Z}} (\rho_w)_{mm'} |m\rangle \langle m'| \\
&= \sum_{m,m' \in \mathbb{Z}} (\rho_w)_{mm'} \left[\frac{1}{2\pi} \int_0^{2\pi} e^{im\phi} |\phi\rangle d\phi \right] \left[\frac{1}{2\pi} \int_0^{2\pi} e^{-im'\phi'} \langle \phi'| d\phi' \right] \\
&= \int_0^{2\pi} \int_0^{2\pi} \underbrace{\sum_{m,m' \in \mathbb{Z}} (\rho_w)_{mm'} e^{i(m\phi - m'\phi')} }_{\rho(\phi, \phi')} |\phi\rangle \langle \phi'| \frac{d\phi d\phi'}{(2\pi)^2}. \tag{90}
\end{aligned}$$

We have found now the function $\rho(\phi, \phi')$, which is the kernel of the ρ_w density matrix in the continuous basis. The first step of the walk means that we will apply the evolution operator \mathcal{E}_{V^2} (V^2 tracing scheme) to the density matrix ρ_w such that

$$\mathcal{E}_{V^2}(\rho_w) = \int_0^{2\pi} \int_0^{2\pi} \underbrace{\sum_{m,m' \in \mathbb{Z}} (\rho_w)_{mm'} e^{i(m\phi - m'\phi')} }_{\rho(\phi, \phi')} \mathcal{E}_{V^2}(|\phi\rangle \langle \phi'|) \frac{d\phi d\phi'}{(2\pi)^2}, \tag{91}$$

with

$$\begin{aligned}
\rho(\phi, \phi') &= \sum_{m,m' \in \mathbb{Z}} (\rho_w)_{mm'} e^{i(m\phi - m'\phi')} \\
&= \mathcal{F}[(\rho_w)_{mm'}], \tag{92}
\end{aligned}$$

being the Fourier transform of the density matrix elements. Therefore, to compute the action of $\mathcal{E}_{V^2}(\rho_w)$, we need to compute $\mathcal{E}_{V^2}(|\phi\rangle \langle \phi'|)$. The map \mathcal{E}_{V^2} is representing the \mathcal{E} quantization rule using the tracing scheme V^2 . The V^k QW model is described by the map

$$\mathcal{E}_{V^k}(\rho_w) = Tr_c \{ V_{cl}[\mathcal{E}_k \otimes \mathbf{1}] \dots [V_{cl}[\mathcal{E}_1 \otimes \mathbf{1}] (\rho_c \otimes \rho_w) V_{cl}^\dagger] \dots V_{cl}^\dagger \}. \tag{93}$$

The V^2 QW model is

$$\begin{aligned}
\mathcal{E}_{V^2}(\rho_w) &= Tr_c\{Ad(V_{cl}) \cdot (\mathcal{E}_\tau \otimes \mathbf{1})Ad(V_{cl}) \cdot (\mathcal{E}_t \otimes \mathbf{1}) \cdot (\rho_c \otimes \rho_w)\} \\
&= Tr_c\{Ad(V_{cl}) \cdot (\mathcal{E}_\tau \otimes \mathbf{1})Ad(V_{cl}) \cdot \mathcal{E}_t(\rho_c) \otimes \rho_w\} \\
&= Tr_c\{V_{cl}(\mathcal{E}_\tau \otimes \mathbf{1})[V_{cl} \cdot [\mathcal{E}_t(\rho_c) \otimes \rho_w]V_{cl}^\dagger]V_{cl}\}. \tag{94}
\end{aligned}$$

For $\rho_w = |\phi\rangle\langle\phi'|$, we have that

$$\begin{aligned}
\mathcal{E}_{V^2}(|\phi\rangle\langle\phi'|) &= Tr_c\{V_{cl}(\mathcal{E}_\tau \otimes \mathbf{1})[V_{cl}[\mathcal{E}_t(\rho_c) \otimes |\phi\rangle\langle\phi'|]V_{cl}^\dagger]V_{cl}^\dagger\} \\
&= |\phi\rangle\langle\phi'| Tr\{V_{cl}\mathcal{E}_\tau[V_{cl}[\mathcal{E}_t(\rho_c)]]V_{cl}^\dagger\}V_{cl}^\dagger \\
&= |\phi\rangle\langle\phi'| Tr\{Ad^2(V_{cl})(\mathcal{E}_{\tau+t}(\rho_c))\}. \tag{95}
\end{aligned}$$

Thus, $\mathcal{E}_{V^2}(\rho_w)$ is described as

$$\mathcal{E}_{V^2}(\rho_w) = \int_0^{2\pi} \int_0^{2\pi} \mathcal{F}[(\rho_w)mm'] Tr\{Ad^2(V_{cl})(\mathcal{E}_{\tau+t}(\rho_c))\} |\phi\rangle\langle\phi'| \frac{d\phi d\phi'}{(2\pi)^2}. \tag{96}$$

2.2.3 Asymptotics and the Double Horn Distribution

Investigating the density matrix, we will analyse and construct the characteristic asymptotic PDF of the QW bearing the distinct double horn shape.

Initially, at time $t = 0$, the walker density (matriceq. (89)) becomes

$$\rho_w^{(0)}(\phi, \phi') = 1. \tag{97}$$

We assume the coin is initialized as a pure state with density matrix $\rho_c = |c\rangle\langle c|$, $|c\rangle = \cos x|+\rangle + i \sin x|-\rangle$. Our system runs with the V_q^k tracing scheme evolving the walker

density matrix as

$$\begin{aligned}
|\phi\rangle\langle\phi'| &\xrightarrow{\mathcal{E}} \mathcal{E}_{V_q^k}(|\phi\rangle\langle\phi'|) = \text{Tr}_c\{(V_q^k)(\rho_c \otimes |\phi\rangle\langle\phi'|)(V_q^k)^\dagger\} \\
&= A_+(k, \Phi; c) |\phi\rangle\langle\phi'| A_+(k, \Phi; c)^\dagger \\
&\quad + A_-(k, \Phi; c) |\phi\rangle\langle\phi'| A_-(k, \Phi; c)^\dagger \\
&= (A_+(k, \phi; c) A_+(k, \phi'; c)^* \\
&\quad + A_-(k, \phi; c) A_-(k, \phi'; c)^*) |\phi\rangle\langle\phi'| \\
&= A(k, \phi, \phi'; c) |\phi\rangle\langle\phi'|, \tag{98}
\end{aligned}$$

with

$$A_\pm(k, \Phi; c) = \langle \pm | V^k(\Phi) | c \rangle, \tag{99}$$

being Kraus generators. For the n -th step, we simply obtain

$$\mathcal{E}_{V_q^k}^n(|\phi\rangle\langle\phi'|) = A(k, \phi, \phi'; c)^n |\phi\rangle\langle\phi'|, \tag{100}$$

where $A(k, \phi, \phi'; c)$ is called the *characteristic function* of the QW. From eq. (89) and eq. (100) we resolve the final walker density matrix

$$\begin{aligned}
\mathcal{E}_{V_q^k}^n(\rho_w) &= \mathcal{E}_{V_q^k}^{(n-1)} \left(\sum_{i=\pm} A_i(k, \Phi; c) \rho_w A_i(k, \Phi; c)^\dagger \right) \\
&= \int_0^{2\pi} \int_0^{2\pi} \rho(\phi, \phi') A(k, \phi, \phi'; c)^n |\phi\rangle\langle\phi'| d\phi d\phi'. \tag{101}
\end{aligned}$$

Using the evolution operator for n number of steps, the position operator L has a

quantum moment of

$$\begin{aligned}
\langle L^s \rangle_n &= Tr\{L^s \mathcal{E}_{V_q^n}(\rho_w)\} \\
&= \frac{1}{2\pi i^s} \int_0^{2\pi} d\phi \theta_\phi^s [\rho(\phi, \phi') A^n(k, \phi, \phi'; c)]_{\phi'=\phi} \\
&= \sum_{k \in \mathbb{Z}} k^s P_k^{(n)} \equiv \langle k^s \rangle_n,
\end{aligned} \tag{102}$$

with

$$P_k^{(n)} = \langle k | \mathcal{E}_{V_q^n}(\rho_w) | k \rangle, \tag{103}$$

being the probability distribution for the walker to be in position k after n number of steps, and $\langle k^s \rangle_n$ are the statistical moments of the walker's position. For large n , eq. (102) behaves as

$$\langle L^s \rangle_n = \langle n^s \rangle_n = \frac{n^s}{2\pi i^s} \int_0^{2\pi} h(2\phi; t) d\phi \left[\rho(\phi, \phi') \left(\frac{\theta}{\theta\phi} A(k, \phi, \phi'; c) \right)^s \right]_{\phi'=\phi} + O(n^{s-1}). \tag{104}$$

From eq. (104) we observe that $\frac{m}{n}$ converges weakly to

$$h(\phi; k, c) = -i \left[\frac{\theta}{\theta\phi} A(k, \phi, \phi'; c) \right]_{\phi=\phi'}, \tag{105}$$

with ϕ being a random variable with probability $p_\phi = \frac{\rho(\phi, \phi)}{2\pi}$. A closer approach of eq. (105) to our study is

$$h(\phi; k, c) = Tr\{(\sigma + V(\phi)^\dagger \sigma V(\phi) + \dots + V(\phi)^\dagger (k-1) \sigma V(\phi)^{(k-1)}) \rho_c\}, \tag{106}$$

with $\sigma := U_0^\dagger \sigma_3 U_0$.

In order to find the asymptotic pdf of the QW we will make use of the dual map

$$\mathcal{E}_{V_q^n}^* : B(H_w) \longrightarrow B(H_w), \tag{107}$$

defined on the set of bounded operators acting on the walker Hilbert space H_w of some given CPTP map

$$\mathcal{E}_{V_q^k} : D(H_w) \longrightarrow D(H_w), \quad (108)$$

operating on the density matrices $\rho_w \in D(H_w)$, with operator sum realization

$$\mathcal{E}_{V_q^k}(\rho_w) = \sum_{i=\pm} A_i(k, \Phi; c) \rho_w A_i(k, \Phi; c)^\dagger. \quad (109)$$

This dual map is defined to act on bounded operators $X \in B(H_w)$, as

$$\mathcal{E}_{V_q^k}^*(X) = \sum_{i=\pm} A_i(k, \Phi; c)^\dagger X A_i(k, \Phi; c). \quad (110)$$

After n number of steps, the walker density matrix is

$$\rho_w^{(n)} = \mathcal{E}_{V_q^k}^n(\rho_w), \quad (111)$$

and the scaled quantum moments of the position operator are found to be

$$\left\langle \left(\frac{L}{n} \right)^s \right\rangle_n = Tr \left\{ \rho_w^{(n)} \left(\frac{L}{n} \right)^s \right\}, \quad (112)$$

or

$$\left\langle \left(\frac{L}{n} \right)^s \right\rangle_n \equiv \left\langle \mathcal{E}_{V_q^k}^{*n} \left(\frac{L}{n} \right)^s \right\rangle_0 = Tr \left\{ \rho_w \mathcal{E}_{V_q^k}^{*n} \left(\frac{L}{n} \right)^s \right\}, \quad (113)$$

if we apply the dual map eq. (110).

For the V_q^2 tracing scheme with the initial states defined earlier,

the limit PDF is

$$\lim_{n \rightarrow \infty} \left\langle \mathcal{E}_{V_q^2}^{*n} \left(\frac{L}{n} \right)^s \right\rangle_0 = \int_0^{2\pi} h(\phi)^s \frac{d\phi}{2\pi} = \int_{-1}^1 \frac{y^s}{\pi \sqrt{1-y^2}} dy. \quad (114)$$

The final term of eq. (114) seems like a scaled version of the general double horn

(fig. 3) formula

$$P(y) = \frac{1}{\pi\sqrt{1-y^2}}, \quad -1 \leq y \leq 1, \quad (115)$$

with the scale factor being the random variable y^s .

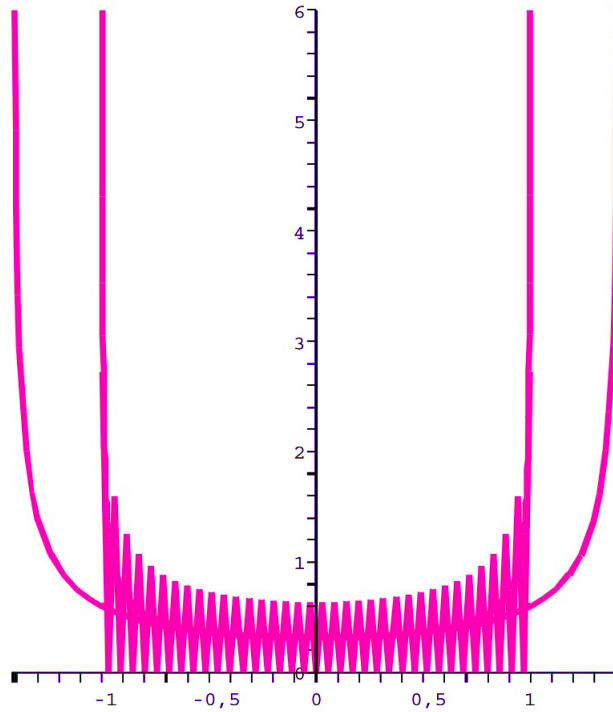


Figure 3: Occupation values vs normalized walker positions for a number of steps $n = 36$, showing the double horn asymptotic, characteristic of the QW.

Chapter 3

Quantum – Classical Transitions

From the previous chapter, we saw how a QW evolution operator is made by the incorporation of an appropriate reshuffling matrix U to the CRW evolution operator giving

$$\begin{aligned} V_q &= V_{cl}U \otimes \mathbf{1} \\ &= P_+U \otimes E_+ + P_-U \otimes E_-. \end{aligned} \tag{116}$$

In fig. 4, we see the typical CRW behaviour which yields a spread of $\sigma = O(\sqrt{n})$ and the typical QW behaviour which yields a spread of $\sigma = O(n)$, both which occur, in a way, independently of one another. For a given walk, from an initially ballistic motion (quantum behaviour), we will approach a diffusive motion (classical behaviour) as time passes. As a motivation to find ways to interpolate between these two marginal behaviours, we construct a novel reshuffling matrix by introducing a concept of physical noise in our quantum systems, and experimenting with different noise strength values, we will observe fluctuations at the rate of this behaviour traversal, explaining the title of this work. We will work with two mathematical models, the discrete time model named the ε -model and the continuous time model named the χ -model, although very different from each other, manipulated in the right way, we will arrive at these said transitions and in fact, for the same reasons.

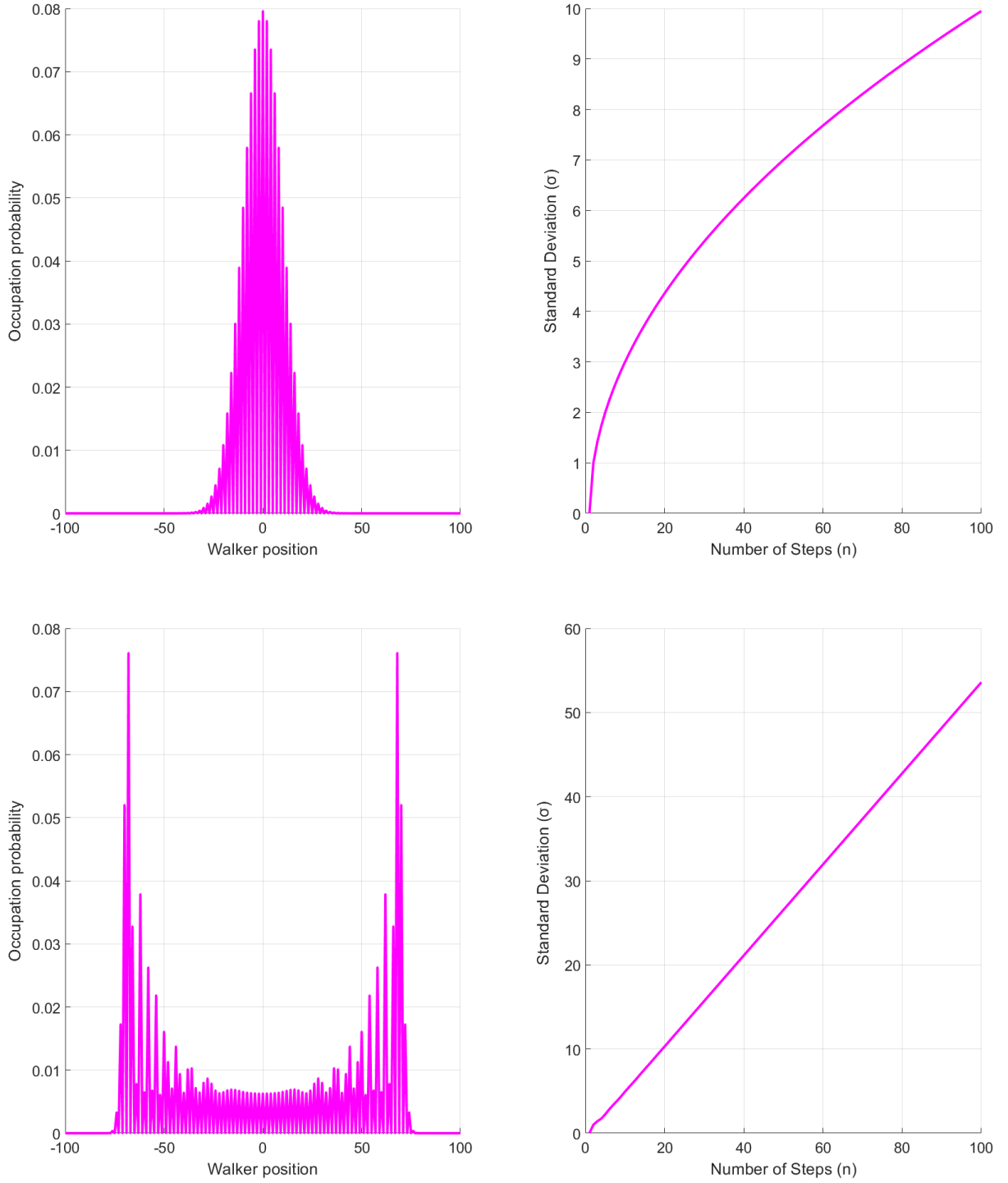


Figure 4: **Left:** Occupation probabilities for every position the walker occupies vs the number of steps, n , executed from the initial walker position $X = 0$. **Right:** Standard deviation vs number of steps, n , of the walk on the left. **Top:** Typical CRW algorithm run with the evolution operator V_{cl} ($U = \mathbf{1}$). **Bottom:** Typical QW algorithm run with the evolution operator in eq. (116) with $U = \frac{1}{\sqrt{2}} \begin{pmatrix} 1 & 1 \\ -1 & 1 \end{pmatrix}$.

3.1 The ε -Model

Let's introduce the classical noise parameter, represented as $\varepsilon \in [0, 1]$, considered to be a measure of randomness strength, something which entangles our system with the outside world annihilating quantum coherence, and an equally distributed dichotomic random variable $s \in \{\pm 1\}$ which yields an extra stochastic dimension to work with later [20]. We infuse those variables to the off-diagonal elements of the QW reshuffling matrix as

$$U(s; \varepsilon) = \mathcal{N} \begin{pmatrix} 1 & s\varepsilon \\ -s\varepsilon & 1 \end{pmatrix}, \quad \mathcal{N} \equiv \frac{1}{\sqrt{1 + \varepsilon^2}}. \quad (117)$$

The newly introduced variables ε and s are such that they retain the unitarity of the reshuffling matrix, so

$$U(s; \varepsilon)U(s; \varepsilon)^* = U(s; \varepsilon)^*U(s; \varepsilon) = \mathbf{1}. \quad (118)$$

Our new QW evolution operator is now explicitly written as

$$V_q(s; \varepsilon) = P_+U(s; \varepsilon) \otimes E_+ + P_-U(s; \varepsilon) \otimes E_-. \quad (119)$$

We begin our experimentation of this novel reshuffling matrix by applying the two extreme ε values, starting with $\varepsilon = 0$,

$$\begin{aligned} U(s; 0) &= \frac{1}{\sqrt{1+0}} \begin{pmatrix} 1 & 0 \\ 0 & 1 \end{pmatrix} \\ &= \begin{pmatrix} 1 & 0 \\ 0 & 1 \end{pmatrix} = \mathbf{1} = U(\pm 1; 0), \end{aligned} \quad (120)$$

$U(\pm 1; 0)$ becomes the identity matrix, so eq. (116) returns to its original V_{cl} form, without portraying any novel quantum behaviours.

For $\varepsilon = 1$,

$$\begin{aligned} U(s;1) &= \frac{1}{\sqrt{1+1}} \begin{pmatrix} 1 & s \\ -s & 1 \end{pmatrix} \\ &= \frac{1}{\sqrt{2}} \begin{pmatrix} 1 & s \\ -s & 1 \end{pmatrix} \Rightarrow \end{aligned} \quad (121)$$

$$U(\pm 1;1) = \frac{1}{\sqrt{2}} \begin{pmatrix} 1 & \pm 1 \\ \mp 1 & 1 \end{pmatrix}, \quad (122)$$

$U(\pm 1;1)$ becomes a non-diagonal matrix, something that promotes quantum characteristics in eq. (116).

For which ε does the unitary $U(s;\varepsilon) = \frac{1}{\sqrt{1-\varepsilon^2}} \begin{pmatrix} 1 & s\varepsilon \\ -s\varepsilon & 1 \end{pmatrix}$ spreads the walk faster?

We expect a non-diagonal reshuffling matrix to give a faster walk diffusion than its diagonal counterpart. We shall analyse in detail this query soon.

For now, let's observe how the QW behaves for various noise strength values. We begin by plotting the QW introducing the two extreme values $\varepsilon \in \{0, 1\}$ and we set $s = 1$.

In the top left plot of fig. 5, we see for the initial position of the QW (#steps = 0), there is a definite chance that the walker stands in the initial position $X = 0$, trivial. For the rest of the walk, the possible walker positions increase, anti-diametrically, one by one, with the number of steps moved, with an equal probability amplitude of $p_{\pm} = \frac{1}{2}$. The linearity of σ in the top right plot of fig. 5 also attests this behaviour. It's worth noticing that the σ lines for every different case, thus, colours, extend up to their respective number of steps.

What we find in the bottom left plot of fig. 5 is a more complex position occupancy. The distribution turns to a double-horn, which widens as the number of steps increases. Note how the values of the Y -axis in the bottom plots of fig. 5 dropped compared to those on top. So far, we encountered the unexpected! For a more off-diagonalized reshuffling matrix, that is for a bigger ε , we observe a slower diffusion. The terms 'matrix diagonality'

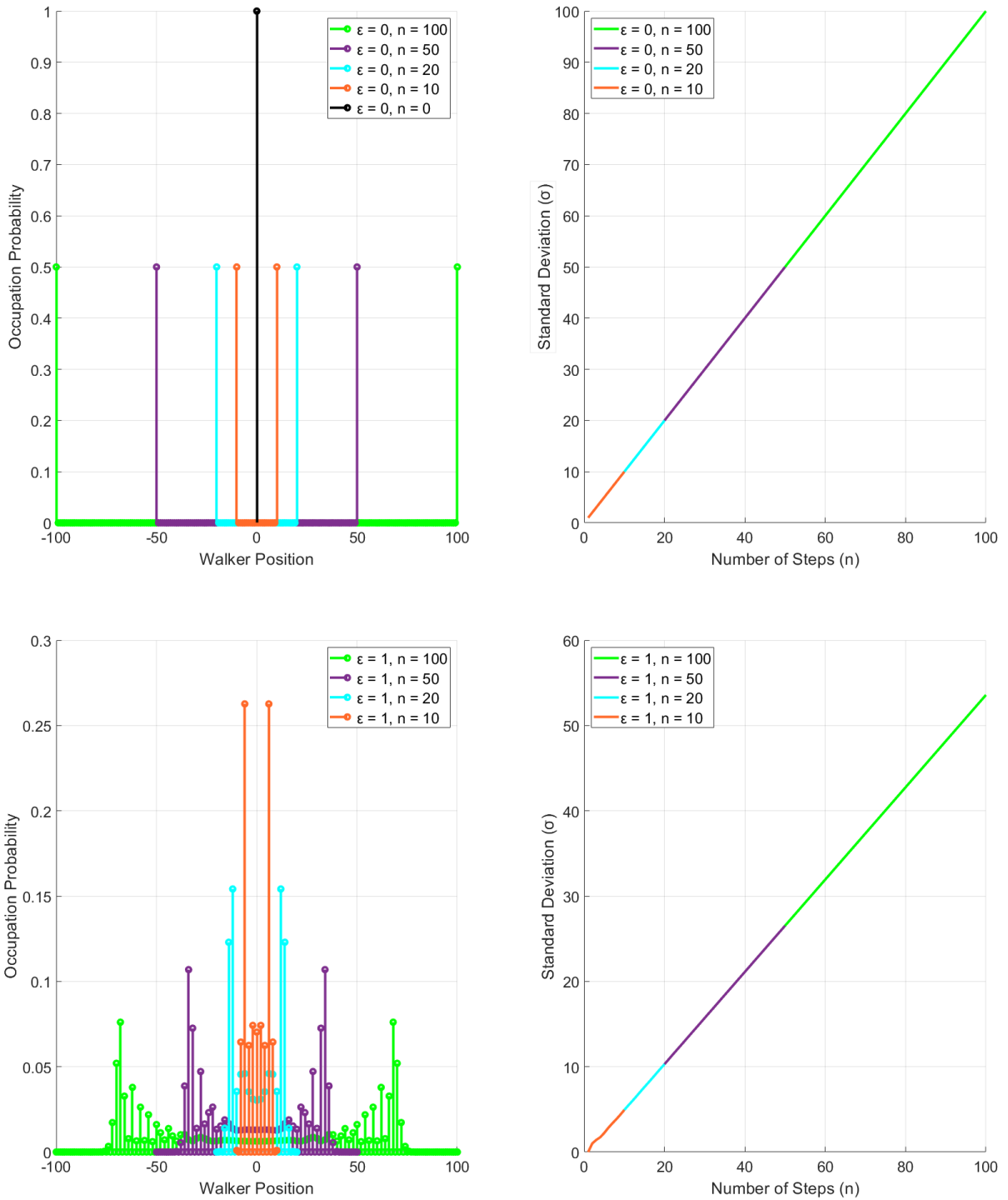


Figure 5: **Left:** Occupation probabilities for every position the walker occupies vs the number of steps, n , executed from the initial walker position $X = 0$. This graph is achronous, but with the use of colouration we can see different time (in this case steps— n) instances. **Right:** Standard deviation vs number of steps, n , of each corresponding walk from the left, maintaining the colouration. **Top:** We set $\epsilon = 0$ for which eq. (120) stands true. **Bottom:** We max-out the possible noise strength to $\epsilon = 1$ for which eq. (122) stands true.

and ‘strength of randomness’ appear opposite. A strong off-diagonality promotes a strong randomness, something which localizes the walker.

Because a QW algorithm may run with fluctuating s values, we must be capable of overcoming this stochastic situation with some method, one of which is the computation of the average value. In the case of the unbiased random variable s , that is, when we have an equal probability ($p_{\pm} = \frac{1}{2}$) of the s values, we evolve the QW from the n -th to the $(n+1)$ -th step as

$$\rho_{n+1} = \frac{1}{2} \sum_{s=\pm 1} V_q(s; \varepsilon) \rho_n V_q(s; \varepsilon)^\dagger, \quad (123)$$

in that case we have the *stochastic average* of the QW and since the sign of ε is flipped during this procedure, there is no reason to experiment with negative ε values. In the case of eq. (120), where the variable s disappears from the reshuffling matrix, the results with or without the stochastic averaging will coincide.

Let’s try some QW combinations with and without statistical averaging for various strengths of the noise parameter.

In the right plots of fig. 6 and fig. 7 we observe the two curves to diverge from one another while the green curve moves its orientation correspondingly.

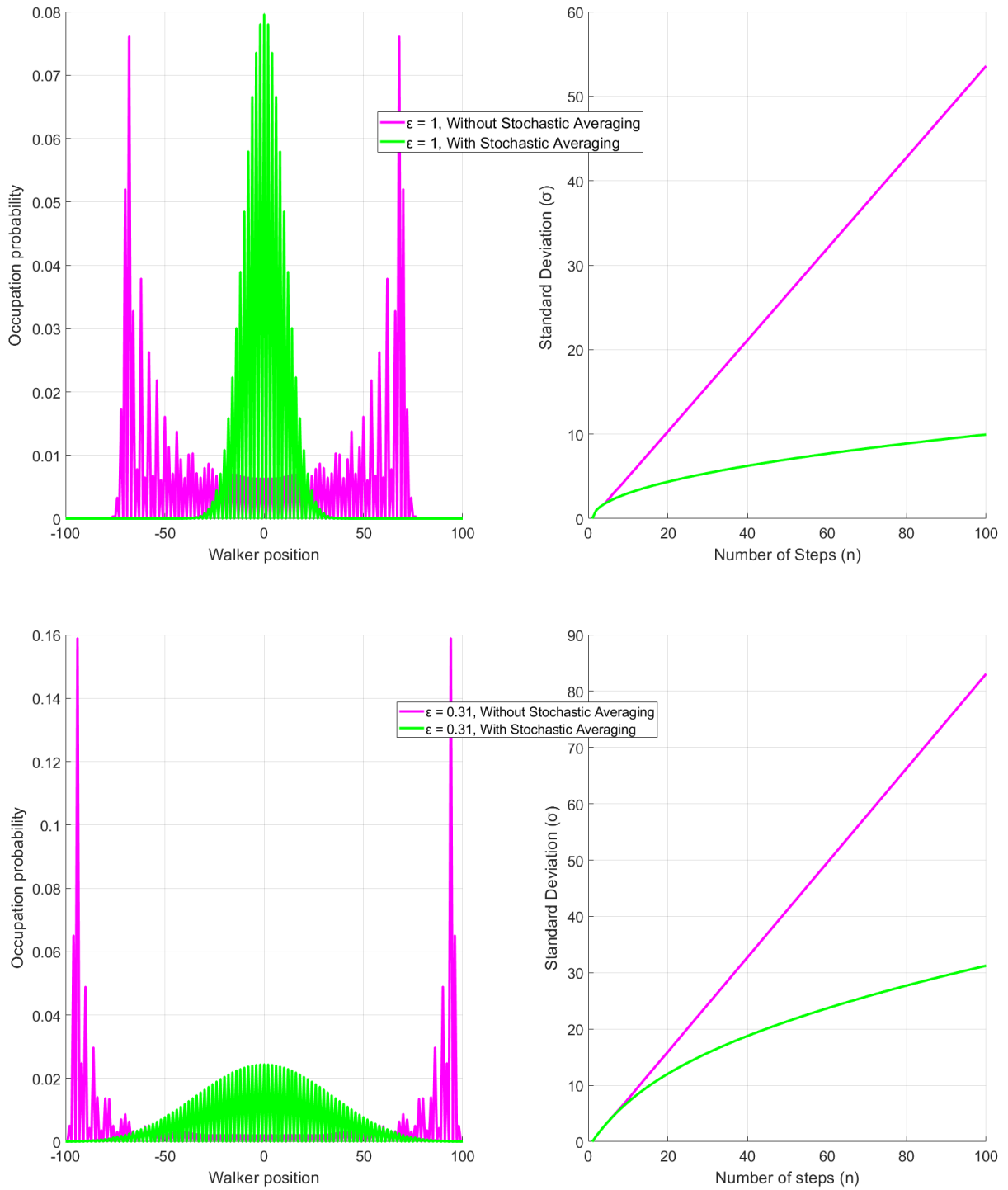


Figure 6: **Left:** Occupation probabilities for every position the walker occupies vs the number of steps, n , executed from the initial walker position $X = 0$, for the same ϵ with, and without stochastic averaging. **Right:** Standard deviation vs number of steps, n , of each corresponding walk from the left, maintaining the colouration. **Top:** $\epsilon = 1$. **Bottom:** $\epsilon = 0.31$.

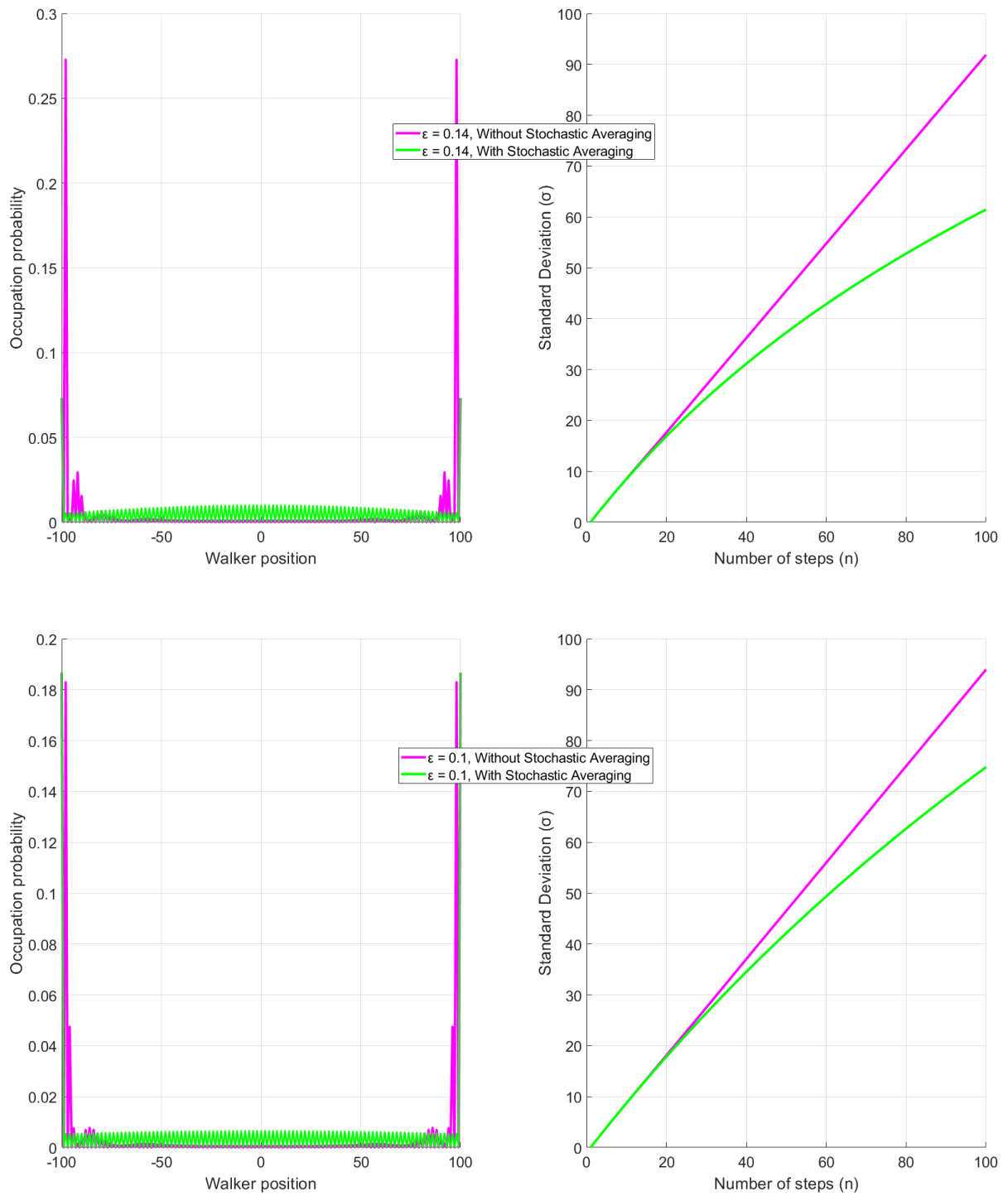


Figure 7: **Left:** Occupation probabilities for every position the walker occupies vs the number of steps, n , executed from the initial walker position $X = 0$, for the same ϵ with, and without stochastic averaging. **Right:** Standard deviation vs number of steps, n , of each corresponding walk from the left, maintaining the colouration. **Top:** $\epsilon = 0.14$. **Bottom:** $\epsilon = 0.1$.

Until now, we executed the QW algorithm with a stationary noise strength value and the increment of the step variable n . We can also work with a more fine ε structure to interpolate more of this kind of figures. A new concept is to alter the noise strength value while the walker walks. For this approach, we hold the step variable n on a given value and run the QW with a varying noise strength amount. These approaches are realized in fig. 8.

In fig. 8 we notice that as ε lessens, the σ curve values increase non-linearly, so the system adopts a quantum behaviour—and vice versa. This free selection of ε values, allows us to travel through the whole quantum – classical σ spectrum, implying that the changeover occurs continuously, though, with some gradient.

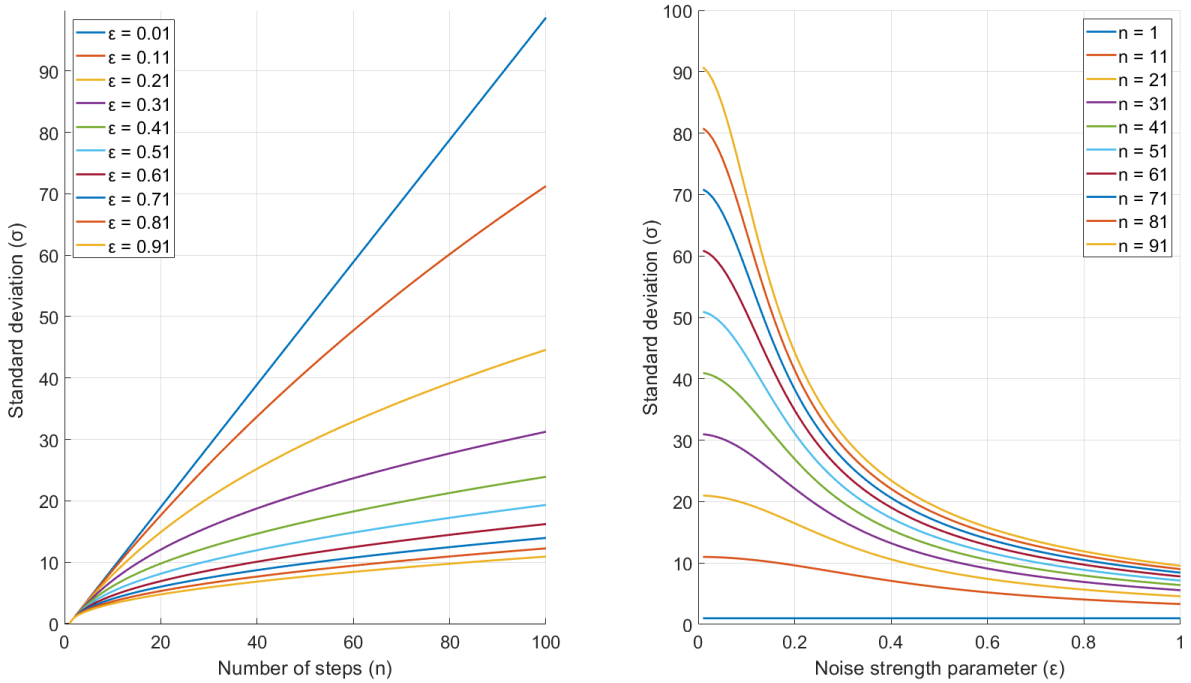


Figure 8: **Left:** Standard deviation, σ , vs the number of steps, n , for ten σ curves of various ε values and a total number of steps $N = 100$. **Right:** Standard deviation, σ , vs noise parameter, ε , for ten σ results of various numbers of steps accomplished and an increasing noise of strength $\varepsilon \in [0.01, 1]$. A vertical incision on the left plot corresponds to a σ curve on the right plot. Both algorithms ran with stochastic averaging.

Two brief experiments are given in fig. 9 in which ε switches between uncorrelated values at certain locations of the QW runtime (or rather, walktime...). In this figure, for every 50 steps of the walker, the ε parameter is tweaked. Because of its nature, we call this algorithm the ‘ ε switch’ algorithm.

In the top plots of fig. 9, we want to see how the position of the ε value changes the QW behaviour. We observe that even though the σ curves on the top right plot remain collided until mid-end of the QW procedure, the occupation behaviours on the top left plot seem opposing.

In the bottom plots of fig. 9, we want to see which QW diffuses faster and if there is a connection of the position and the value of ε . We observe that even though the σ curves on the bottom right plot separate from virtually the beginning of the walk, the occupation behaviours on the bottom left plot seem ‘dazzlingly’ similar.

In the σ vs #steps plot, the $X = Y$ line occurs for $\varepsilon = 0$, which is not allowed, so we can presume it as an upper asymptote. Also, we cannot move under the X -axis, trivial, so we can assume it as a lower asymptote. Therefore, the allowed variances live in-between these asymptotes, forming an 45° angle space. The upper asymptote gives the fastest diffusion, while the lower asymptote gives the slowest diffusion. So there exists a general ‘delay’ which is determined by setting one (or more, in the process of time) selected ε with big delays, causing the ‘trapping’ of the walker on the mean value.

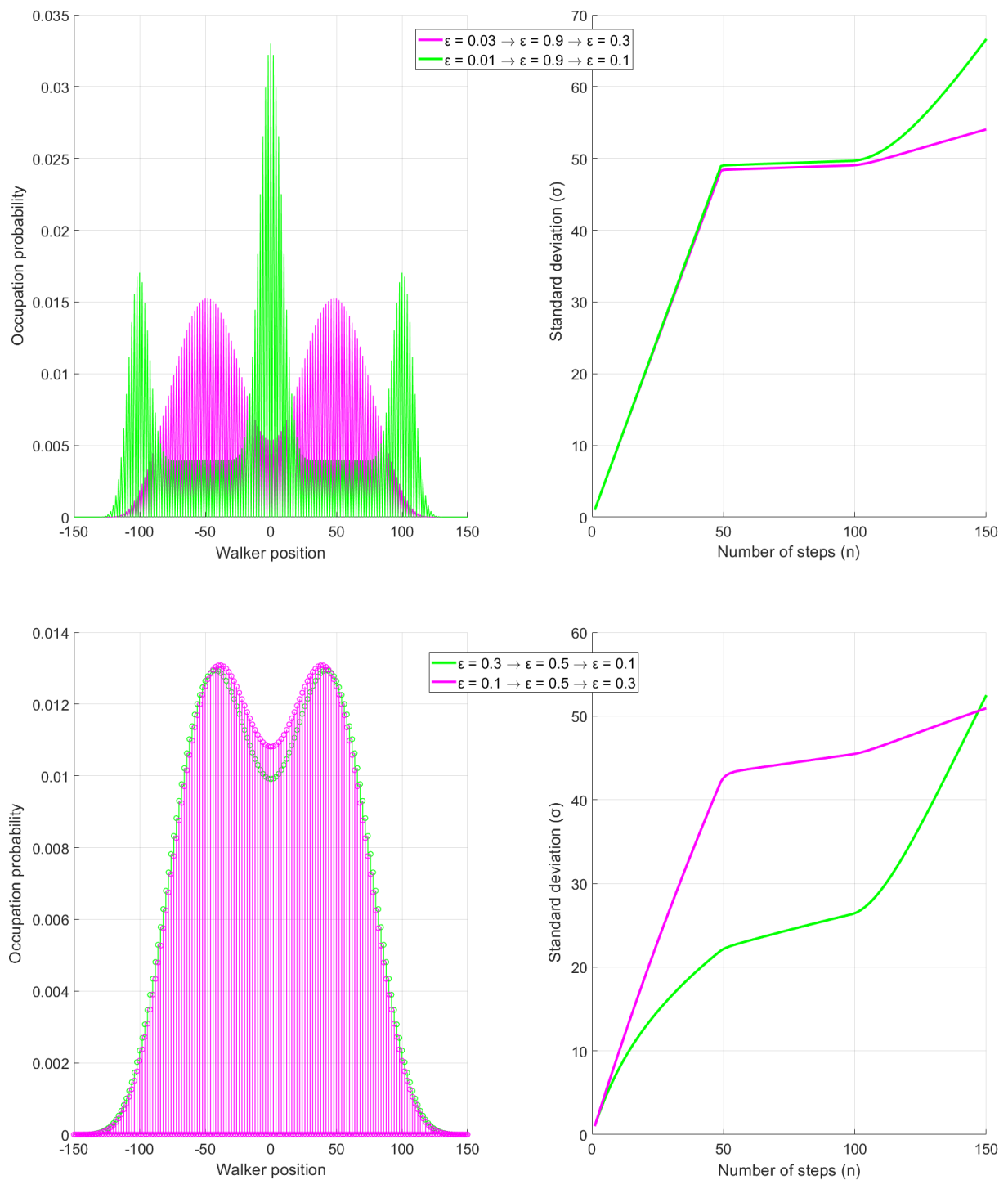


Figure 9: **Left:** Occupation probabilities for every position the walker occupies vs the number of steps, n , executed from the initial walker position $X = 0$, for the same ϵ with stochastic averaging. **Right:** Standard deviation vs number of steps, n , of each corresponding walk from the left, maintaining the colouration. **Top:** We start two QW with a similar ϵ value, in the middle of the process we set a mutual ϵ value, and lastly we set two different ϵ values. **Bottom:** We start two QW with two different ϵ values, in the middle of the process we set a common ϵ value, and lastly we set again the initial ϵ values but in inverse order.

The standard deviation indicates how far the leftmost and rightmost sites of the curve have been separated in the course of the evolution of the walk, without providing any information about what's happening in between these sites. However, another interesting point is that we would like to find a kind of index that indicates a number of occupied sites, and not only the edge sites.

In order to do this, we have to utilize the occupation probability of the sites, although they are able to provide some measure, they are not suitable as such. One reason is they are not free, they are constrained and in order to get rid of the normalization constraint ($\sum_i p_i = 1$), we take the square of each site occupation probability p_i , so now they must not satisfy any constraint. We now assume that each one of them contributes to the participation of the site into the whole picture. To keep things tight, we place the sum under a fraction, and we end up with the IPR index eq. (66).

For this aim, we point out the following remarks [21].

Remark #1. In terms of the probability distribution sequence

$$p = (p_i)_{i=1}^n, \quad 0 \leq p_i \leq 1 \quad (124)$$

the index

$$IPR(p) = \sum_i p_i^2, \quad (125)$$

satisfies the bounds

$$\frac{1}{n} \leq IPR(p) \leq 1. \quad (126)$$

To prove this, we need to show

$$\frac{1}{n} \leq \sum_{i=1}^n p_i^2 \leq 1. \quad (127)$$

The Cauchy-Schwarz inequality

$$\langle x, y \rangle^2 \leq \langle x, x \rangle \langle y, y \rangle, \quad (128)$$

for the vectors

$$x = (x_i)_{i=1}^n, \quad y = (1)_{i=1}^n, \quad (129)$$

yields

$$1 \leq \left(\sum_{i=1}^n p_i^2 \right) n \implies \frac{1}{n} \leq IPR(p). \quad (130)$$

As to the RHS congruence rule of the bound inequalities, the relations $0 \leq p_i \leq 1$, $p_i^2 \leq p_i$ lead to

$$\sum_{i=1}^n p_i^2 \leq \sum_{i=1}^n p_i = 1. \quad (131)$$

Remark #2. The question of the amount of participation of sample space sites $i \in \{1, 2, \dots, n\}$ in a probability distribution $p = (p_i)_{i=1}^n$, can be understood as finding a measure to quantify the difference of distribution p from the *sharp distribution* $p_0 = (\delta_{0i})_{i=1}^n$ and the *uniform distribution* $p_u = (\frac{1}{n})_{i=1}^n$, with minimal and maximal participation respectively. To this end, an order is defined among distributions, named the *majorization order* (\prec).

Two distributions $p = (p_i)_{i=1}^n$, and $q = (q_i)_{i=1}^n$ are ordered as $p \prec q$ iff

$$\sum_{i=1}^k p_i^\downarrow \leq \sum_{i=1}^k q_i^\downarrow, \quad k = 1, \dots, n; \quad (132)$$

here, the terms of the distribution sequence have been put in non-increasing order i.e., e.g., $p_i^\downarrow \leq p_{i+1}^\downarrow$.

Moreover, it is valid that if $p \prec q$ then $S(p) \leq S(q)$, where

$$S(p) = - \sum_{i=1}^n p_i \ln p_i, \quad (133)$$

is the Shannon entropy; see [15] and references therein.

The IPR index offers an alternative way of ordering distribution in relation to the participation of the sites, i.e., $IPR(p) \leq IPR(q)$ means that the distribution p has fewer sample sites occupied in comparison to that of distribution q . This measure has been employed to compare the distribution with regard to the Anderson localization in the context of QWs with random coin space reshuffling.

In fig. 10, we observe the behaviour of the QW's σ next to that of the IPR index. It is obvious that as ε increases, after a certain point, the stochastic distribution curve goes under the non-stochastic curve and tends to converge towards the X-axis, which means that the distribution tends to localize. This phenomenon corresponds to the Anderson localization, suggesting that in the presence of strong noise, quantum states seem to be localized [22], [23], [24].

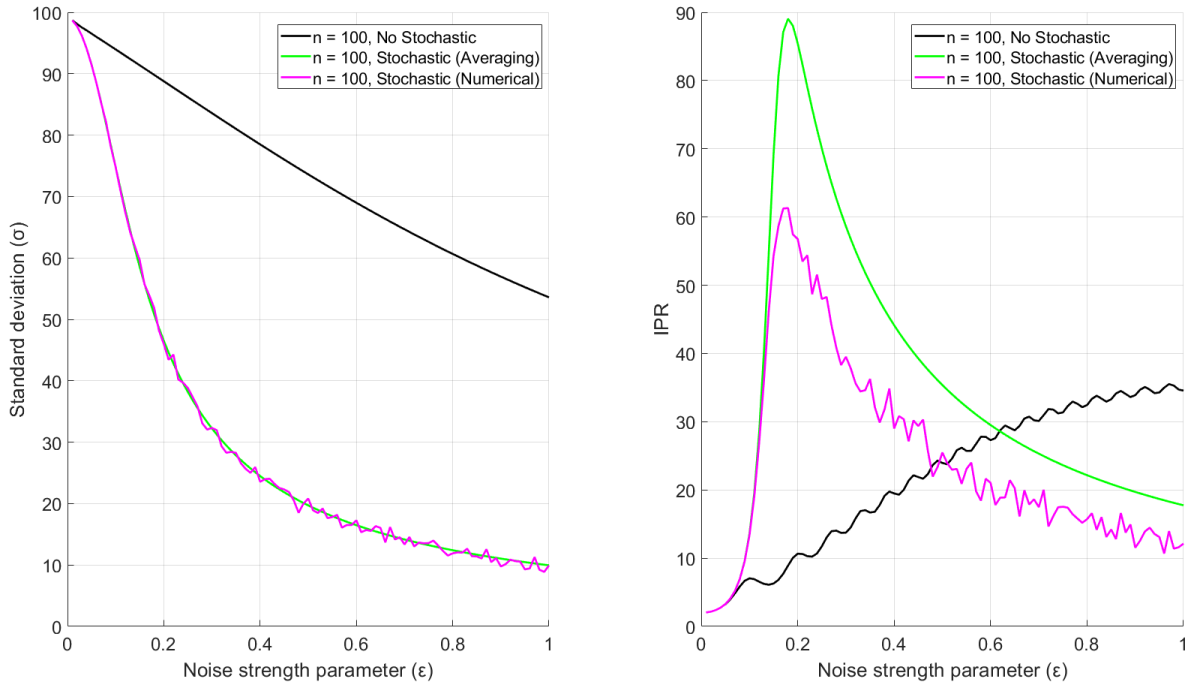


Figure 10: **Left:** Standard deviation, σ , vs noise strength value, $\epsilon \in [0.01, 1]$. **Right:** Inverse participation ratio, (IPR) vs noise strength value, $\epsilon \in [0.01, 1]$. The plots came from applying the three layers QW_1 , QW_2 , QW_3 , with stochastic noise on the second layer QW_2 , in the form of random dichotomic variable $s \in \{\pm 1\}$ with equal probability $p_{\pm} = \frac{1}{2}$ (mean of 10 runs) (magenta), stochastic averaging (green) and without stochastic noise (black).

We saw how the applied $U(s; \varepsilon)$ matrix behaves for various ε values with or without stochastic averaging. We introduced and toyed with this ε parameter because it's crisp, flexible, and it can be chosen at will. We also introduced the s variable to help us realize QW instances with stochastic averaging.

Looking back at the critical fig. 8, we see different characteristic behaviours, i.e., σ being analogous to the number of steps (fast diffusion), a fraction of the number of steps (moderate diffusion), or the square root of the number of steps (slow diffusion). These curves came circumstantially, and we don't know the roots of these behaviours, though, it's important to find out because these extreme behaviours seem to portray a powerful classical – quantum transition.

The core interest of this work is the inspection of this adjustable QW model to prove the correlation of n with ε and to connect them in a common cause such that we could drive and parametrize this behaviour in order to go from one regime to the other and back continuously, if this is possible. The best way to display these results is by looking at a new pair of axes, the ε - n plane, which plays the role of a decision plane for the category of the walker's behaviour. This plane will be demarcated by an equation into two pieces, out of which we are going to extract all the information we need in order to adjust the passing from the classical to the quantum behaviour and vice versa.

We will now make use of this newly introduced reshuffling matrix, so we can study the effect it has on the spread of the QW.

A Theoretical Analysis on the ε - n Plain.

We start from the initial density matrix being

$$\begin{aligned}
 \rho_0 &= \rho_0^c \otimes \rho_0^w \\
 &= P_0^c \otimes P_0^w \\
 &= |0; c\rangle \langle 0; c| \otimes |0; w\rangle \langle 0; w|.
 \end{aligned} \tag{134}$$

We generate the total system density matrices $\rho_0, \rho_1, \rho_2, \dots, \rho_n, \dots$, using the transformation

$$\rho_n \rightarrow V_q(s; \varepsilon) \rho_n V_q(s; \varepsilon)^\dagger = \rho_{n+1}. \tag{135}$$

E.g., for $n = 1$ the density matrix is

$$\begin{aligned}
 \rho_1 &= V_q(s; \varepsilon) \rho_0 V_q(s; \varepsilon)^\dagger \\
 &= \frac{1}{\sqrt{1 + \varepsilon^2}} \begin{pmatrix} h & s\varepsilon h \\ -s\varepsilon h^\dagger & h^\dagger \end{pmatrix} \begin{pmatrix} |0; w\rangle \langle 0; w| & 0 \\ 0 & 0 \end{pmatrix} \begin{pmatrix} h & s\varepsilon h \\ -s\varepsilon h^\dagger & h^\dagger \end{pmatrix} \frac{1}{\sqrt{1 + \varepsilon^2}}.
 \end{aligned} \tag{136}$$

We name the stochastic average of coin+walk density matrices $\rho_0, \langle \rho_1 \rangle, \langle \rho_2 \rangle, \dots, \langle \rho_n \rangle, \dots$, with

$$\langle \rho_n \rangle = \frac{1}{2^n} \sum_{s_n = \pm 1} \cdots \sum_{s_1 = \pm 1} V_q(s_n; \varepsilon) \cdots V_q(s_1; \varepsilon) \rho_0 V_q(s_1; \varepsilon)^\dagger \cdots V_q(s_n; \varepsilon)^\dagger. \tag{137}$$

E.g., the statistical average of the density matrix for $n = 1$ is

$$\begin{aligned}
\langle \rho_1 \rangle &= \frac{1}{2} \sum_{s=\pm 1} V_q(s; \varepsilon) \rho_0 V_q(s; \varepsilon)^\dagger \\
&= \frac{1}{2} \{ V_q(1; \varepsilon) \rho_0 V_q(1; \varepsilon)^\dagger + V_q(-1; \varepsilon) \rho_0 V_q(-1; \varepsilon)^\dagger \} \\
&= \frac{1}{2} \frac{1}{1 + \varepsilon^2} \sum_{s=\pm 1} \begin{pmatrix} |1; w\rangle \langle 1; w| & -s\varepsilon |1; w\rangle \langle -1; w| \\ -s\varepsilon |-1; w\rangle \langle 1; w| & s^2 \varepsilon^2 |-1; w\rangle \langle -1; w| \end{pmatrix} \\
&= \frac{1}{1 + \varepsilon^2} \begin{pmatrix} |1; w\rangle \langle 1; w| & \\ & \varepsilon^2 |-1; w\rangle \langle -1; w| \end{pmatrix} \\
&= \frac{1}{1 + \varepsilon^2} \begin{pmatrix} 1 & 0 \\ 0 & \varepsilon^2 \end{pmatrix} \otimes |1; w\rangle \langle 1; w| + \begin{pmatrix} & \\ 0 & \varepsilon^2 \end{pmatrix} \otimes |-1; w\rangle \langle -1; w|, \tag{138}
\end{aligned}$$

which is a diagonal density matrix in coin-walker spaces. It can be shown (e.g., by induction), that eq. (137) is also diagonal, i.e.,

$$\langle \rho_n \rangle = \sum_{k=-n}^n \begin{pmatrix} \alpha_{n,k} & \\ & \beta_{n,k} \end{pmatrix} \otimes |k; w\rangle \langle k; w|, \tag{139}$$

where the elements $\alpha_{n,k}, \beta_{n,k}, k \in \{0, \pm 1, \dots, \pm n\}$, satisfy the respective recurrence relations

$$\alpha_{n+1,k} = \mathcal{N}^2(\alpha_{n,k-1} + \varepsilon^2 \beta_{n,k-1}), \tag{140}$$

and

$$\beta_{n+1,k} = \mathcal{N}^2(\beta_{n,k-1} + \varepsilon^2 \alpha_{n,k-1}). \tag{141}$$

eq. (140) leads to the occupation probability for finding the head of the coin, and the walker in k state, at the n -th step of the evolution

$$p_{n,k}^{head} = |\alpha_{n,k}|^2, \tag{142}$$

eq. (141) leads to the occupation probability for finding the tail of the coin, and the walker in k state, at the n -th step of the evolution

$$p_{n,k}^{tails} = |\beta_{n,k}|^2, \quad (143)$$

and by summing eq. (142) and eq. (143) we get the occupation probability for finding the walker in k state, at the n -th step of the evolution

$$p_{n,k} = |\alpha_{n,k}|^2 + |\beta_{n,k}|^2. \quad (144)$$

Obviously, trying to solve eq. (140), eq. (141) for other than $\varepsilon \in \{0, 1\}$, would not give exact results. So, we resort to the *quantum moments* of the probability distribution.

$$A_n^{(p)} = \sum_{k=-\infty}^{\infty} \alpha_{n,k} k^p, \quad p = 0, 1, \dots, \quad (145)$$

represents the p -th moment of the probability distribution after a number of steps n , showing the head of the coin, and respectively

$$B_n^{(p)} = \sum_{k=-\infty}^{\infty} \beta_{n,k} k^p, \quad p = 0, 1, \dots, \quad (146)$$

represents the p -th moment of the probability distribution after a number of steps n , showing the tail of the coin.

The total system probability distribution is

$$S_n^{(p)} = A_n^{(p)} + B_n^{(p)}. \quad (147)$$

We can express these terms explicitly as

$$A_n^{(p)} = Tr(P_+ \otimes \widehat{L}^p \rho_n) \equiv \langle P_+ \otimes P_k \rangle_n, \quad (148)$$

$$B_n^{(p)} = Tr(P_- \otimes \widehat{L}^p \rho_n) \equiv \langle P_- \otimes P_k \rangle_n, \quad (149)$$

$$\begin{aligned} S_n^{(p)} &= Tr((P_+ + P_-) \otimes \widehat{L}^p \rho_n) \\ &= Tr(\mathbf{1}_c \otimes \widehat{L}^p \rho_n) \\ &=: Tr(\widehat{L}^p \rho_n^{(w)}). \end{aligned} \quad (150)$$

We solve eq. (148) and eq. (149) for the 0-th moment

$$A_n^{(0)} = \frac{1}{2}(1 + r^n \cos(2\gamma)), \quad \gamma \in [0, \pi] \quad (151)$$

$$B_n^{(0)} = \frac{1}{2}(1 - r^n \cos(2\gamma)), \quad \gamma \in [0, \pi] \quad (152)$$

for the 1st moment of eq. (150) we obtain

$$S_n^{(1)} = r \cos(2\gamma)[1 - r^n]/[1 - r], \quad (153)$$

and for the 2nd moment of eq. (150) we obtain

$$S_n^{(2)} = n(1 + r)/(1 - r) - 2r(1 - r^n)/(1 - r)^2. \quad (154)$$

The second total moment, i.e., the expectation value of the square of the position operator L , can also be written as

$$S_n^{(2)} = Tr(L^2 \rho_n^{(w)}) \equiv \langle L^2 \rangle_n \quad (155)$$

$$= \frac{1}{2\epsilon^4}(2n\epsilon^2 - 1 + \epsilon^4 - (1 - \epsilon^2)^{n+1}/(1 + \epsilon^2)^{n-1}). \quad (156)$$

For a preconditioned epsilon value, and for a variable number of steps n , such that

$$\boxed{\frac{1}{\varepsilon^2} \gg n \gg 1}, \quad (157)$$

we get the first diffusion regime, and eq. (156) becomes

$$\boxed{S_n^{(2)} = n^2 + \frac{1}{2\varepsilon^4} O((n\varepsilon^2)^3)}. \quad (158)$$

This growth rate of the second moment for n , is $\sqrt{\langle L^2 \rangle_n} \sim O(n)$, is called ‘ballistic’ or ‘inertial’ regime and is a characteristic of a QW.

For a preconditioned epsilon value, and for a variable number of steps n , such that

$$\boxed{n \gg \frac{1}{\varepsilon^2} \gg 1}, \quad (159)$$

we get the second diffusion regime, and eq. (156) becomes

$$\boxed{S_n^{(2)} = \frac{n}{\varepsilon^2} \left\{ 1 + O\left(\frac{1}{n\varepsilon^2}\right) \right\}}. \quad (160)$$

This growth rate of the second moment for n , is $\sqrt{\langle L^2 \rangle_n} \sim O(\sqrt{n})$, is called ‘diffusive’ regime and is a characteristic of a CRW.

For a small number of steps n , the probability distribution seems like that of a QW. As the number of steps increasingly reaches large numbers, no matter how small the epsilon value is, the changeover will eventually occur, showing the probability distribution behaviour of a CRW [20], [21].

This transition happens at the borderline and the relation between $n - \varepsilon$ is

$$\boxed{n\varepsilon^2 \approx 1}, \quad (161)$$

from which we define as $n - critical$ (n^*) that for which the transition happens

$$\boxed{n^* \approx \frac{1}{\varepsilon^2}}, \quad (162)$$

and, respectively, we define as $\varepsilon - critical$ (ε^*) that for which the transition happens

$$\boxed{\varepsilon^* \approx \frac{1}{\sqrt{n}}}. \quad (163)$$

From eq. (157), we get that $\varepsilon \neq 0$, so eq. (120) is out of the game. Also, from eq. (159), we see that $\varepsilon \leq 0.1$ so there is an order difference between the inequalities. We conclude the feasible ε value range to be $\varepsilon \in (0, 0.1]$. In order to maintain eq. (161), as ε diminishes, we have more QW steps n .

By welding together multiple plot instances of the standard deviation, σ , vs the number of steps, n , for various noise strength values, ε , we form a plane which is partitioned by the crossover equation eq. (161) in two parts. In the left part we have a region for which eq. (159) stands true and eq. (160) connects the σ - n - ε variables, promoting a slow diffusion ($O(\sqrt{n})$), while in the right part we have a region for which eq. (157) stands true and eq. (158) connects the σ - n - ε variables, promoting a fast diffusion ($O(n)$). This Q - C change becomes apparent in fig. 11.

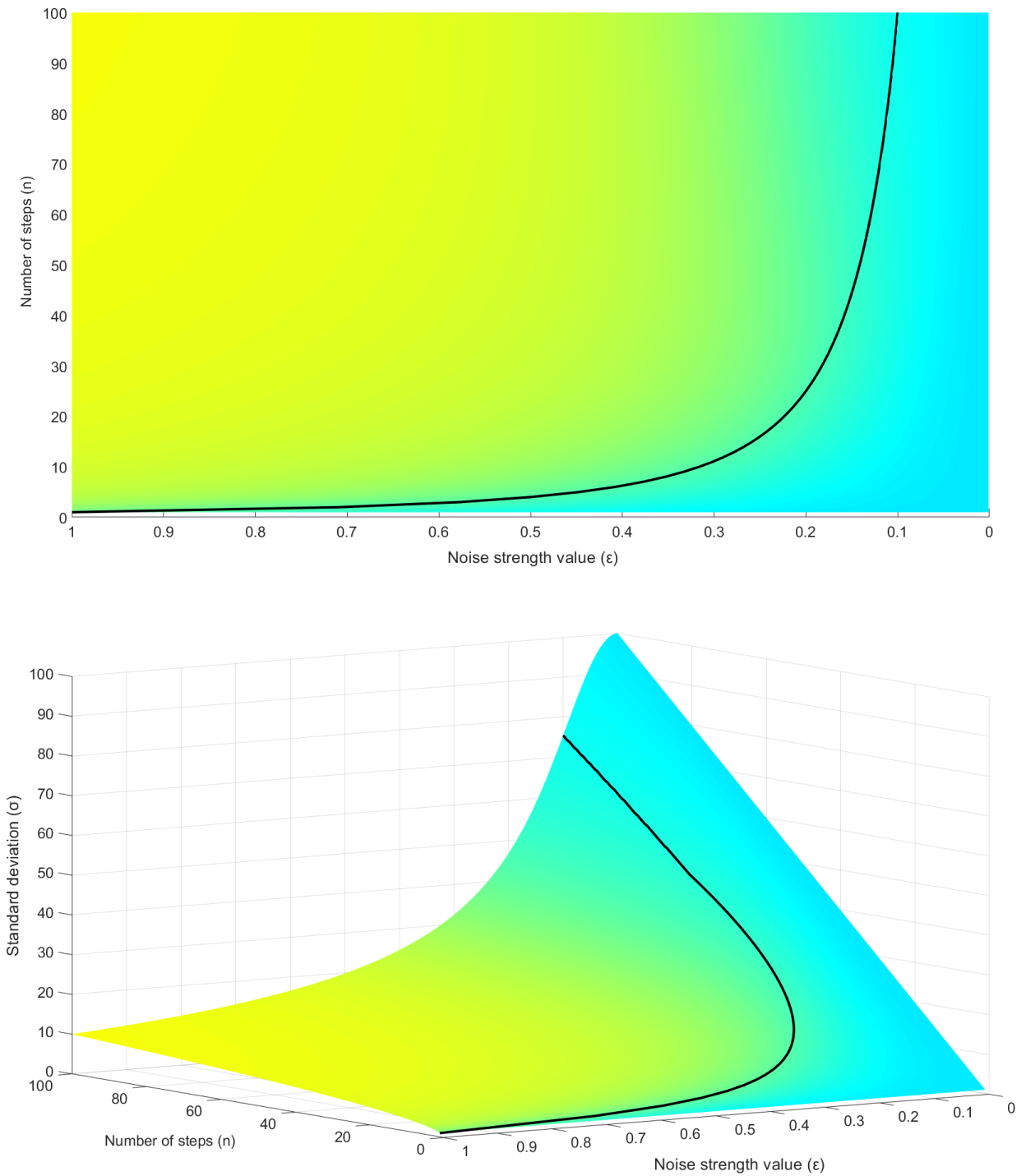


Figure 11: **Top:** Number of steps, n , vs noise strength, ϵ , represented as a surface in which lighter colours express slowly changing values and darker colours represent faster changing values, in a horizontal fashion, for a total number of steps $N = 100$. The black borderline which splits the two coloured plains is drawn from $\epsilon = \frac{1}{\sqrt{n}}$. **Bottom:** Three dimensional version of the above, with the standard deviation now present in the form of the surface altitude and the crossover line (black) elevated by the corresponding σ value so that it stays on top of the figure's surface. We can easily perceive the steepness of the "cliff" at the higher numbers of steps the walker has travelled for lesser ϵ values.

3.2 Detection of a Hidden Random Layer via Q – C Transition

We are asked to transmit particles through an area made out of three stacked layers. The particle movement behaves like a QW containing a reshuffling matrix determined by noise strength parameters $\epsilon_1, \epsilon_2, \epsilon_3$ and layer widths n_1, n_2, n_3 respectively associated to the QW_1, QW_2, QW_3 corresponding to the particle movement on each of the three layers. This passing through the different layers gives a characteristic terminal distribution probability measurement of the particles entered, identified as a QW behaviour.

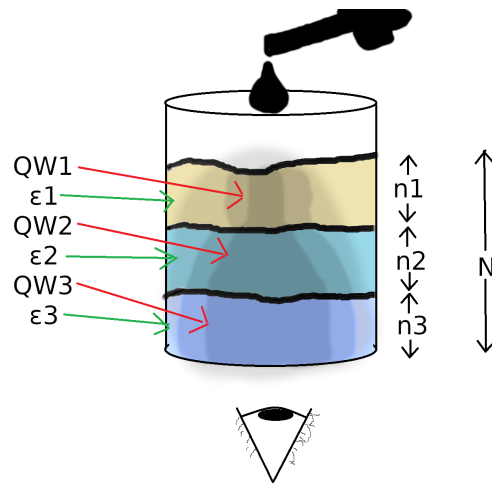


Figure 12: A drop of ink, representing some kind of particle, drips down through three substance layers, darkening the colours it comes in contact. The viscosity ϵ_i can be seen as the different colours of each layer, with the corresponding width counted in number of steps n_i . The diffusion speed of each QW_i can be perceived as the angle of darkness expansion as the drop flows down through the layers.

Our initial QW theory is that we have a single reshuffling matrix with some pre-determined noise strength value ϵ , which gives a measurement like that of fig. 13. In this state of things, theory and measurement agree.

Suddenly, we obtain an experimental measurement as seen in the left of fig. 14, rendering our initial theory outdated.

Why is the system failing?

It seems there is some kind of anomaly in the probability distribution.

How can we overcome this problem?

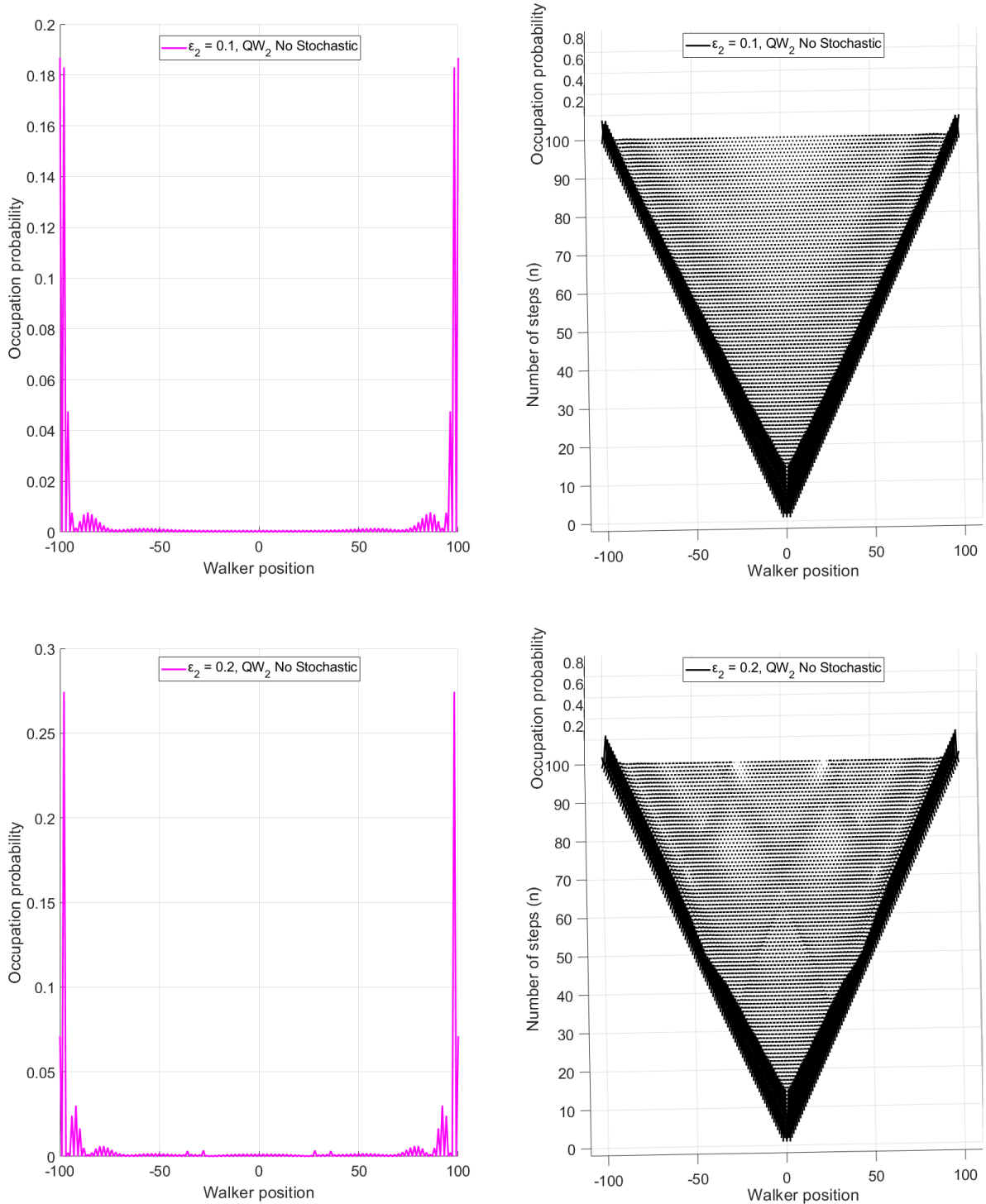


Figure 13: **Left:** Occupation probability vs walker position final step profile after applying the three layers QW_1, QW_2, QW_3 , without stochastic noise. **Right:** Number of steps vs walker position vs occupation probability 3-D profile during the evolution of the three layers QW_1, QW_2, QW_3 , without stochastic noise. **Top:** $n_1 = n_2 = n_3 = 33$, $\epsilon_1 = \epsilon_2 = \epsilon_3 = 0.1$. Given these values, from the crossover equation we obtain $n^* = 100 > n_2 = 33$, so the layer isn't thick enough for the transition to occur. **Bottom:** $n_1 = n_2 = n_3 = 33$, $\epsilon_1 = \epsilon_3 = 0.1$ and $\epsilon_2 = 0.2$. Given these values, from the crossover equation we obtain $n^* = 25 < n_2 = 33$, so the layer is thick enough for the transition to occur.

We can hypothesize that a layer has been exposed to stochastic noise, e.g., the random dichotomic variable, $s = \pm 1$, $p_{\pm} = \frac{1}{2}$, is applied in the reshuffling matrix of QW_2 , fluctuating the sign of ε_2 and thus, creating some kind of motion randomization in the middle layer.

Is this enough to create this distribution rearrangement?

From the output probability distribution of the diffusing particles, we must determine the existence of the hidden random layer (HRL).

Our initial QW theory lacks the stochastic noise filter and does not still fit the picture, so we introduce the element of stochastic noise in our QW in order to troubleshoot this disagreement between theory and measurement. The new QW theoretical model is now stochastically noisy with a deterministic noise strength value application.

The averaging factor acts as another diffusion mechanism that changes the system's diffusion behaviour affecting the terminal probability distribution, even if the averaging is applied to a non-terminal part of the route of the QW. Thus, we can reverse the question and say, when the walker passes through this total layer of $n_1+n_2+n_3$ steps, and we see some kind of anomaly at the terminal profile, we can hypothesize that there exists a hidden random layer which is based on the Q - C transitions. This scenario is generally quite modular, we can have layers of the same width, or not. Could we have more diversion of the terminal profile if the layers had different widths? When we alter the width, the crossover statement determines if this width is sufficient for the transition to occur or not. We also have a secondary diffusion mechanism which, for a given ε , it has width requirements for the alterations to take place. So, generally we can maintain a balance of things depending on which variable we want to parametrize.

The averaging algorithm features a reshuffling matrix which consists of both the possible s values with equal probabilities, giving a probability distribution as seen in the right plots of fig. 14. The case, in real systems, is that the coin can only have one discrete possible outcome. To simulate this real world experimental approach, a change on the

QW algorithm was made, so that the coin gets a value conditionally, controlled by some classical random number generator. This leads to the *stochastic numerical* outcome of the QW and is the type of measurement that occurred in our system, giving the left plots of fig. 14.

We will now make use of the known Q - C transition in a noisy environment to provide detection tools and the analytic condition between parameters ε and n that characterize this transition, to determine quantified measures that manifest the existence and extent of the hidden random layer. If $\mathcal{E}_{\varepsilon_1}, \mathcal{E}_{\varepsilon_2}, \mathcal{E}_{\varepsilon_3}$ stand for the CPTP maps governing the diffusion by the respective QW_1, QW_2, QW_3 layers, \mathcal{B} stands for the stochastic numerical map and \mathcal{D} stands for the stochastic averaging map, investigate the difference generated on the terminal distribution of the occupation probabilities of the composite maps

$$\mathcal{E}_{\varepsilon_3} \times \mathcal{E}_{\varepsilon_2} \times \mathcal{E}_{\varepsilon_1},$$

$$\mathcal{E}_{\varepsilon_3} \times \mathcal{B} \mathcal{E}_{\varepsilon_2} \times \mathcal{E}_{\varepsilon_1},$$

and

$$\mathcal{E}_{\varepsilon_3} \times \mathcal{D} \mathcal{E}_{\varepsilon_2} \times \mathcal{E}_{\varepsilon_1}. \quad (164)$$

Determine value intervals for the parameters $\varepsilon_{1,2,3}, n_{1,2,3}$ and possible interrelations between those intervals as well as the parameters between them, so that to determine necessary conditions for the solution of the HRL problem.

For our experiments, we choose the QW algorithm to walk a total number of steps $n = 100$. For simplicity and to maintain equal layer widths we divide by the number of layers, in our case 3 layers, so each layer is of width $n_1 = n_2 = n_3 = 33$, though differentiate these layers by means of the varying ε values, preferring layers QW_1, QW_3 to be thin enough for the change over to not occur e.g., we choose $\varepsilon_1 = \varepsilon_3 = 0.1$ giving $n^* \approx 100 > n_{1,3} = 33$. The value assignment for variable ε_2 is made with a similar approach, in one case we want it to be small enough, so the changeover doesn't occur (see n^* for $\varepsilon = 0.1$),

and in the other case we want the changeover to occur, so we choose $\varepsilon = 0.2$ giving $n^* = 25 < n_2 = 33$.

Although the numerical outcomes, seen in the left of fig. 14 (fig. 15, giving the total time-space evolution), and their deterministic relatives seen in the right, have definite outcome alterations, those being harsh terminal profiles and a chaotic time-space evolution for the numerical runs, they maintain strikingly similar deviations as seen in fig. 16. Both of these runs apply a stochastic noise in QW_2 which can be diagnosed by the bumps that occur in the mid-range of the terminal distribution profile.

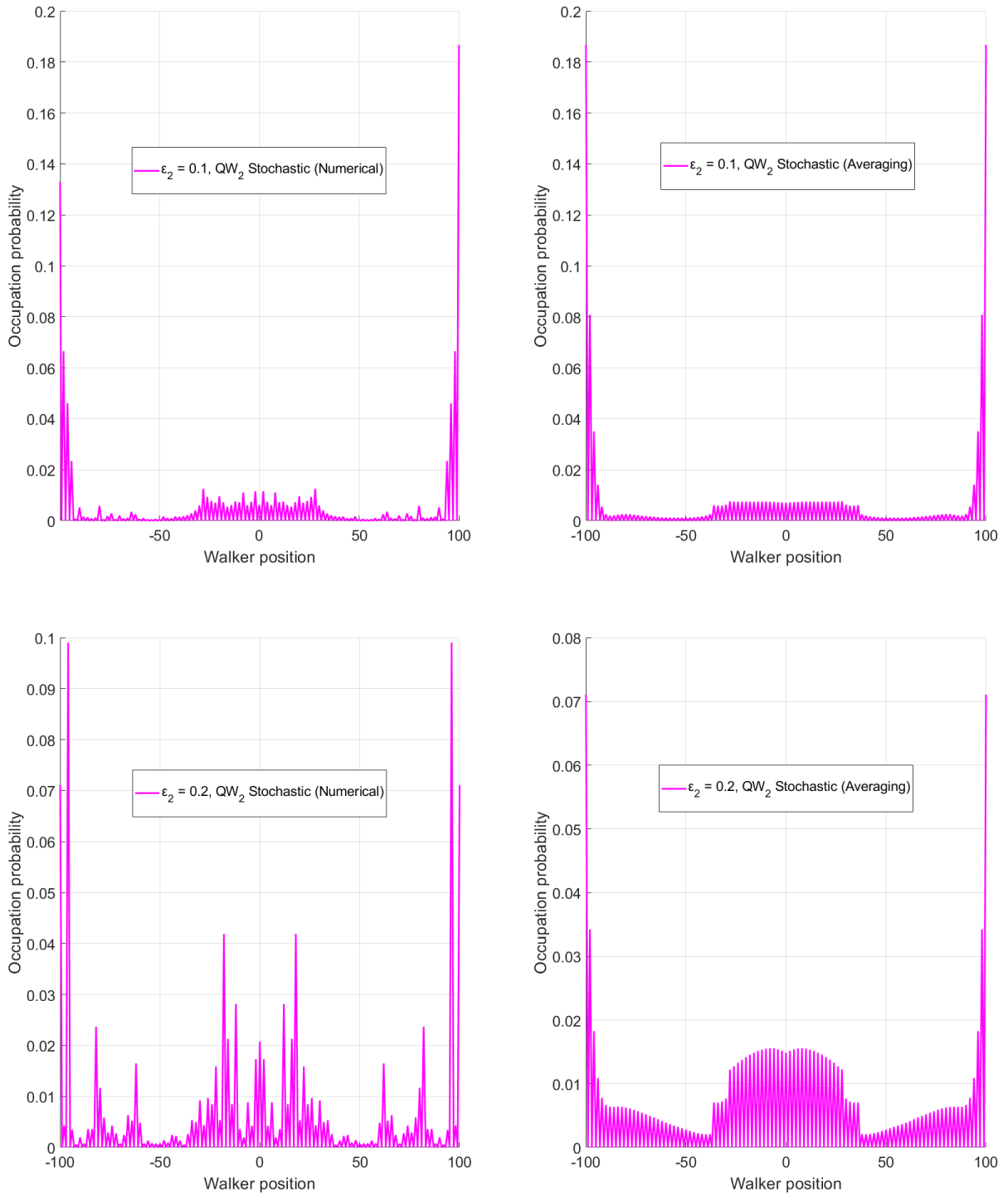


Figure 14: **Left:** Occupation probability vs walker position final step profile after applying the three layers QW_1, QW_2, QW_3 , with stochastic noise in the form of random numerical values of the dichotomic variable $s \in \{\pm 1\}$ with equal probability $p_{\pm} = \frac{1}{2}$ on the middle layer QW_2 . **Right:** Occupation probability vs walker position final step profile after applying the three layers QW_1, QW_2, QW_3 , with stochastic noise in the form of stochastic averaging on the middle layer QW_2 . **Top:** $n_1 = n_2 = n_3 = 33$, $\epsilon_1 = \epsilon_2 = \epsilon_3 = 0.1$. Given these values, from the crossover equation we obtain $n^* = 100 > n_2 = 33$, so the layer isn't thick enough for the transition to occur. **Bottom:** $n_1 = n_2 = n_3 = 33$, $\epsilon_1 = \epsilon_3 = 0.1$ and $\epsilon_2 = 0.2$. Given these values, from the crossover equation we obtain $n^* = 25 < n_2 = 33$, so the layer is thick enough for the transition to occur.

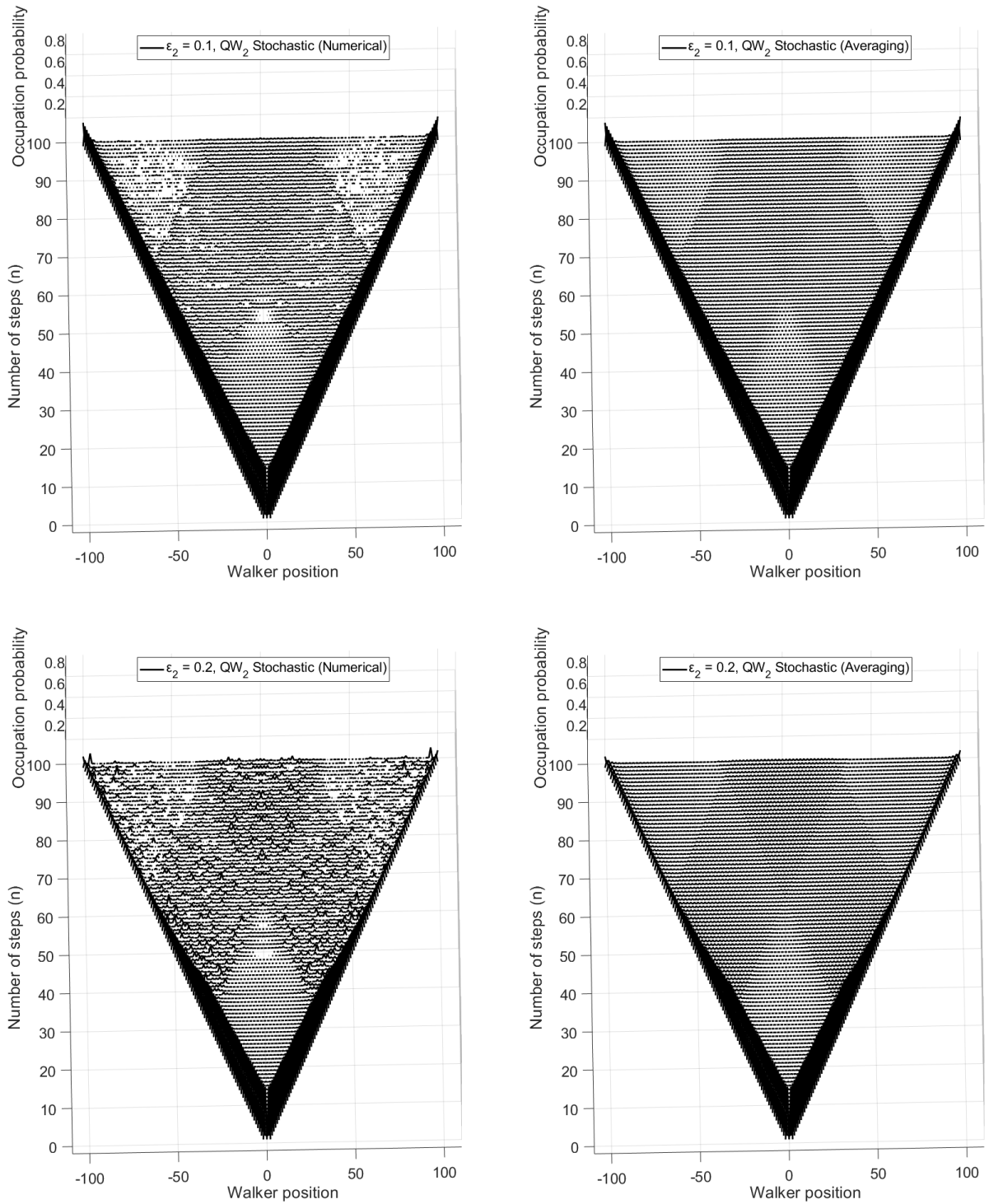


Figure 15: **Left:** Number of steps vs walker position vs occupation probability 3-D profile during the evolution of the three layers QW_1 , QW_2 , QW_3 , with stochastic noise in the form of random numerical values of the dichotomic variable $s \in \{\pm 1\}$ with equal probability $p_{\pm} = \frac{1}{2}$ on the middle layer QW_2 . **Right:** Number of steps vs walker position vs occupation probability 3-D profile during the evolution of the three layers QW_1 , QW_2 , QW_3 , with stochastic noise in the form of stochastic averaging on the middle layer QW_2 . **Top:** $n_1 = n_2 = n_3 = 33$, $\epsilon_1 = \epsilon_2 = \epsilon_3 = 0.1$. Given these values, from the crossover equation we obtain $n^* = 100 > n_2 = 33$, so the layer isn't thick enough for the transition to occur. The noise in QW_2 is applied as a stochastic average value. **Bottom:** $n_1 = n_2 = n_3 = 33$, $\epsilon_1 = \epsilon_3 = 0.1$ and $\epsilon_2 = 0.2$. Given these values, from the crossover equation we obtain $n^* = 25 < n_2 = 33$, so the layer is thick enough for the transition to occur.

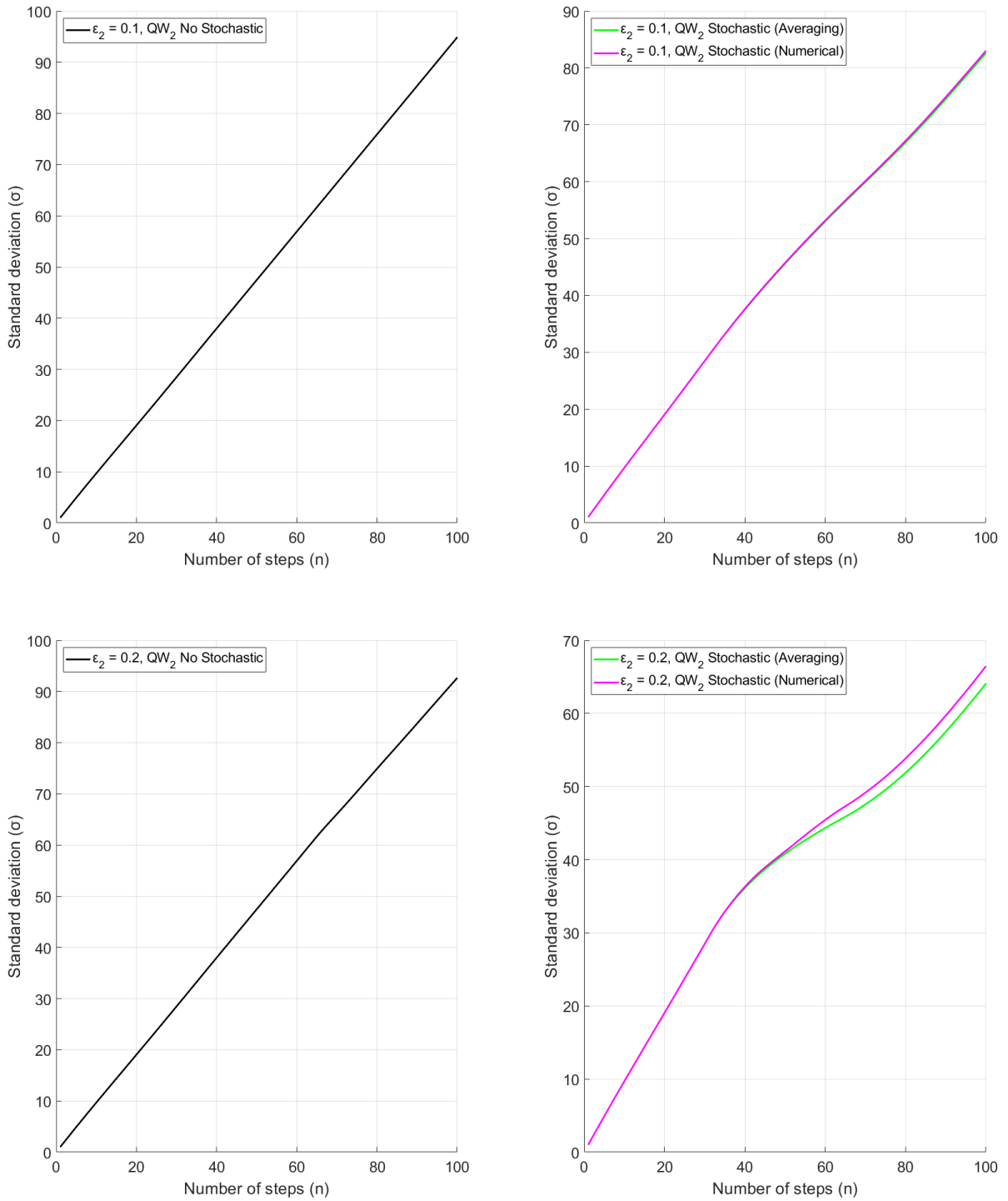


Figure 16: **Left:** Standard deviation vs number of steps upon applying the three layers QW_1 , QW_2 , QW_3 , without stochastic noise. **Right:** Standard deviation vs number of steps upon applying the three layers QW_1 , QW_2 , QW_3 , with stochastic noise on the second layer QW_2 , in the form of random dichotomic variable $s \in \{\pm 1\}$ with equal probability $p_{\pm} = \frac{1}{2}$ (green) and stochastic averaging (magenta). **Top:** $n_1 = n_2 = n_3 = 33$, $\epsilon_1 = \epsilon_2 = \epsilon_3 = 0.1$. Given these values, from the crossover equation we obtain $n^* = 100 > n_2 = 33$, so the layer isn't thick enough for the transition to occur. **Bottom:** $n_1 = n_2 = n_3 = 33$, $\epsilon_1 = \epsilon_3 = 0.1$ and $\epsilon_2 = 0.2$. Given these values, from the crossover equation we obtain $n^* = 25 < n_2 = 33$, so the layer is thick enough for the transition to occur.

Another interesting experiment, of similar approach, is to send the particle through more than one opening, corresponding to more than one initial walker positions. Our example has two initial walker positions $x_{init} = \pm 10$, $p_{\pm} = \frac{1}{2}$. As observed in fig. 17 fig. 18, fig. 19, and fig. 20 the basic behaviour of the QW still remains, though with the extra peaks driven by the initial positions.

Again, starting from the initial QW theoretical model (fig. 17) giving a pure double (in this case quadruple) horn distribution, an experimental measurement like that on the left of fig. 18 joins the game. An update on our QW theory is needed to obtain the right plots that can explain the bumps in-between the now quadruple horns. These right plots are achieved by introducing the stochastic noise in the middle layer QW_2 , and can determine the existence or not of the hidden random layer.

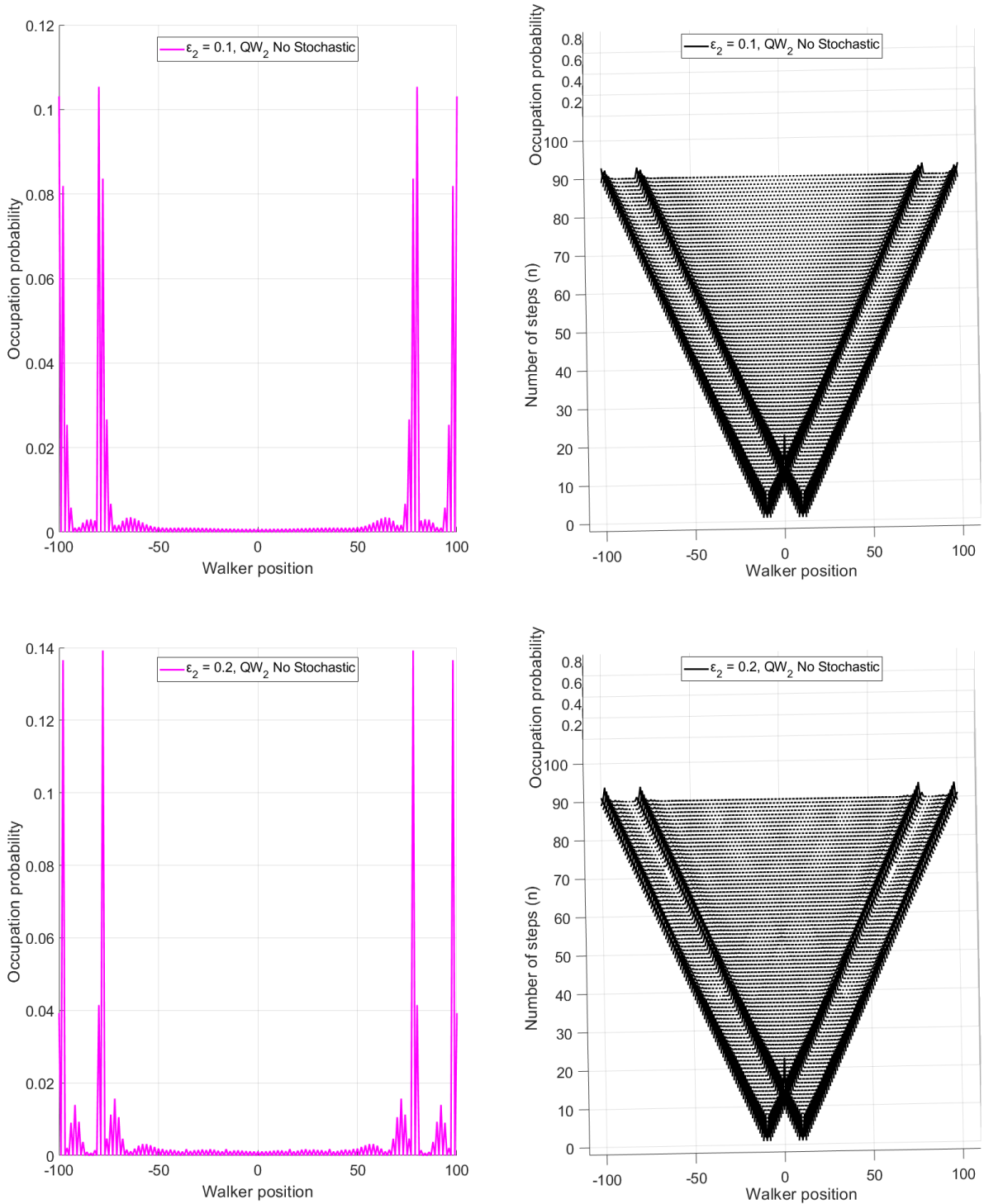


Figure 17: *QW* runs with starting walker positions ± 10 with equal probability $p_{\pm} = \frac{1}{2}$. **Left:** Occupation probability vs walker position final step profile after applying the three layers QW_1, QW_2, QW_3 , without stochastic noise. **Right:** Number of steps vs walker position vs occupation probability 3-D profile during the evolution of the three layers QW_1, QW_2, QW_3 , without stochastic noise. **Top:** $n_1 = n_2 = n_3 = 33$, $\epsilon_1 = \epsilon_2 = \epsilon_3 = 0.1$. Given these values, from the crossover equation we obtain $n^* = 100 > n_2 = 33$, so the layer isn't thick enough for the transition to occur. **Bottom:** $n_1 = n_2 = n_3 = 33$, $\epsilon_1 = \epsilon_3 = 0.1$ and $\epsilon_2 = 0.2$. Given these values, from the crossover equation we obtain $n^* = 25 < n_2 = 33$, so the layer is thick enough for the transition to occur.

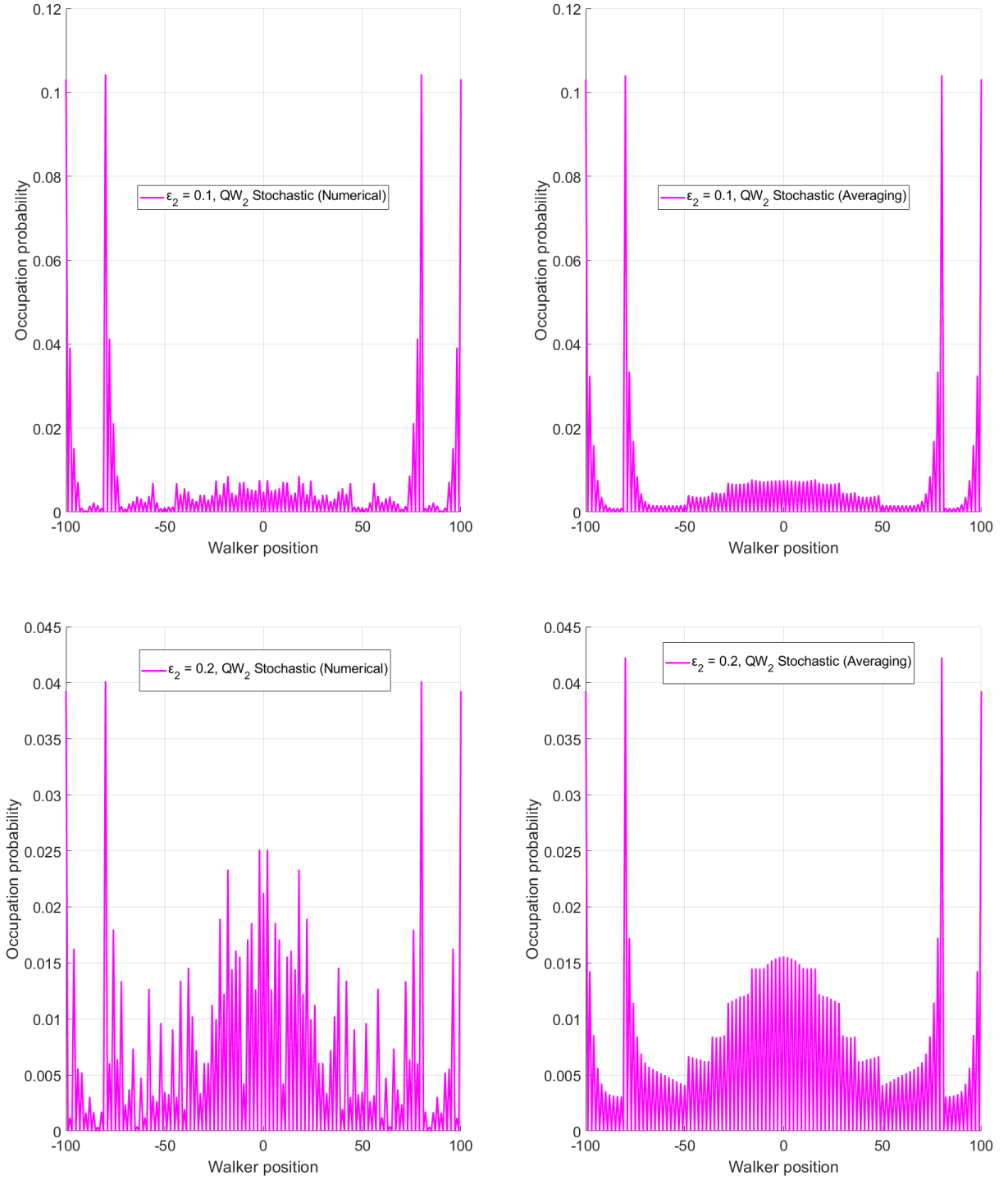


Figure 18: *QW runs with starting walker positions ± 10 with equal probability $p_{\pm} = \frac{1}{2}$. **Left:** Occupation probability vs walker position final step profile after applying the three layers QW_1, QW_2, QW_3 , with stochastic noise in the form of random numerical values of the dichotomic variable $s \in \{\pm 1\}$ with equal probability $p_{\pm} = \frac{1}{2}$ on the middle layer QW_2 . **Right:** Occupation probability vs walker position final step profile after applying the three layers QW_1, QW_2, QW_3 , with stochastic noise in the form of stochastic averaging on the middle layer QW_2 . **Top:** $n_1 = n_2 = n_3 = 33$, $\epsilon_1 = \epsilon_2 = \epsilon_3 = 0.1$. Given these values, from the crossover equation we obtain $n^* = 100 > n_2 = 33$, so the layer isn't thick enough for the transition to occur. **Bottom:** $n_1 = n_2 = n_3 = 33$, $\epsilon_1 = \epsilon_3 = 0.1$ and $\epsilon_2 = 0.2$. Given these values, from the crossover equation we obtain $n^* = 25 < n_2 = 33$, so the layer is thick enough for the transition to occur.*

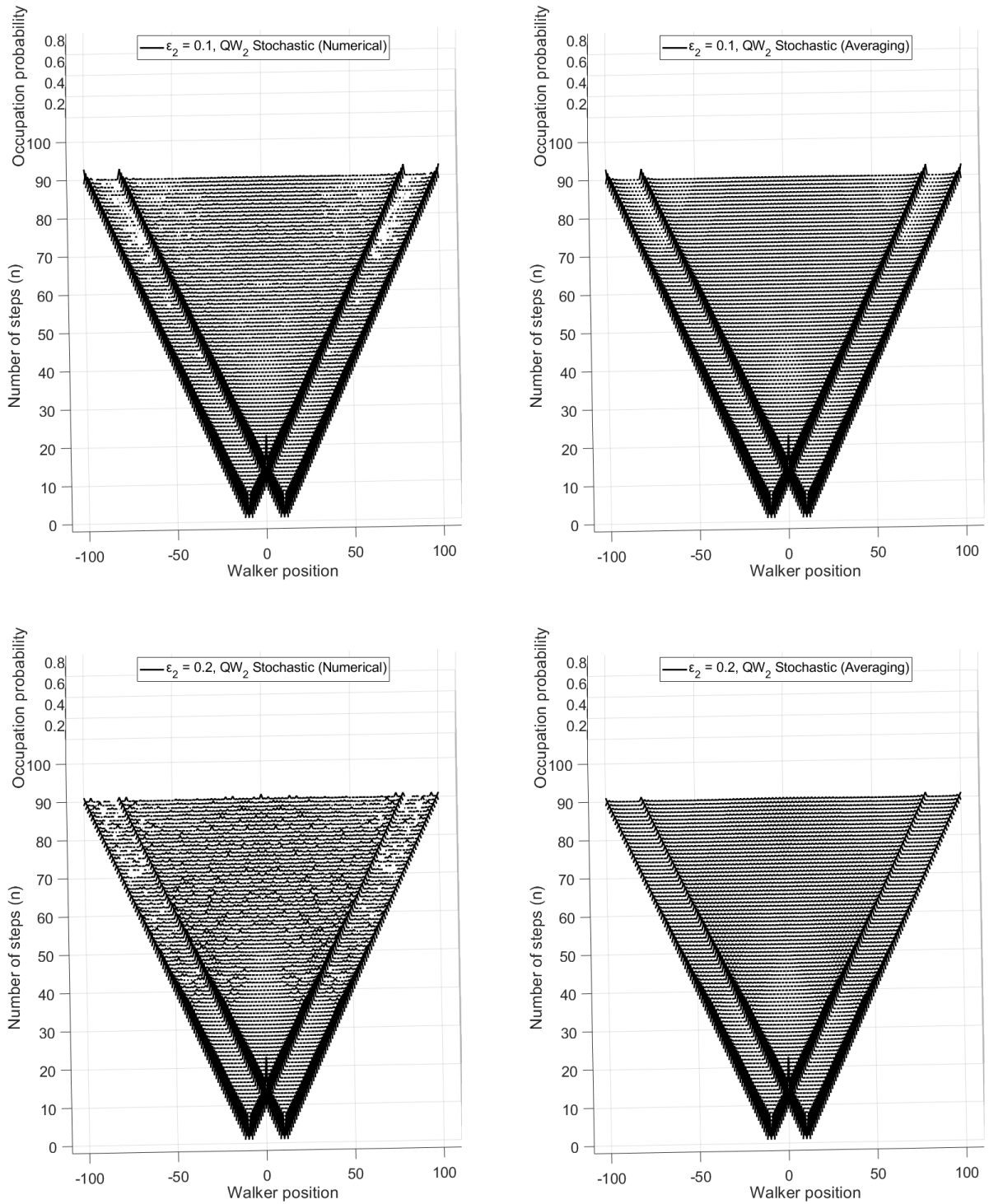


Figure 19: *QW* runs with starting walker positions ± 10 with equal probability $p_{\pm} = \frac{1}{2}$. **Left:** Number of steps vs walker position vs occupation probability 3-D profile during the evolution of the three layers QW_1 , QW_2 , QW_3 , with stochastic noise in the form of random numerical values of the dichotomic variable $s \in \{\pm 1\}$ with equal probability $p_{\pm} = \frac{1}{2}$ on the middle layer QW_2 . **Right:** Number of steps vs walker position vs occupation probability 3-D profile during the evolution of the three layers QW_1 , QW_2 , QW_3 , with stochastic noise in the form of stochastic averaging on the middle layer QW_2 . **Top:** $n_1 = n_2 = n_3 = 33$, $\epsilon_1 = \epsilon_2 = \epsilon_3 = 0.1$. Given these values, from the crossover equation we obtain $n^* = 100 > n_2 = 33$, so the layer isn't thick enough for the transition to occur. The noise in QW_2 is applied as a stochastic average value. **Bottom:** $n_1 = n_2 = n_3 = 33$, $\epsilon_1 = \epsilon_3 = 0.1$ and $\epsilon_2 = 0.2$. Given these values, from the crossover equation we obtain $n^* = 25 < n_2 = 33$, so the layer is thick enough for the transition to occur.

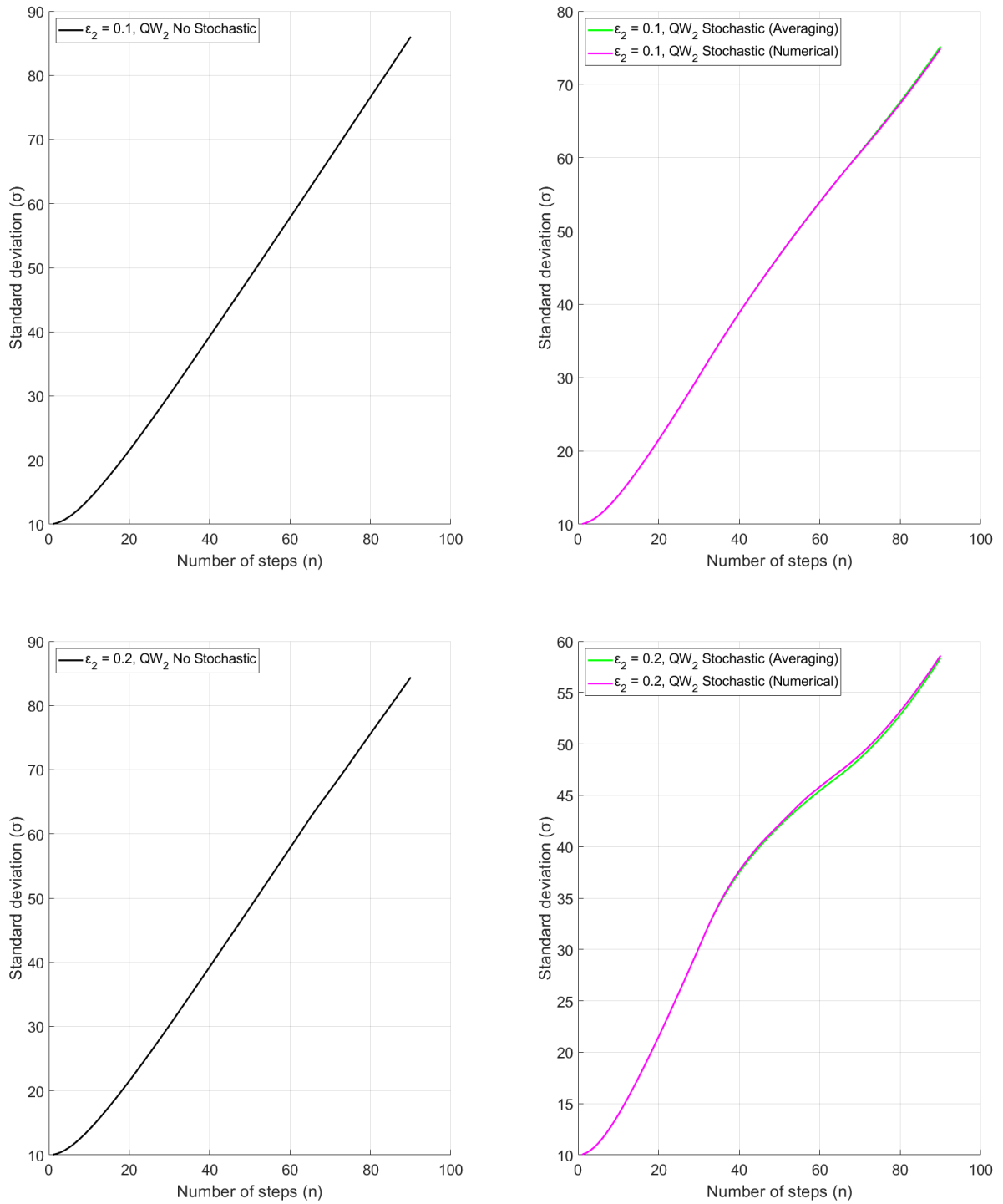


Figure 20: *QW runs with starting walker positions ± 10 with equal probability $p_{\pm} = \frac{1}{2}$. **Left:** Standard deviation vs number of steps upon applying the three layers QW_1 , QW_2 , QW_3 , without stochastic noise. **Right:** Standard deviation vs number of steps upon applying the three layers QW_1 , QW_2 , QW_3 , with stochastic noise on the second layer QW_2 , in the form of random dichotomic variable $s \in \{\pm 1\}$ with equal probability $p_{\pm} = \frac{1}{2}$ (green) and stochastic averaging (magenta). **Top:** $n_1 = n_2 = n_3 = 33$, $\epsilon_1 = \epsilon_2 = \epsilon_3 = 0.1$. Given these values, from the crossover equation we obtain $n^* = 100 > n_2 = 33$, so the layer isn't thick enough for the transition to occur. **Bottom:** $n_1 = n_2 = n_3 = 33$, $\epsilon_1 = \epsilon_3 = 0.1$ and $\epsilon_2 = 0.2$. Given these values, from the crossover equation we obtain $n^* = 25 < n_2 = 33$, so the layer is thick enough for the transition to occur.*

3.3 The χ -Model

Ellinas et al. [25], [26] talk about a case in which a single electromagnetic mode system and a single two-level atomic system interact with each other while on resonance, we name these two systems the coin system and walker system respectively, and they exist independently of this discussion and research of the walk theory. Though a completely different setup from the type of model we are interested in, we will keep the essentials of the model to employ it for our purpose. We don't emphasize the physical aspects, but we simply want to use it as a second version of this adjustable model between the classical and quantum walk, therefore instead of a unitary matrix of the walk we introduce a hamiltonian, and it's by means of this hamiltonian that it produces the unitary operator which involves both the coin and the walker system.

We will focus on the Jaynes-Cummings Model (JCM) with its resonance hamiltonian operator

$$H_{JC} = \lambda(\sigma^+ \alpha + \sigma^- \alpha^\dagger) = \lambda \begin{pmatrix} 0 & \alpha^\dagger \\ \alpha & 0 \end{pmatrix}, \quad (165)$$

where α^\dagger , α are the creation and annihilation operators of quanta of the EM field, σ^+ , σ^- act as step operators in the atomic 'quantum coin' system state space, and λ is the field-atom coupling constant, consequently if $\lambda = 0$, there exists no mixture between the coin and the walker.

The unitary evolution operator of the χ -model walk reads

$$V_{JC}(t) = e^{itH_{JC}}, \quad (166)$$

promoting an unconditional coin – walker entanglement [25], something convenient in this case, compared to the evolution operator of the kind $P_0 \otimes E_0 + P_1 \otimes E_1$, which promotes an if-else behaviour for the two measurable coin outcomes $|c\rangle \in \{|0\rangle, |1\rangle\}$.

Using the quaternion extended Euler's formula, we obtain the χ -model's reshuffling

matrix

$$\begin{aligned}
U(\chi) &= e^{i\chi\sigma_2} \\
&= \cos \chi \mathbf{1} + i \sin \chi \sigma_2 \\
&= \begin{pmatrix} \cos \chi & \sin \chi \\ -\sin \chi & \cos \chi \end{pmatrix},
\end{aligned} \tag{167}$$

in which

$$\cos \chi = \frac{1}{\sqrt{1 - \varepsilon^2}}, \tag{168}$$

and

$$\sin \chi = \frac{\varepsilon}{\sqrt{1 - \varepsilon^2}}. \tag{169}$$

If we solve eq. (168) and eq. (169) for χ , we get

$$\chi_\varepsilon = \arccos \left(\frac{1}{\sqrt{1 - \varepsilon^2}} \right), \tag{170}$$

and

$$\chi_\varepsilon = \arcsin \left(\frac{\varepsilon}{\sqrt{1 - \varepsilon^2}} \right). \tag{171}$$

This means that χ_ε is a ε driven variable, consequently, we could change the notation of the reshuffling matrix to

$$U_\varepsilon(\chi_\varepsilon) = \begin{pmatrix} \cos \chi_\varepsilon & \sin \chi_\varepsilon \\ -\sin \chi_\varepsilon & \cos \chi_\varepsilon \end{pmatrix}. \tag{172}$$

The fact that we have retained the ε -valued matrix from the previous model in this present model, means that we don't promote χ as a random variable but rather as a rotation matrix and χ becomes some angle that is determined by ε , so this model tends to a more geometrical kind. The incorporation of $U(\chi)$ in the V_{JC} evolution operator reminds us of

the forging of V_q that we were interested about in the previous model.

We choose the χ -model initial coin state to be

$$\begin{aligned}
|0; c\rangle &= \cos \chi |0\rangle + i \sin \chi |1\rangle \\
&= \begin{pmatrix} \cos \chi \\ i \sin \chi \end{pmatrix} = \begin{pmatrix} \cos \chi & -i \sin \chi \\ i \sin \chi & \cos \chi \end{pmatrix} \begin{pmatrix} 1 \\ 0 \end{pmatrix} \\
&= U(\chi) |0\rangle.
\end{aligned} \tag{173}$$

On the bell circuit shown in fig. 1, we used the Hadamard gate to create a local superposition of the input. In case, though, our input is already in a superposition, the Hadamard gate is of no need. Something similar happens in the χ -model. We can either, have the mixed coin state $|c\rangle = \cos \chi |0\rangle + i \sin \chi |1\rangle$, or we can propagate the randomness of χ in the 2×2 reshuffling matrix $U(\chi)$ later on, leaving $|c\rangle$ in a pure state e.g., $|0\rangle$, as seen in eq. (173). Both cases present an entangled coin and walker state, speeding up the diffusion.

With an initial walk state $|0; w\rangle$, the evolution of the combined system reads

$$|0; c\rangle \otimes |0; w\rangle \xrightarrow{V_{JC}} V_{JC}(t) |0; c\rangle \otimes |0; w\rangle \tag{174}$$

$$= V_{JC}(t) (U(\chi) |0\rangle \otimes \mathbf{1}_w) \otimes |0; w\rangle \tag{175}$$

$$= V_{JC}(t) (U(\chi) \otimes \mathbf{1}_w) (|0\rangle \otimes |0; w\rangle). \tag{176}$$

In density matrix formalism

$$\rho_w^{(0)} = |0\rangle \langle 0|, \tag{177}$$

and

$$\rho_c^{(0)} = |c\rangle \langle c| = U(\chi) |0\rangle \langle 0| U(\chi)^\dagger. \tag{178}$$

Again, we can interpret the total system with or without the reshuffling matrix $U(\chi)$.

Is this a QW?

Yes! The reason is that we can identify the two systems as if they are one system for the coin and one system for the walker with the coin reshuffling matrix $U(\chi)$ affecting only the coin system, and the evolution operator V_{JC} which acts on the total system.

We can now proceed on calculating the SD with the same steps as in the ε -model. Because the evolution operator V_{JC} is slightly more complicated than the V_{cl} in the ε -model, this new SD is going to have extra parameters, of which only two are important, the time spent in the cavity, and the mixing angle introduced in the new reshuffling matrix. Also, because this model runs in the continuous time domain, we transform the discrete number of steps n into continuous time t or we could use a switchable continuous time, stroboscopically.

The first optical cavity transforms $\rho_c = |c\rangle\langle c|$ to $\mathcal{E}_U(\rho_c)$. If we choose $|0; c\rangle$ such that $|0; c\rangle = \cos \chi |0\rangle + i \sin \chi |1\rangle$, we obtain the mixed coin state

$$\begin{aligned} \mathcal{E}_U(\rho_c) &= \frac{1}{2} \mathbf{1} + \frac{1}{2} \sin(2\chi) \cos(\lambda \eta t) \cos(\lambda \theta t) \sigma_2 \\ &\quad + \frac{1}{2} [\cos(2\lambda \eta t) \cos^2 \chi - \cos(2\lambda \theta t) \sin^2 \chi] \sigma_3. \end{aligned} \quad (179)$$

To solve the dynamic of the problem, we must calculate the n -th (or t -th), power of this χ -model walk, and we do this through the $|\phi\rangle$ base using the characteristic function

$$\begin{aligned} h(\phi; \chi, t) &= (-\cos(2\lambda t \eta) \cos^2 \chi + \cos(2\lambda t \theta) \sin^2 \chi) \cos(2\phi) \\ &\quad + (\sin(2\chi) \cos(\lambda t \eta) \cos(\lambda t \theta)) \sin(2\phi). \end{aligned} \quad (180)$$

In order to evaluate the limit PDF, we reshape the last equation, with the use of

trigonometric identities, as

$$h(\phi; \chi, t) = C(\chi, t) \cos(2\phi - \Lambda(\chi, t)), \quad (181)$$

with our newly defined variables being

$$A(\chi, t) = -\cos(2\lambda t \eta) \cos^2 \chi + \cos(2\lambda t \theta) \sin^2 \chi, \quad (182)$$

$$B(\chi, t) = \sin(2\chi) \cos(\lambda t \eta) \cos(\lambda t \theta), \quad (183)$$

$$C(\chi, t) = \sqrt{A(\chi, t)^2 + B(\chi, t)^2}, \quad (184)$$

$$\Lambda(\chi, t) = \frac{B(\chi, t)}{A(\chi, t)}. \quad (185)$$

For simplicity, we can set

$$y = h(\phi; \chi, t), \quad (186)$$

so that we get $h'(h^{-1}(y)) = -2\sqrt{C(\chi, t)^2 - y^2}$ resulting in the limit PDF

$$\begin{aligned} P(y; \chi, t) &= \frac{1}{2\pi|h'(h^{-1}(y))|} \\ &= \frac{1}{\pi\sqrt{C(\chi, t)^2 - y^2}}, \quad -1 \leq y \leq 1 \end{aligned} \quad (187)$$

which is nothing else than the occupation probability of the integer node sites, but now represented as sites on a circle.

Supposedly we could calculate the probabilities for every $|\phi\rangle$, but the walk is still within the discrete basis $|n\rangle$. We can Fourier transform the system so that the integer index becomes an angle, e.g., $\phi \in [0, 2\pi]$, or we can Z transform to go to $h(\phi; \chi, t)$. So we have a walk that, instead of spreading out on integers, it spreads around a circle. Because of the ease of integral transformations, we change domain, calculate easier, and return if needed.

We have now transformed $n \rightarrow \phi$ and from eq. (181), and eq. (186) we obtain

$$y = C(\chi, t) \cos(2\phi - \Lambda(\chi, t)), \quad (188)$$

for a second system transformation $\phi \rightarrow y$. We can say $y \in [-C, +C]$ is a time-dependent pseudo angle with an enhanced value range.

Because the walk evolves through time, to find the probability distribution for a given site, we should now also include the question ‘for which time instance?’. At some point in the far asymptotic limit, there exists an asymptotic behaviour, something like a transient state, and after that, we go to an asymptotic state which does not change (think of a drop of paint in a glass of water, the water turns blue and then stays blue, Brownian motion). At that point the distribution becomes continuous, and there is no point in talking for discrete sites.

The base change with the Z transform is not only for our ease of use, but is also helpful to understand the model on its physical aspect. Because $C(\chi, t)$ is time dependant, for different time values, we may find y in different positions with various probabilities. Now we are interested in defining the value range of y .

E.g., if $y \in [-5, 5]$, what is the probability of hitting that range?

The relationship

$$\int_{-1}^1 \frac{dy}{\sqrt{1-y^2}} = \int_{-|C(\chi, t)|}^{|C(\chi, t)|} \frac{dy}{\sqrt{C(\chi, t)^2 - y^2}}, \quad (189)$$

between the limit distribution of the walk without the driving cavity, and the same one with the driving cavity present, shows that when $C(\chi, t)$ is not zero, the QW asymptotics are robust to the changes caused by the modified coin system, up to a scaling.

Because $A(\chi, t)$ and $B(\chi, t)$ themselves, depend also on the angle χ and λ , $C(\chi, t)$ holds inside all these dependencies, so instead of observing the left member of eq. (189) with $y \in [-1, 1]$, we can observe the rescaled variable where y is divided with $C(t)$ and

now $y \in [-C, +C]$. The scaling explicitly refers to the changes $y(\chi, t) \rightarrow \frac{y(\chi, t)}{|C(\chi, t)|}$, $(-1, 1) \rightarrow (-|C(\chi, t)|, |C(\chi, t)|)$ in the limit random variable and its interval of values, respectively.

Do we need to observe the original y or its scaled alter-ego?

The statistical moments derived by the new distribution are now time dependent; e.g., the first moment reads

$$\begin{aligned}\mu &= \lim_{n \rightarrow \infty} \left\langle \frac{L}{n} \right\rangle_n \\ &= \int_0^{2\pi} h(2\phi; \chi, t) \frac{d\phi}{2\pi} \\ &= 0,\end{aligned}\tag{190}$$

so the walk remains unbiased, while the second moment reads

$$\begin{aligned}\sigma(\chi, t)^2 &= \lim_{n \rightarrow \infty} \left\langle \left(\frac{L}{n} \right)^2 \right\rangle_n \\ &= \int_0^{2\pi} h(2\phi; \chi, t) h(\phi; \chi, t)^2 \frac{d\phi}{2\pi} \\ &= \frac{C(\chi, t)^2}{2}.\end{aligned}\tag{191}$$

The influence of the first cavity is now expressed by the double dependence of the distribution, first on the time spend in the cavity, i.e., the coin-field interaction time, and second on the initial coin state by means of the dependence of $C(\chi, t)$, via $A(\chi, t)$ and $B(\chi, t)$, on the angle χ of the coin vector.

To further probe the behaviour of the QW and especially the influences upon the asymptotics of the driving cavity, we first note that for $t = 0$, that is in the absence of the first cavity, the characteristic function h depends on the initial state of the quantum coin system by means of its angle χ , i.e., $h(\phi; \chi, 0) = -\cos(2\phi + 2\chi)$. However, the dependence does not show up in the asymptotic regime since its probability distribution $P(y) = \frac{1}{\pi\sqrt{1-y^2}}$

([25]) appears to have a universal character, and is independent of the initial coin state, provided it is of the form considered here.

On the other hand, as eq. (180), eq. (187) indicate in the case where there is a first cavity present, the dependence of the characteristic function on the initial coin state survives in the asymptotic regime of the χ -model. Indeed, by inspection of the functions $A(\chi, t)$, $B(\chi, t)$ and, $C(\chi, t)$ as given above, we see that they do depend on the χ angle, and this dependence harbours the possibility of controlling the asymptotic statistics of the walk.

For certain values of t , as shown below

$$t = \left\{ \frac{(2k+1)\pi}{4\lambda\eta}, \frac{(2k+1)\pi}{4\lambda\theta}, \frac{(2k+1)\pi}{4\lambda\eta}, \frac{(2k+1)\pi}{4\lambda\theta} \right\}, \quad k \in \mathbb{Z} \quad (193)$$

we enforce

$$A(\chi, t) = 0. \quad (194)$$

For certain values of χ , as shown below

$$\chi = \left\{ 0, \frac{\pi}{2}, \pi, \frac{3\pi}{2} \right\}, \quad (195)$$

we enforce

$$B(\chi, t) = 0, \quad \forall t. \quad (196)$$

For $A(\chi, t) = 0$ and $B(\chi, t) = 0$ we also get $C(\chi, t) = 0$. Then, the aforementioned χ, t values force the coin density matrix to a couple of different combinations with their appropriate interaction times, viz

$$\rho_c = |0\rangle\langle 0|, \quad t = \frac{(2k+1)\pi}{4\lambda\eta}, \quad (197)$$

and

$$\rho_c = |1\rangle\langle 1|, \quad t = \frac{(2k+1)\pi}{4\lambda\theta}. \quad (198)$$

As we can see in the bottom plots of fig. 21, the left valley, occurring for the first and third χ values of eq. (195), can be found from eq. (197), while the right valley, occurring for the second and fourth χ values of eq. (195), can be found from eq. (198).

If each of these two conditions occur, we say that a *resonance condition* arises in the first cavity between the field and the two-level atom.

The resonance condition implies that the standard deviation becomes zero, hence the limit PDF collapses, and more importantly that $\langle L^2 \rangle_n \sim n$, so we lose the quadratic diffusion time speed up, characterizing the quantum random walk. In such a case, the asymptotic behaviour of the standard deviation agrees with that of a classical random walk.

In the ε -model, by applying different ε values, we obtain various SD values and behaviours. In the χ -model case, while the SD depends crucially on the resonance function $C(\chi, t)$, in the long term, the QW asymptotics ‘wash out’ the variable χ_{JC} obtaining the limit PDF behaviour. This reminds us of the first model, while there existed a strong dependence from the step index n , and the noise strength value ε , in the long term, the QW spread turned sub-ballistic, regardless of the ε value. The second moment of both models, portrayed in eq. (155) and eq. (191), prove this resemblance.

We can see that the resonance function $C(\chi, t)$ behaves like the crossover function in eq. (161).

These two models are manifestations of something more general.

We claim this SD variety, created by manipulation of specific variables, is the *Quantum – Classical Transition* [20], [21].

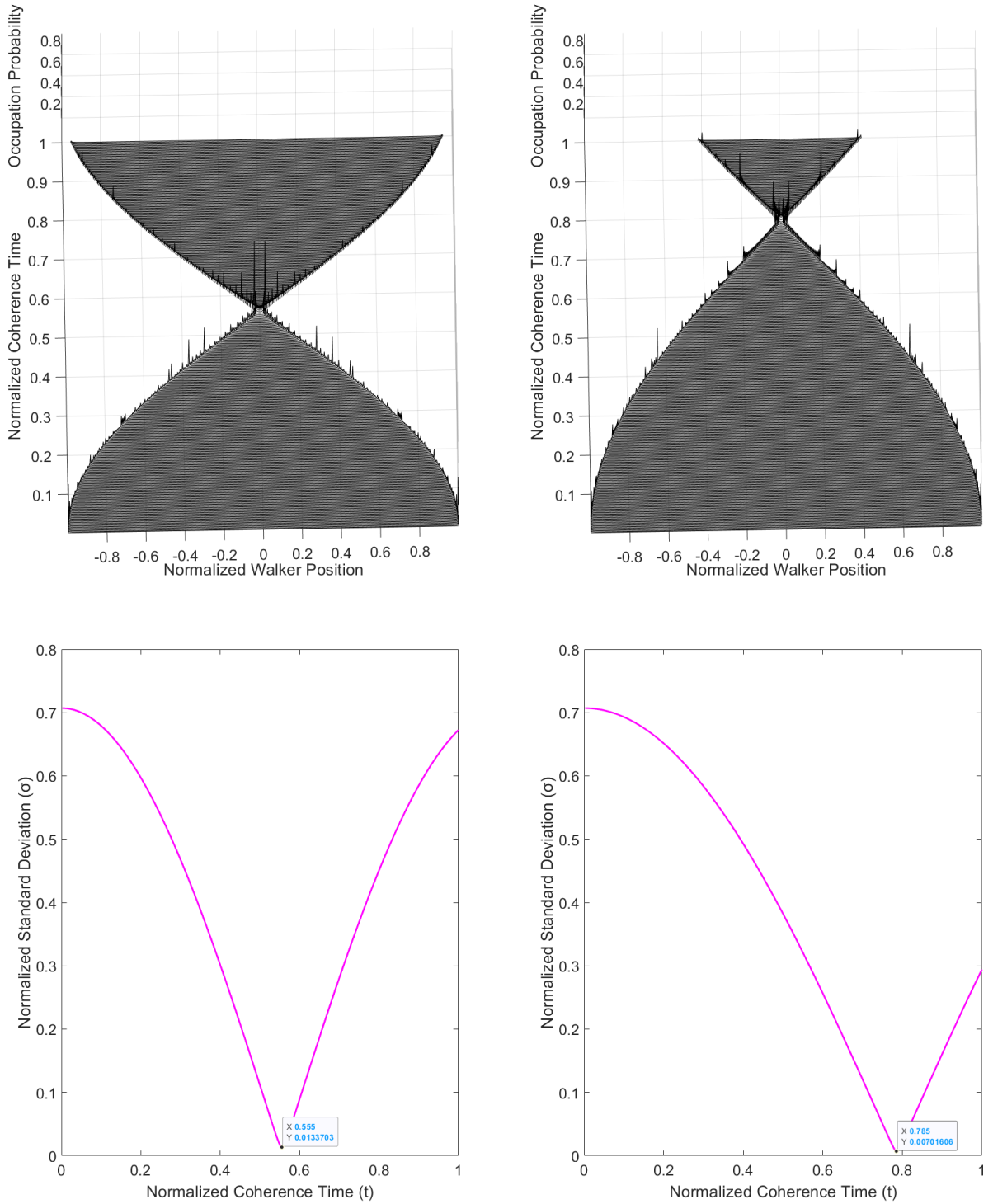


Figure 21: **Top:** Occupation probability vs normalized walker position vs normalized coherence time 3-D asymptotic profile for a time interval of 400, with the number of steps at each run being maxed-out. **Bottom:** Normalized standard deviation vs normalized coherence time in the asymptotic regime. The data tip labels show the lowest points of the σ curve. The time, for which we have the lowest σ , can be seen in the top figures, where the pinching of the hourglass happens and may remind us of the CRW diffusion rate opposed to the expanded limits for normalized coherence time $t = 0$ with maximum σ giving a similar approach of the QW diffusion. This means that the σ varies according to key parameters, reminding us of the $Q - C$ transitions mentioned in the ε -model. **Left:** Vector entry angle $\chi \in \{0, \pi\}$ (same behaviour for both values). **Right:** Vector entry angle $\chi \in \{\frac{\pi}{2}, \frac{3\pi}{2}\}$ (same behaviour for both values). The rest parameters are set to $k = 0$, $\lambda = 1$, $\eta = \sqrt{2}$, $\theta = 1$ for both cases of the vector entry angle.

Conclusion

We investigated the QW's Q – C transition phenomenon with two mathematical models, one theoretical, designed ad hoc for this purpose and one which exists regardless of this subject and was applied usefully here by exploiting some of its parameters.

Firstly, in order to transform the CRW to a QW, we displayed the U and \mathcal{E} walk quantization rules. These refer to the integration of a reshuffling matrix to the mathematical model of the already known CRW.

Following this, we simulated the behaviour of a basic discrete time QW, so we could have a visual perspective of the subject. Key variables are the number of steps n , and the noise strength value ε infused in the reshuffling matrix. The reshuffling matrix's off-diagonality and noise strength terms were correlated in a way that opposes our intuition about the QW behaviour. With statistical analysis, we exposed the second moment of the QW in order to specify the crossover equation for which the transition occurs, that is $N\varepsilon^2 \approx 1$.

Next, we worked up the mathematical background of the physical QW implementation driven by an optical cavity. We exposed several variables of the model, with two of them playing an important role in the transition. The coherence time t of a beam spent in the cavity and the beam's entry vector angle χ expressing the amount of correlation between the model's coin and walker elements, fluctuating the system's entanglement. Last in this model, we analysed the behaviour of the cavity's resonance levels with the use of $C(\chi, t)$, a variable relative to the SD of the model's QW.

Finally, we demonstrated a brief, potential real world, problem in which a particle passing through a set of layers, one of which was exposed to noise factors, altered the behaviour of the particle passing through promoting classical characteristics in the final experimental measurement. The detection of a hidden random layer was achieved by

exploiting the stochastic noise introduced in the ε -model and its Q – C transitions.

The level of importance of this matchmaking, between the given models, gives an optimistic perspective for future implementation of this very useful random walk phenomenon.

Appendix A Appendix

A.1 The Adjoint Action

The adjoint action [18] of an arbitrary matrix A is described as

$$Ad(A)X = AXA^\dagger. \quad (199)$$

The adjoint action of the product AB of two arbitrary matrices A and B is

$$Ad(AB)X = Ad(A)Ad(B)X, \quad (200)$$

also, the power k of an adjoint action of A is

$$Ad^k(A)X = Ad(A^k)X. \quad (201)$$

A.2 Euclidean Group $E(2)$

Let the operator position L and the step operators E_{\pm} satisfying the commutation relations of the Euclidean algebra [17], [27]

$$E(2) \equiv ISO(2) = span\{L, E_+, E_-\}, \quad [L, E_{\pm}] = \pm E_{\pm}, \quad [E_+, E_-] = 0. \quad (202)$$

If the phase operator $\hat{\Phi}$ is defined from the relation $E_{\pm} = e^{\pm i\hat{\Phi}}$, then the phase-position operators satisfy the canonical algebra $[L, \hat{\Phi}] = i\mathbf{1}$.

There are two irreducible representations of Euclidean algebra generators carried out by vector spaces H_w and H_w^* which are respectively the eigenspace of position operator L and of unitary step operators E_{\pm} as well as of Hermitian phase operator $\hat{\Phi}$. The latter are inter-related as $E_{\pm} = e^{\pm i\hat{\Phi}}$.

Explicitly, the two vector spaces are **(a)** the Hilbert space

$$H_w = l_2(\mathbb{Z}), \quad (203)$$

and its discrete spanning set of vectors $span\{|m\rangle\}_{m \in \mathbb{Z}}$, forming an orthogonal ($\langle m|m'\rangle = \delta_{mm'}$) and complete ($\sum_{m \in \mathbb{Z}} |m\rangle \langle m| = \mathbf{1}_{H_w}$) basis, and **(b)** its dual space

$$H_w^* = L_2\left([0, 2\pi), \frac{d\phi}{2\pi}\right), \quad (204)$$

with its continuous spanning set of vectors $\{|\phi\rangle; \phi \in [0, 2\pi), \frac{d\phi}{2\pi}\}$, forming a generalized orthogonal ($\langle \phi|\phi'\rangle = \delta(\phi - \phi')$) and complete ($\int_0^{2\pi} |\phi\rangle \langle \phi| \frac{d\phi}{2\pi} = \mathbf{1}_{H_w^*}$) basis, inter-related as

$$|\phi\rangle = \sum_{m \in \mathbb{Z}} e^{i\phi m} |m\rangle, \quad (205)$$

and

$$|m\rangle = \int_0^{2\pi} e^{-i\phi m} |\phi\rangle \frac{d\phi}{2\pi}. \quad (206)$$

The respective differential representations of the generators in the continuous basis are

$$E_{\pm} |\phi\rangle = e^{\pm i\phi} |\phi\rangle, \quad (207)$$

and

$$L |\phi\rangle = \frac{1}{i} \frac{\theta}{\theta\phi} |\phi\rangle. \quad (208)$$

The corresponding generators in the discrete basis are

$$E_{\pm} |m\rangle = |m \pm 1\rangle, \quad (209)$$

and

$$L |m\rangle = m |m\rangle. \quad (210)$$

A.3 Discrete Time Fourier Transform

A discrete time Fourier transform is part of the family of Fourier transforms. It transforms a function $f(n)$ of a discrete time variable $n \in \mathbb{Z}$ into a continuous, periodic spectrum $F(\omega)$ [17]. Let $f : \mathbb{Z} \rightarrow \mathbb{C}$ be a complex function over the integers, then its discrete Fourier transform $\mathcal{F} : [-\pi, \pi] \rightarrow \mathbb{C}$ is given by

$$\mathcal{F}\{f(n)\} = F(\omega) = \sum_{n=-\infty}^{\infty} f(n)e^{-j\omega n}. \quad (211)$$

The inverse discrete time Fourier transform is defined as the process of finding the discrete time sequence $f(n)$ from its frequency response $F(\omega)$ as

$$f(n) = \frac{1}{2\pi} \int_{-\pi}^{\pi} F(\omega)e^{j\omega n} d\omega. \quad (212)$$

A.4 Qiskit QW Circuit Implementation

A basic QW circuit implementation using qiskit is given in fig. 22. This model uses 3 walker space qubits (q_0, q_1, q_2) and one coin qubit (q_3) for the total system setup. The measurement is projected onto the 3 *walker* bits of classical information representing in binary the four odd occupation sites ($001_2 = 1_{10}, 011_2 = 3_{10}, 101_2 = 5_{10}, 111_2 = 7_{10}$) [28], [29].

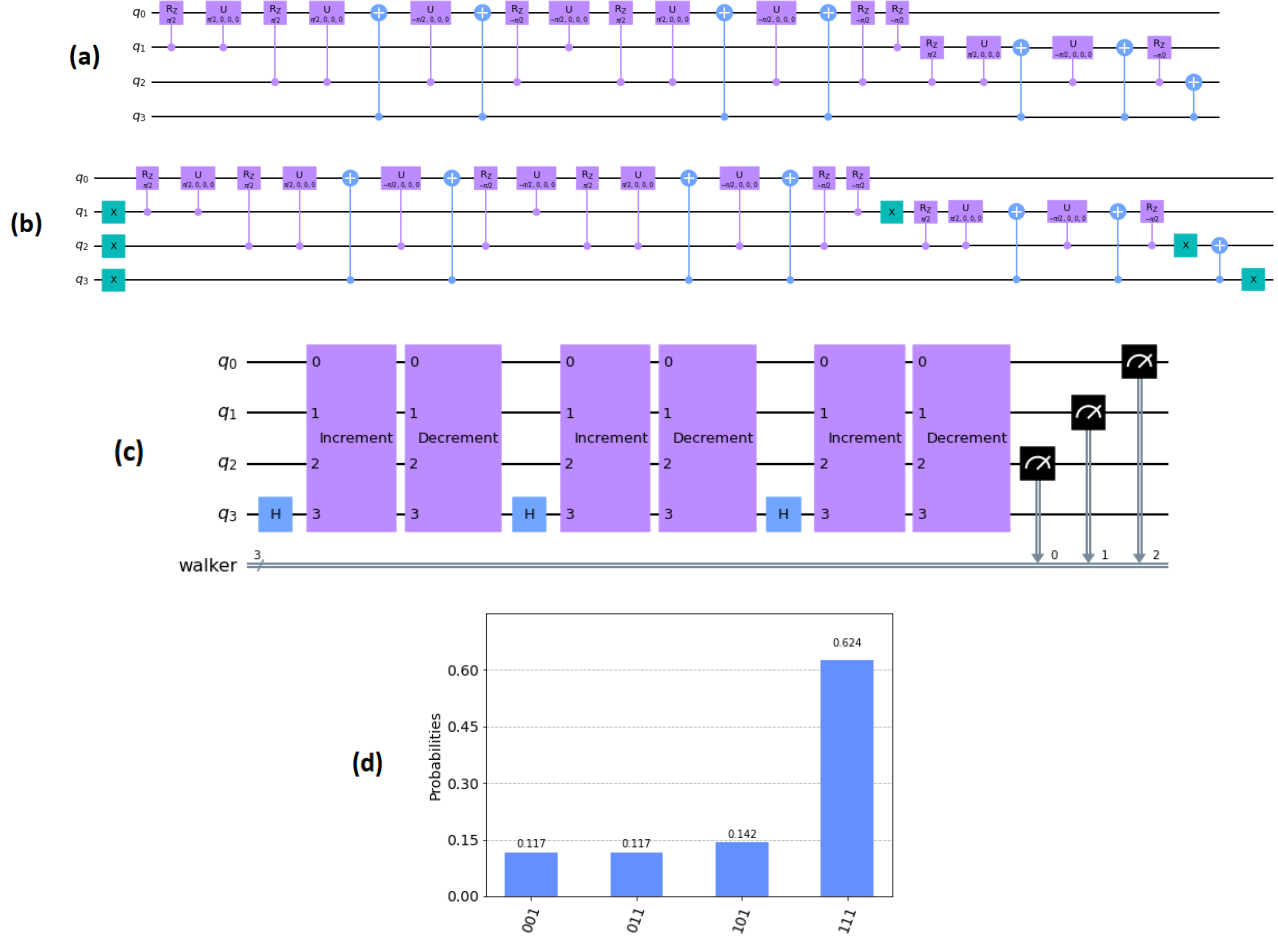


Figure 22: (a): Explicit increment circuit implementation in its purest form. The circuit consists of control not gates with one target qubit and control qubits corresponding to the number of walker qubits underneath the target qubit. Because qiskit has no intrinsic control-not gate for more than 2 qubits, a custom one was made consisting of Z and $\frac{\pi}{2}$ rotations. (b): Explicit decrement circuit implementation in its purest form. The gate setup is related to that of the increment circuit, with the sole difference being the not-gates at the beginning and at the end of the decrement function of each qubit respectively, indicating the inversion of the increment circuit function. (c): QW circuit implementation, with the increment and decrement circuits now represented as black boxes. The Hadamard gate, acted on the coin qubit q_3 , creates the superposition which will then be dispersed on the walker qubits through the increment & decrement gates to provide quantum characteristics. (d): Occupation probability vs walker position after a measurement of 3 QW steps. The even binary positions are not displayed because they have zero occupation probability, trivial.

```

import math
import numpy as np
from qiskit import *
from qiskit.circuit.library import MCMT
from qiskit.tools.monitor import job_monitor
from qiskit.visualization import plot_histogram
aer_sim = Aer.get_backend('qasm_simulator')

pi = math.pi
q = QuantumRegister(4,'q')
cw = ClassicalRegister(3,"walker")
qc = QuantumCircuit(q, cw)

# Custom multiple control not gate
def cnx(qc, *qubits):
    if len(qubits) >= 3:
        last = qubits[-1]
        # A matrix: (made up of Z and n/2 rotations)
        qc.crz(np.pi/2, qubits[-2], qubits[-1])
        qc.cu(np.pi/2, 0, 0, 0, qubits[-2],qubits[-1])

        # Control not gate
        cnx(qc,*qubits[:-2],qubits[-1])

        # B matrix (opposite angle)
        qc.cu(-np.pi/2, 0, 0, 0, qubits[-2], qubits[-1])

        # Control not gate
        cnx(qc,*qubits[:-2],qubits[-1])

        # C matrix (final rotation)
        qc.crz(-np.pi/2,qubits[-2],qubits[-1])
    elif len(qubits)==3:
        qc.ccx(*qubits)
    elif len(qubits)==2:
        qc.cx(*qubits)

# Increment circuit for cyclical crossing
increment_circuit = QuantumCircuit(4, name = "Increment")
cnx(increment_circuit,q[3],q[2],q[1],q[0])
cnx(increment_circuit,q[3],q[2],q[1])
cnx(increment_circuit,q[3],q[2])
custom_increment = increment_circuit.to_instruction()

display(increment_circuit.draw(output = 'mpl'))

# Decrement circuit for cyclical crossing
decrement_circuit = QuantumCircuit(4, name = "Decrement")
decrement_circuit.x(q[3])
decrement_circuit.x(q[2])
decrement_circuit.x(q[1])
cnx(decrement_circuit,q[3],q[2],q[1],q[0])
decrement_circuit.x(q[1])
cnx(decrement_circuit,q[3],q[2],q[1])
decrement_circuit.x(q[2])
cnx(decrement_circuit,q[3],q[2])
decrement_circuit.x(q[3])
custom_decrement = decrement_circuit.to_instruction()

display(decrement_circuit.draw(output = 'mpl'))

def runQWC(qc, times):
    for i in range(times):
        qc.h(q[3])
        qc.append(custom_increment, [0,1,2,3])
        qc.append(custom_decrement, [0,1,2,3])
    return qc

for step in range(1,4):
    # Display histograms for 1-4 steps
    qc = QuantumCircuit(q, cw)
    ys = ('000':[], '001':[], '010':[], '011':[], '100':[], '101':[], '110':[], '111':[])

    #qc.x(2) # Starting walker position
    #qc.x(1) # Starting walker position
    #qc.x(0) # Starting walker position

    qc = runQWC(qc, step)
    qc.measure([2,1,0], [0,1,2]) # Inverse matching for better histogram understanding

    display(qc.draw(output = 'mpl'))

    print('\nExecuting job for step =',step,'...\n')
    tx = transpile(qc, aer_sim)
    qobj = assemble(tx)
    results = aer_sim.run(qobj).result()
    counts = results.get_counts()

    for i,state in enumerate(ys.keys()):
        try:
            ys[state].append(counts[state])
        except KeyError:
            ys[state].append(0)

    for i,state in enumerate(ys.keys()):
        ys[state] = sum(ys[state])

    display(plot_histogram(ys))

```

Figure 23: Qiskit code for the implementation of the circuits in fig. 22

References

- [1] J. Kempe, “Quantum random walks – an introductory overview,” 2008.
- [2] Y. Aharonov, L. Davidovich, and N. Zagury, “Quantum random walks,” *Physical Review A*, vol. 48, no. 2, p. 1687, 1993.
- [3] N. Shenvi, J. Kempe, and K. B. Whaley, “A quantum random walk search algorithm,” *Physical Review A*, vol. 67, no. 5, p. 052307, 2003.
- [4] D. Aharonov, A. Ambainis, J. Kempe, and U. Vazirani, “Quantum walks on graphs,” *Proceedings of ACM Symposium on Theory of Computation (STOC’01)*, vol. 41, no. 7, pp. 50–59, 2001.
- [5] A. M. Childs and J. Goldstone, “Spatial search by quantum walk,” *Physical Review A*, vol. 70, no. 022314, 2004.
- [6] E. Farhi and S. Gutmann, “Quantum computation and decision trees,” *Physical Review A*, vol. 58, no. 915, 1998.
- [7] A. M. Childs, R. Cleve, E. Deotto, E. Farhi, S. Gutmann, and D. A. Spielman, “Exponential algorithmic speedup by quantum walk,” *Proc. 35th ACM Symposium on Theory of Computing*, pp. 59–68, 2002.
- [8] A. Ambainis, E. Bach, A. Nayak, A. Vishwanath, and J. Watrous, “One-dimensional quantum walks,” *STOC ’01: Proceedings of the thirty-third annual ACM symposium on Theory of computing*, pp. 37–49, 2001.
- [9] T. A. Brun, H. A. Carteret, and A. Ambainis, “Quantum random walks with decoherent coins,” *Physical Review A*, vol. 67, no. 032304, 2003.
- [10] N. Konno, “Quantum random walks in one dimension,” *Quantum Information Processing*, vol. 1, no. 5, pp. 345–354, 2002.
- [11] V. Kendon and B. Tregenna, “Decoherence can be useful in quantum walks,” *Physical Review A*, vol. 67, no. 042315, 2003.
- [12] D. Ellinas and I. Smyrnakis, “Quantization and asymptotic behaviour of evk quantum random walk on integers,” *Physica A: Statistical Mechanics and its Applications*, vol. 365, no. 1, pp. 222–228, 2006.
- [13] G. Moutzianou, “Quantum walk on integers and maximum likelihood parametric estimation,” *Technical University of Crete, School of ECE*, 2013.

- [14] A. M. Childs, E. Farhi, and S. Gutmann, “An example of the difference between quantum and classical random walks,” *Quantum Information Processing*, vol. 1, no. 35, 2002.
- [15] A. J. Bracken, D. Ellinas, and I. Tsohanjis, “Pseudo memory effects, majorization and entropy in quantum random walks,” *Journal of Physics A: Mathematical and General*, vol. 37, pp. 91–97, 2004.
- [16] B. C. Sanders and S. D. Bartlett, “Quantum quincunx in cavity quantum electrodynamics,” *Physical Review A*, vol. 67, no. 042305, 2003.
- [17] M. A. Nielsen and I. L. Chuang, “Quantum computation & quantum information,” *Cambridge University Press*, 2010.
- [18] D. Ellinas, “Quantum information: Lecture notes,” *Technical University of Crete, School of ECE*, 2021.
- [19] B. C. Travaglione and G. J. Milburn, “Implementing the quantum random walk,” *Physical Review A*, vol. 65, no. 032310, 2002.
- [20] D. Ellinas, A. J. Bracken, and I. Smyrnakis, “Discrete randomness in discrete time quantum walk: Study via stochastic averaging,” *Reports on Mathematical Physics*, vol. 70, no. 2, pp. 221–227, 2012.
- [21] D. Ellinas *et al.*, “Dating with a phase transition: Quantum to classical in quantum walks,” *to appear*,
- [22] C. Guan and X. Guan, “A brief introduction to anderson localization,” *Department of Physics, Massachusetts Institute of Technology*, 2019.
- [23] A. Lagendijk, B. A. van Tiggelen, and D. Wiersma, “Fifty years of anderson localization,” *In proceedings of the twenty-eighth annual ACM symposium on Theory of computing*, pp. 212–219, 1996.
- [24] M. Zeng and E. H. Yong, “Discrete-time quantum walk with phase disorder: Localization and entanglement entropy,” *Scientific Reports*, vol. 7, no. 1, 2017.
- [25] D. Ellinas and I. Smyrnakis, “Asymptotics of a quantum random walk driven by an optical cavity,” *Journal of Optics B: Quantum and Semiclassical Optics*, vol. 7, no. 2, pp. 152–157, 2005.
- [26] ———, “Quantum optical random walk: Quantization rules and quantum simulation of asymptotics,” *Physical Review A*, vol. 76, 2007.

- [27] W.-K. Tung, “Group theory in physics, an introduction to symmetry principles, group representations, and special functions in classical and quantum physics,” *Michigan University, USA*, 1985.
- [28] A. Abbas, S. Andersson, A. Asfaw, A. Corcoles, L. Bello, Y. Ben-Haim, M. Bozzo-Rey, S. Bravyi, N. Bronn, L. Capelluto, A. C. Vazquez, J. Ceroni, R. Chen, A. Frisch, J. Gambetta, S. Garion, L. Gil, S. D. L. P. Gonzalez, F. Harkins, T. Imamichi, P. Jayasinha, H. Kang, A. h. Karamlou, R. Loredo, D. McKay, A. Maldonado, A. Macaluso, A. Mezzacapo, Z. Mineev, R. Movassagh, G. Nannicini, P. Nation, A. Phan, M. Pistoia, A. Rattew, J. Schaefer, J. Shabani, J. Smolin, J. Stenger, K. Temme, M. Tod, E. Wanzambi, S. Wood, and J. Wootton., “Learn quantum computation using qiskit,” 2020.
- [29] B. L. Douglas and J. B. Wang, “Efficient quantum circuit implementation of quantum walks,” *School of Physics, The University of Western Australia, 6009, Perth, Australia.*, 2009.